Republic of Iraq
Ministry of Higher Education & Scientific Research
University of Babylon
College of Education for Pure Sciences
Department of Physics

Silicon dioxide nanoparticles impact on the Physical Properties of Polymer Nanocomposites

A Thesis

Submitted to the Council of the College of Education for Pure Sciences, University of Babylon in Partial Fulfillment of the Requirements for the Degree of Master in Education / Physics

By

Athar Iqbal Alawi abd alshahid

B.Sc. in physics

(University of Babylon, 2009)

Supervised by

Prof. Dr. Ehssan Dhiaa Jawad Al-Bermany

2023 A.D. **1445 A.H.**

بسم الله الرحمن الرحيم

﴿ قُل لَّوْ كَانَ ٱلْبَحْرُ مِدَادًا لِّكَلِمَٰتِ رَبِّى لَنَفِدَ ٱلْبَحْرُ قَبْلَ أَن تَنفَدَ كَلِمَٰتُ رَبِّى وَلَوْ جِئْنَا بِمِثْلِهِۦ مَدَدًا ﴾

صدق الله العلي العظيم

سورة الكهف: آية (١٠٩)

Silicon
https://doi.org/10.1007/s12633-023-02477-5

RESEARCH

Newly Fabricated Ternary PAAm-PVA-PVP Blend Polymer Doped by SiO_2: Absorption and Dielectric Characteristics for Solar Cell Applications and Antibacterial Activity

Athar Iqbal Alawi[1,2] · Ehssan Al-Bermany[1]

Received: 4 March 2023 / Accepted: 18 April 2023

Abstract
Silicon oxide nanoparticles (SiO_2 NPs) attractive nanomaterials for tuning the structure, characterizations, band gap, and dielectric properties. Newly ternary blend polymers nanocomposites reinforced using SiO_2 nanoparticles were fabricated and investigated. Poly(acrylamide) (PAAm), poly(vinyl alcohol) (PVA), and poly(vinyl pyrrolidone) (PVP) were mixed with different ratios and loaded with different ratios of SiO_2 (x = 0.00, 0.01, 0.03, and 0.05) wt. % applying green-easy solution-casting procedure. X-ray diffraction (XRD), infrared Fourier-transform spectroscopy (FTIR), optical microscopy (OPM), field emission scanning electron microscope (FE-SEM), UV–visible spectrophotometer, DC electrical meter and antibacterial activity of the nanocomposite were used to characterizations the samples. FTIR spectra exhibited significant interfacial interaction between the component matrixes. XRD patterns for samples showed a broad peak between ~ 10–50°. OPM and FESEM images showed a homogeneous surface and excellent distribution of nanoparticles in the matrix. The optical absorption results enhanced from 0.73 to 0.91 at 200 nm, and the energy gap improved from 4.8 to 3.4 eV for allowed indirect transition and from 4.2 to 3.1 eV for forbidden indirect transition. The dielectric constant and loss improved from 0.20 to 0.53, and outstanding enhancement was presented in the electrical conductivity. SiO_2 NPs exhibited notable improvement in the inhibited zone of antibacterial activity from 0.00 to 24 mm of S. aureus and 23 mm of E. coli compared to ternary blend polymers. These nanocomposites are promising for various applications, such as solar cells, optoelectronic, and bioenergy applications.

Keywords SiO_2 · PAAm · PVP · PVA · Absorption · Dialectical · Optoelectronic · Antibacterial · Nanocomposites

1 Introduction

The efficiency of polymer-based solar cells could be lower than silicon based solar cells, which could relate to the lack of absorbing the whole solar light by the photoactive layer. The polymer with a large band gap presented emission quenching, which is a problem by presenting only one donor compared to the two acceptors in the ternary blend [1]. Therefore, many researchers tried solving this issue using binary blend counterparts. Other investigated using ternary blend polymers that showed better absorption optical range and can be easily expanded. This impact comes from additional absorption of the third material that can be more expeditiously get donor/acceptor interfaces through the transfer of the long-range energy [2]. Compared to binary blend counterparts, there is a significant enhancement to the photocurrent generation of ternary blend polymer solar cells [1, 2]. Recently, a ternary structure has been a promising strategy to enhance the performances in binary polymer, fullerene, and bulk heterojunction polymer (BHJ) devices [3]. To boost the achievement in the material properties, incorporating the nanostructures such as SiO_2, TiO_2, GO, and Ag nanoparticles in these ternary blends polymer can play a unique role in improving the emission of the large band gap polymer by a mechanism, which is named charge trapping [1].

Silicon is a promising material with significant characterizations because it has chemical stability, a high melting

✉ Ehssan Al-Bermany
ehssan@uobabylon.edu.iq

[1] Department of Physics, College of Education for Pure Science, University of Babylon, Babylon, Iraq

[2] Educational Directorate of Babylon, Ministry of Education, Baghdad, Iraq

Published online: 27 April 2023

Prof. Dr. Ehssan Al-Bermany <ehssan@itnet.uobabylon.edu.iq>

Notification of Full Paper (Decision) 2ICSRI 2023 - Paper ID (2ICSRI-6687)

1 message

2ICSRI 2023 <2icsri2023@easychair.org> 18 June 2023 at 17:48
To: Prof Ehssan Al-Bermany <ehssan@itnet.uobabylon.edu.iq>

Dear Author(s),

On behalf of the International Programme Committee of The second International Conference on Scientific Research and Innovation 2023 (2ICSRI 2023), We are very pleased to inform you that your submitted paper with ID (2ICSRI-6687) and titled "Silicon Nanoparticle Impact on some of the Properties of Polymer Nanocomposites", has been [accepted with Major Revisions] (Conditional Acceptance).

Please, review the comments below and the attached files of the referees.
The paper would be reconsidered after requisite modifications per the conference's comments and instructions (Author Guidelines) https://opqc.org/2icsri.
Kindly make the changes according to the comments and the attached files and resend the revised manuscript along with clarifications for all the comments, clearly indicating the areas where the changes have been made by highlighting it in Yellow.
You may log in to your EasyChair account to upload the revised paper:
https://easychair.org

The Scientific Programme Committee of the 2ICSRI 2023 allows FIVE days for the revision of the manuscript.

Thank you for submitting your valuable research work to the 2ICSRI 2023.

Please ensure that your paper is written in correct English before submission with a plagiarism score of less than 20%. If you need assistance in the Language Editing Services, please do not hesitate to contact us at info@opqc.org

Kind regards,

Duha Saadi

Programme Committee Member of 2ICSRI 2023

https://opqc.org/2icsri
Duha.S.Ahmed@uotechnology.edu.iq

SUBMISSION: 6687
TITLE: Silicon Nanoparticle Impact on some of the Properties of Polymer Nanocomposites

---------- REVIEW 1 ----------
SUBMISSION: 6687
TITLE: Silicon Nanoparticle Impact on some of the Properties of Polymer Nanocomposites
AUTHORS: Athar Alawi and Prof Ehssan Al-Bermany

---------- Review Form ----------
SCORE: 1 (Accept after major revisions (conditional acceptance): the paper will be reconsidered after the authors make the major changes suggested by the reviewers and/or editors)
----- TEXT:
Accept after major revisions.

1. Scientific and grammar mistakes are everywhere. I JUST MARKED SOME EXAMPLES OF THESE MISTAKES. THE WHOLE ARTICLE SHOULD BE REVISED IN A PROPER MANNER REGARDING THE SCIENTIFIC AND GRAMMAR STYLES.

2. The images, plots, and curves came with bad resolution and non clear details and scales of measurements.

The second International Conference on Scientific Research and Innovation (2ICSRI 2023)

Organized by

Oakland Publishing and Quality Conferences

Ohio Publishing and Academic Services

Cincinnati, OH, United States, August 25-26, 2023

Acceptance Letter

Date: 21/07/2023

Manuscript Title: Exploring the Impact of Silicon Nanoparticles on Polymer Nanocomposites: Advancements in Fabrication Techniques and Exciting Applications in Solar Cells, Photoelectronics, and Sensors.

Manuscript ID: 2ICSRI-6687

Dear Athar Alawi and Ehssan Al-Bermany,

We are pleased to inform you that the manuscript with the above title has been accepted for oral presentation in the **Second International Conference on Scientific Research & Innovation (2ICSRI 2023)**, organized by *Oakland Publishing and Quality Conferences*, and *Ohio Publishing and Academic Services*, which will be held in **Cincinnati, OH, United States, August 25-26, 2023**, and the publication will be in **AIP Conference Proceedings (E-ISSN:1551-7616).** The concept note and draft agenda will be sent to you at a later time.

We look forward to your attendance.

Thank you very much for your participation.

Prof. Dr. Justin Link
Scientific Chairman

Assoc. Prof. Dr. Haider Raad
Publication Chairman

Dr. Thaer Al-Jadir
Organizing Chairman

Acknowledgments

Thankfulness, praise be to Allah, the grace that befits his holy self, and peace and blessings be upon our messenger, Muhammad Bin Abd Allah, May Allah's prayers and peace be upon him and his family and companions. After completing this work, it is my pleasure to extend my sincere thanks and appreciation to the owner of the generous hands, who contributed with his abundance of knowledge, his valuable time, and his sincere help in helping in my preparation of this letter, Professor Dr. Ehssan Dhiaa Jawad Al-Bermany.

Thanks to the Deanery of the College of Education for the Pure Sciences/ University of Babylon and the Department of Physics for allowing me to complete my letter. I also would like to thank all the teachers, instructors, and students of the Department of Physics for their assistance. Finally, many thanks go to those who supported me and alleviated the difficulties I have faced during my work and to everyone who helped me in one way or another while preparing this letter.

Athar

Dedication

To the best man in the universe, my father

To the best woman in the universe, my mother

To who gave me the endurance to complete my road, my husband

To my brother and my sister

To my close friends

My beloved country Iraq

The martyrs of Iraq with all the love and appreciation

Athar

Summary

Silicon oxide nanoparticles (SiO_2 NPs) attracted nanomaterials for tuning the structure, characterizations, band gap, and dielectric properties. This investigation focused on the impact of the SiO_2 on newly ternary blend polymers to fabricate new nanocomposites. Polyacrylamide (PAAm), polyvinyl alcohol (PVA), and polyvinyl pyrrolidone (PVP) were mixed with different ratios and loaded with different ratios of SiO_2 (x = 0.00, 0.01, 0.03, and 0.05) wt. % applying green-easy solution-casting procedure.

The study was divided into five chapters, chapter one focused on the introduction and literature survey, chapter two explained the thermotical parts, chapter three explained the experimental part, chapter four presented and discussed the results, and finally, chapter five summarized the conclusions and future works.

Different characterizations used to investigate these new nanomaterials' X-ray diffraction (XRD), infrared Fourier transform spectrometer (FTIR), optical microscopy (OM), field emission scanning electron microscope (FE-SEM), UV visible light spectrometer (UV visible light spectrometer), AC ammeter and anti-efficacy used for bacteria to examine samples and a Giger counter to detect susceptibility to ionizing radiation absorption.

FTIR spectra showed a significant interaction between the polymer mixture and the nanomaterial. X-ray diffraction (XRD) patterns of the samples showed a wide peak between10 ^{o}- ~50^{o}. The OM and FE-SEM images showed a homogeneous surface and an excellent distribution of nanoparticles in the mixture.

The optical properties showed enhancement absorption from 0.73 to 0.91 at 200 nm, and the energy gap improved from 4.8 to 3.4 eV for allowed indirect transition and from 4.2 to 3.1 eV for forbidden indirect transition. The absorption coefficient refractive index, extinction coefficient, real and imaginary dielectric constant, and optical conductivity improved with increasing the concentration of

SiO_2 NPs, while the transmittance reduced with increasing concentration of SiO_2 NPs. The dielectric constant and loss improved from 0.20 to 0.53, and outstanding enhancement was presented in the electrical conductivity.

SiO_2 nanoparticles have shown significant improvement in the inhibition zone of antibacterial activity from 0.00 to 24 mm of S. aureus and 23 mm of coli strip compared to the triple mixture of polymers. These nano compounds are promising for different applications and the results of gamma radiation shield applications for nano compounds have emerged in low transport radiation with increased SiO_2 concentrations. Attenuation factors increase with the increased concentration of SiO_2 nanoparticles. These nanocomposites are promising for solar cells, optoelectronics, biology applications, and light shielding applications.

Contents

List of Figures

List of Tables

List of Symbols

Symbol	Physical Meanings	Unites
A	Absorbance	a.u
A_a	Area	cm^2
B	constant depending on the type of material	-
C_o	Capacitance vacuum	F
C_p	Capacitance	F
c	Speed of light	m/s
D	crystallite size	nm
d_{hkl}	Distance to miller	Å
E	Energy	ev
E_{ph}	Energy of phonon	ev
$\boldsymbol{E_g^{OPt}}$	Optical energy gap	ev
ε	Complex dielectric constant	-
ε_r	Real dielectric constant	-
ε_i	Imaginary dielectric constant	-
$\grave{\varepsilon}$	Dielectric constant	-
ε''	Dielectric Loss	-

ε_o	Vacuum permittivity	F/cm
h	Planck's constant	J. s
I	Electrical Current	A
$\mathbf{I_T}$	Transmittance Ray	Lux
$\mathbf{I_q}$	Capacitate Current	A
$\mathbf{I_p}$	Conduction Current	A
$\mathbf{I_o}$	Incident Intensity of Light	Lux
$\mathbf{I_A}$	Absorbed Light Intensity	Lux
i	Imaginary Number	-
$\mathbf{k_o}$	Extinction Coefficient	-
N	Complex refractive Index	-
$\mathbf{N_o}$	Number of transmitted particles	-
n	Refractive Index	-
n	Diffraction rating	-
R	Reflectance	-
$\mathbf{R_v}$	Volume Electrical Resistance	Ohm
$\mathbf{R_P}$	Parallel Resistance	Ohm
r	Exponential constant	-

T	Transmittance	-
T_g	Glass Transition Temperature	^oC
T_m	Melting Temperature	^oC
t	The thickness of the film	μm
V_m	Maximum voltage	V
W	Weight of the Sample	g
X	Sample thickness	μm
Z	Total Prohibition	ohm
ω	Angular frequency	Rad. s^{-1}
α	Absorption coefficient	cm^{-1}
λ	Wavelength of Light	nm
σ_{op}	Optical conductivity	S^{-1}
σ_{ac}	Electrical conductivity	S/cm
δ	Dielectric loss angle	-
θ	The incident angles	Degree
ν	Photon Frequency	Hz
ΔK	Wave number	cm^{-1}
μ	The linear absorption coefficient	cm^{-1}

μ_m	the mass absorption coefficient	cm^2/g
ρ	Density	g/mL
χ½	The half thickness	cm
β	Full Width at Half Maximum (FWHM)	-

List of Abbreviations

Abbreviations	Physical Meanings
A.C	Alternating current
APTES	3-Aminopropyl triethoxysilane
AFM	atomic force microscopy
Ag	Silver
BP1	blend polymers
C.B	Conductive band
CS	chitosan
DOX	doxorubicin
DW	Distill water
EDS	energy dispersive X-ray spectrometry
E. coli	Escherichia coli
FE-SEM	Field emission scanning electron microscope
FTIR	Fourier transform infrared
GO	Graphene oxide
IR	Infrared
MW	Molecular weights

NC2	Nanocomposites with SiO_2 concentrations of %1
NC3	Nanocomposites with SiO_2 concentrations of 3%
NC4	Nanocomposites with SiO_2 concentrations of 5%
NIPS	Non-solvent Induced Phase Separation
NPs	Nanoparticle
OLM	Optical Light Microscope
OM	Optical Microscopy
PAAm	Poly acryl amide
PEO	Poly ethylene oxide
PS	Polystyrene
PVDF	Polyvinylidene fluoride
PVA	Poly Vinyl alcohol
PVP	Poly Vinyl pyrrolidone
PMMA	Polymethyl methacrylate
ROS	Reactive Oxygen Species
RT	Room Temperature
S. aureus	Staphylococcus aureus

Sb_2O_3	Antimony trioxide
SEM	Scanning Electron Microscopy
SiC	Silicon Carbide
SiO_2	Silicon dioxide
$SrTiO_3$	Strontium Titanate
TEM	Transmission Electron Microscopy
TMSPM	trimethoxysilyl propyl methacrylate
TEOS	Tetraethylorthosilane
UHMWPE	Ultra-High Molecular Weight Polyethylene
UV	Ultraviolet spectrum
UCNPS	Upconverting nanoparticles
V.B	Valence band
Vis	Visible
XRD	X-Ray diffraction

Chapter One

Introduction and Literature Survey

1.1 General Introduction

Triple blending polymers used that showed better absorption optical range and can be easily expanded. This impact comes from additional absorption of the third material that can be more expeditiously get donor acceptor interfaces through the transfer of the long-range energy [1] . Compared to binary blend counterparts, there is a significant enhancement to the photocurrent generation of ternary blend polymer solar cells [1,2]. Recently, a ternary structure has been a promising strategy to enhance the performances in binary polymer, fullerene, and bulk heterojunction polymer devices [3]. To boost the achievement in the material properties, incorporating the nanostructures such as SiO_2 nanoparticles in these ternary blend's polymer can play a unique role in improving the emission of the large band gap polymer by a mechanism, which is named charge trapping [2].

Silicon is a promising material with significant advantages, such as a melting point (1700 °C), high chemical stability. These important features make silicon an essential insulator in electronic technology and a good thermal and electrical insulator [4]. In addition, most of the standard fiber optic connection current is made of silicon [5]. Nanoparticles can be created by depositing a silicon-rich material first, followed by thermal processors that cause excess silicon deposition [5]. silica or Silicon dioxide is the most common silicon dioxide in nature such as quartz [1]. silicon dioxide (SiO_2) a widespread adsorption material that is usually resistant to high temperature, low cost and non-toxic [6]. The evolution of small ranges and the subsequent expansion of the impact range gap results from the drop in the diameter of silicon particles to the nanometric scale. Modern electronics rely heavily on crystal Silicon dioxide to produce nanocomposite materials for semiconductors and microelectronics [2,5]. These nanomaterials can benefit from beneficial features of both parts to manufacture polymer nanomaterials [8].

Generally, the use of most polymers was limited to the manufacture of cheap products used for simple purposes. However, rapid technological development has required replacing some materials used in industry with others for better specifications [7,8]. Later, the development of polymer started to increase by leaps and bounds. Nowadays, scientists seek to produce cheap, flexible, and multi-purpose polymers. it is used in housing, automobiles, and different industrial applications. when these materials have developed, they have played a distinguished role in the evolution of electrical components and equipment [11]. Since most electrical properties are determined largely by primary chemical structure and are relatively insensitive to microstructure, consequently, the electrical behavior of polymers is generally less disparate than its mechanical behavior [12]. Similarly, optical properties also govern a variety of engineering end uses. Polymers as a class have the very high electrical resistivity characteristic of insulators. Conduction in the surface layers of a polymer material is often sensitive to humidity and surface contamination. The surface resistivity is determined from the flow of current between two electrodes in contact with one surface of a thin specimen of polymer material [12].

Additives are constituents added to polymers to provide them with specific characteristics and improve basic properties. These constituents are added in a granular form or as small particles [13]. Nanocomposites can be defined as a composite material in which at least one of the phases (Mostly the filler) shows dimensions in the nanometer range, as the filler, size reaches the nanometer level, the interactions at the interfaces become considerably large with respect to the size of the inclusion and thus the final properties show significant changes [14]. A nanocomposite has two parts, filler and the matrix, a traditional composite typically uses a fiber such as carbon fiber or fiberglass as the filler. The host matrix's crystallinity, polymer chemistry, nature as a thermoplastic or

thermosetting material, surface treatment, interfacial qualities, fill grade, degree of dispersion, and agglomeration are all important factors that affect the properties of nanocomposites. Relative arrangements and subsequent synergy between constituents and synthesis methods [15]. The characteristics of polymer nanocomposites are affected by: the nature of the polymer matrix and filler ,etc dispersion state of the particles, filler- matrix interaction, filler size, surface modification of the filler [16]. Nanocomposites are a major factor in the formation of novel advanced materials suitable for a variety of different applications, such as electrical engineering, nanocomposites have attracted considerable interest in both academia and industry [17].

To understand more the effect of silicon oxide on polymeric materials, we review some of the sources that studied these materials in previous studies.

1.2 Literature Survey

In (2016) M. Shahbazi, *et. al.* [18] deposited poly Vinylpyrrolidone-silicon dioxide- 3-trimethoxysilyl propyl methacrylate thin films on p-type Si substrates using spin coating technique. X-ray diffraction analysis revealed an amorphous structure for all the samples, which was approved by scanning electron microscopy images. On the other hand, the surface morphology of (PVP-SiO_2- trimethoxysilyl propyl methacrylate) was examined using atomic force microscopy (AFM) and scanning electron microscopy (SEM) techniques. The effects of dielectric constant (ὲ), dielectric loss (ε"), loss tangent (tan δ) as well as the real component of electric modulus (M'), imaginary component of electric modulus (M"), and alternating current (AC), electrical conductivity (δ_{AC}) on PVP-SiO_2-TMSPM hybrid thin films were investigated with wide range frequency from 0.1 KHz to 1 MHz. It was found that the values of ὲ, ε", tan δ were reduced with increasing frequency.

In (2016), Z. Li, *et. al.* [19] fabricated Poly Vinylidene fluoride /silicon dioxide - Graphene oxide nanohybrid membranes via thermally induced phase separation (TIPS) method. The results indicate that the (Polyvinylidene fluoride) PVDF/SiO_2@GO nanohybrid membranes experience liquid-liquid phase separation mechanism, and exhibit bi-continual and asymmetric structure. The included SiO_2@GO nanohybrid is uniformly dispersed in the membrane matrix. The addition of SiO_2@GO, the top surface becomes denser and the pore size decreases; but overhigh SiO_2@GO addition for membrane M-5 triggers in the adverse trend. The XRD patterns and FTIR spectra of membranes verify the exclusive α-phase of polyvinylidene fluoride, and the melting temperature (T_m) and crystallinity(x_c) evidently increase with the addition of SiO_2@GO nanohybrid up to 0.9 wt.% in the dopes.

In (2017), Z. Haeri, *et. al.* [20] synthesized SiO_2-GO nanohybrids via one-

Step sol-gel route using a mixture of Tetraethylorthosilane (TEOS) and 3-Aminopropyl triethoxysilane (APTES). The SiO_2-GO nanohybrids were prepared at various hydrolysis times of 24, 48 and 72 h, then 0.2 wt.% of GO, SiO_2-GO nanohybrids were separately incorporated into the epoxy coating. Results revealed that amino functionalized SiO_2 nanoparticles with particle size around 20-30 nm successfully synthesized on the basal plane of GO. Results showed significant improvement of dispersion and interfacial interactions between nanohybrids and epoxy composite arising from covalent bonding between the SiO_2-GO and the epoxy matrix. It was found that the thermal resistance of SiO_2-GO nanohybrids and SiO_2-GO/Epoxy nanocomposite was noticeably higher than GO and epoxy matrix.

In (2018), P. Paik, *et. al.* [21] synthesized Upconverting nano@SiO_2–

GO through a bioconjugation approach and used for drug delivery applications to counter the lack of quantum efficiency of the up-conversion

process and control sustained release. A model anticancer drug (doxorubicin, DOX) was loaded to UCNPs, UCN@SiO_2 NPs and the UCN@SiO_2–GO nanocomposite. The photosensitive release of DOX from the UCN@SiO_2–GO nanocomposite was studied with 980 nm NIR laser excitation and the results obtained for UCNPs and UCN@SiO_2 NPs were compared. It is revealed that the increase in the NIR laser irradiation time from 1 s to 30 s leads to an increasing in the amount of DOX release in a controlled manner. In vitro studies using model cancer cell lines perform to check the effectiveness of materials for controlled drug delivery and therapeutic applications.

In (2019), Gaaboura, [22] prepared nanocomposite films based on chitosan (Cs) and polyacrylamide (PAAM) embedded with silica nanoparticles (SiO_2) via solution casting method. The films were studied and characterized using different techniques. The X-ray diffraction revealed the presence of the semi-crystalline nature of Cs/PAAM blend. The main characteristic Infrared-bands to the vibrational groups for Cs/PAAM were observed. No changes in the position of IR bands are seen after incorporation of SiO_2 nanoparticles. The UV–vis spectra show an absorption band at 253 nm with a sharp absorption edge, which indicates the semi-crystalline nature of Cs/PAAM matrices. The spectra optical parameters were measured and characterized as a function of photon energy. The value of optical energy gap (E_g) is estimated using indirect transition model and explained due to local cross linking in the amorphous regions of Cs/PAAM. The plot of dielectric loss and dielectric constant with the frequency was gradually decreases with the increase of the frequency and reaches to constant values at higher frequencies due to polarization effects.

In (2019), S. A. Haddadi, *et. al.* [23] modified Hummer method was used in the preparation of graphene oxide (GO) nanosheets, and then SiO_2 decorated GO [GO(SiO_2)] nanosheets using the sol–gel method. Ultrahigh-molecular-weight

polyethylene (UHMWPE) nanocomposites loaded with 0.5, 1, 1.5, and 2 wt. % of GO-SiO_2, which were prepared using magnesium ethoxide/GO-SiO_2 supported Ziegler–Natta catalysts via the in-situ polymerization. Morphological study of the prepared polymer powders is assessed using field emission scanning electron microscopy, which shows that GO-SiO_2- nanohybrids have uniformly dispersed and distributed into the UHMWPE matrix. Also, the characterization of the UHMWPE nanocomposites indicates that many characterizations, including the mechanical, thermal, and tribological properties of UHMWPE, are significantly improved by incorporation of these new nanosheets in spite of the molecular weight reduction of the polymeric matrix and the improved flowability and processability of the produced nanocomposite.

In (2019), R. Dong, *et. al* [24] prepared of (SiO_2- GO) by surface Modification of graphene oxide (GO) by the hydrolysis of the tetraethoxysilane (TEOS) and then the SiO_2- GO is added into acrylic resin as reinforcement to prepare acrylic nanocomposites. X-ray diffraction, Fourier transform infrared, Raman, XPS, scanning electron microscopy, and Transmission electron Microscopy results indicated that SiO_2 is well dispersed on the surface of GO. Compared with GO, SEM and TEM results revealed that SiO_2– GO dispersed more uniformly in acrylic resin and had less agglomeration.

In (2020), O. H. Sabr, *et. al*. [25] prepared poly Vinylalcohol (PVA)/ silica nanoparticles (SiO_2 NPs) nanocomposite by solution casting method. The morphological, and optical properties of (PVA/SiO_2) nanocomposite were investigated. The AFM, image show the surface of pure PVA that was smooth and homogenous. The roughness of surface of sample increases after adding of SiO_2 nanoparticles. The optical properties showed that all these properties increase linearly by adding of 5% of silica nanoparticles except the transmittance and indirect energy gap have versus behavior of absorbance.

In (2020) Alsaad AM, *et. al* [26] prepared polymethylmethacrylate (PMMA) and poly Vinyl alcohol (PVA) doped with silica nanoparticles (SiO_2 NPs) by the dip-coating technique. The optical and structural properties, such as Fourier-transform infrared spectroscopy and thermal properties, were determined. The optical bandgap of un-doped PMMA-PVA thin film isestimated to be 4.069 ev. Additionally, refractive indices (n) of undoped PMMA-PVA polymeric thin films are calculated to be in the range (1.48–1.72). The result from FTIR obtained are useful for a better understanding of the lattice dynamics. Moreover, thermal stability of thin films is investigated using thermogravimetric (TGA) technique. Remarkably, TGA reveal that doped thin films are thermally stable below 110 C^o. Consequently, investigated thin films may have the potential to be key candidates for real time optical and optoelectronic devices.

In (2021), Ahmed Hashim [27]**,** fabricated PVA/SiO_2/SiC nanostructures by using casting method. The structural, optical, and dielectric characteristics of PVA/SiO_2/SiC films have studied to be used in flexible, lightweight, high sensitivity, and low-cost pressure sensors compared with the other types of pressure sensors. The results indicates that the optical characteristics which included the absorbance and energy gap of PVA enhances with the rise of SiO_2–SiC NP ratios. The dielectric characteristics shows that the dielectric parameters of PVA improved with the rise in SiO_2–SiC NP ratios. The pressure sensor results of PVA/SiO_2/SiC nanocomposites shows that the dielectric parameters increase with the increasy in pressure for various ratios of SiO_2–SiC NPs. Finally, the increasy in sensitivity is 50.18%, 52%, and 53.46% at 1 kHz, 100 kHz, and 1 MHz, respectively, when the SiO_2–SiC NPs, content reached 3.6 wt.%, which makes it suitable to be used in different electronic, optical, and electric fields.

In (2022), T. S. Soliman, *et. al.* [28]**,** prepared PVA/SiO_2 nanocomposite prepared through a sonication technique followed by a solution casting method.

The structure of PVA/SiO_2 films is evaluated using the experimental results attained by X-ray diffraction (XRD), Fourier transform infrared (FTIR), and scanning electron microscope (SEM) examinations. A thermal stability studies of the nanocomposite films was performed. UV-vis spectra were used to investigate the optical properties of PVA/SiO_2 nanocomposite films. The XRD results confirmed the semicrystalline nature of the PVA. The SEM results ascertained the homogeneity of the SiO_2 nanoparticles in the polymer matrix. From the study, a simultaneous increase of SiO_2 nanoparticle content decreases the direct optical band gap and Urbach energy; however, the refractive index and extinction coefficient are increased.

In (2022), karar Abdali, [29] studied the impact of incorporation SiO_2 on the structural, optical, electrical properties , and relative humidity sensor feature of PVA/ Dextrin polymeric blend using traditional casting procedure .the obtained films were investigated using different common techniques like XRD ,FTIR OM, UV-Vis ,LCR meter and humidity meter. The SiO_2NPs were well diffused in host blend, and up to 97% of UV rays were blocked by the produced films at $\lambda = 270$ nm. the absorption edges decreased from 4.05 to 3.80 eV. The values of the allowed and forbidden energy gap (Eg) decreased from 4.18 to 3.75 eV and from 3.98 to 3.73 eV, respectively. The use of SiO_2 was highly improved dielectric features in the 100Hz -10^6Hz frequency range.

In (2023) Al-Bermany, Ehssan , *et. al.* [7] used it environmentally friendly and straightforward process to create silver and silica nanoparticles a core-shell structure (Ag@SiO_2). After that, the core-shell nanoparticles that had created strengthened the blended polymer matrix and allowed for the creation of new nanocomposites. Nanoscale core particles are inserted into the nanocomposites made of poly Vinyl-mixed polymer (PVA) and ultra-molecular-weight

polyethylene oxide (UHMW-PEO). The optical properties of the spectrum made a major contribution to the enhancement of the UV-vis absorption and the reduced the band gap.

In (2023), N. Karim and M. Habeeb [30] , employed the solution casting method to fabricated nanocomposite films using polystyrene (PS) as the host matrix and antimony trioxide (Sb_2O_3) and silicon carbide (SiC) nanoparticles (0, 2, 4, 6 and 8 wt.%) as fillers in the PNCs materials' advancements. The morphology of the nanocomposite was examined using an optical microscope (OM), which demonstrated that polystyrene is exceptionally miscible due to its finer form and smooth, homogeneous surface, as well as the additive concentration SiC and Sb_2O_3 NPs, which are evenly distributed on the surface of the polymer nanocomposite film. The surface morphology of (PS/SiC/Sb_2O_3) films is revealed by field emission scan electron microscope (FE-SEM) to be uniform and coherent, with a significant number of aggregates or fragments randomly dispersed over the top surface. The results of the optical properties for (PS/SiC/Sb_2O_3) nanocomposites demonstrated that the absorbance, coefficient of absorption, index of refractive, coefficient of extinction, and conductivity of optical of (PS/SiC/Sb_2O_3) nanocomposites increases with increase of SiC/Sb_2O_3 NPs, while the transmittance decreased. The optical energy gap decreased from (4.19 eV to 2.69 eV) and from (3.5 eV to 1.45 eV) for allowed and forbidden indirect transition respectively when concentration reaches 8 wt.%. By raising the SiC/Sb_2O_3 NPs ratio in polystyrene, Klebsiella and Staphylococcus microorganism inhibition zone values rose to 24 and 25 mm.

1.3 Aims of the Work

1- Investigate the impact of silicon dioxide nanoparticles on the morphology, optical and electrical properties for the newly ternary blend polymers

fabricated nanocomposites.

2- Revealed the ability of theses nanocomposites for antibacterial activity and shielding applications.

Chapter Two

Theoretical Part

2.1 Introduction

This chapter covers the general idea of some theoretical aspects of the investigation, such as physical concepts, scientific clarifications, relationships, laws, raw materials and characterizations

2. 2 Polymers

Polymers were first discovered in the 1920s, Many synthetic polymers can be listed; some are well-known, such as polyesters, while others are less well-known, such as those used in medical applications for organs and degradable sutures [31]. The term "polymer" refers to units of high molecular mass molecules that are made up of numerous isolated structural elements and is derived from the Greek terms poly (many) and mars (parts). In other terms, polymers are enormous, highly molecularly weighted molecules, or macromolecules. that are connected together from a variety of little molecules, or monomers. The process of monomers reacting to create polymers is known as polymerization. In a chemical reaction known as polymerization, two or more substances combine with or without the addition of another substance, such as heat, water, or another solvent, to create a high-molecular-weight molecule [32].

2.2.1 Preparation of Polymers

Polymers can be divided into two groups based on their polymerization mechanism [31, 32].

1. Addition polymerization: it is the process of repeatedly adding monomer molecules with double or triple bonds to make addition polymers, which are polymers created without the removal of byproducts. For instance, polypropene and polyethylene are both derived from propane [33].

2. Condensation polymerization: It occurs when two monomers are combined after small molecules like water, alcohol, or NH3 have been eliminated. nylon 6, 6, nylon 6, and so forth are a few examples. Hexamethylenediamine and adipic acid, for instance, are combined to create nylon 6.6 [33].

2.2.2 Polymer Structure

The physical properties of polymer materials are not determined only by their molecular weight but also by their molecular structure. Polymer chains come in a variety of shapes and sizes that can be listed below and shown in Figure (2-1) [35].

1. Linear polymers: represent the van der Waals bond between the chains. Examples: Polyethylene and Nylon. Figure (2-1A)
2. Branched polymers: have a lower density than linear polymers and have a lower chain packing efficiency. Figure (2-1B)
3. Cross-linked polymers: chain is connected by covalent bonds. Often, it is achieved by adding atoms or molecules that form covalent links between chains. Many rubbers have this structure. Figure (2-1C)
4. Network polymers: made of three-functional layers in the form of three-dimensional networks. Examples include phenol-formaldehyde and epoxy. Figure (2-1D).

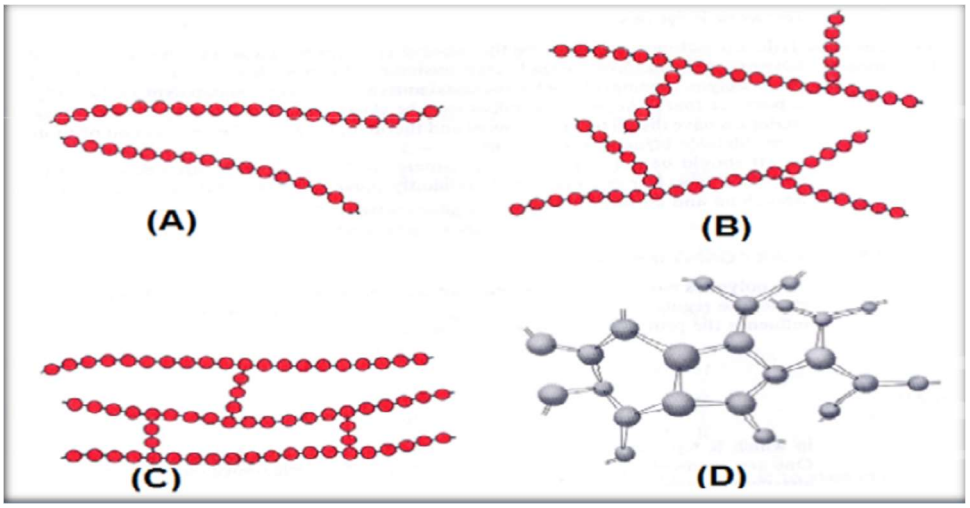

Figure (2-1). Polymer chains in a variety of shapes and sizes (A) linear polymers(B) branched polymers, (C) cross-linked, and (D) network polymers [35]**.**

2.2.3 Crystallinity of Polymers

The process of polymer crystallization involves the partial alignment of the polymer's molecular chains. Lamellae is ordered areas that make up larger spheroidal structures.it is created when these chains fold together. Polymers may crystallize following melting, mechanical stretching, or solvent evaporation. Crystallization has an impact on the polymer's chemical, mechanical, thermal, and optical characteristics [36]. The crystallinity of the polymer refers to how closely the chains of the polymer are aligned with one another. However, for this to occur, there must be some degree of stereoregularity. so, because the crystalline regions are produced by the stereoregular blocks of the polymer chain. When a polymer is melted, the long polymer chains entangle with one another in erratic coil-like formations. Some polymers' chains are highly irregular, and as the melted polymer cools to a solid state, it retains its tangled, chaotic configuration (stereo random). These polymers are known as amorphous polymers.

Additionally, if the chain has any branching regions, there won't be any stereoregularity, which will preclude [37].

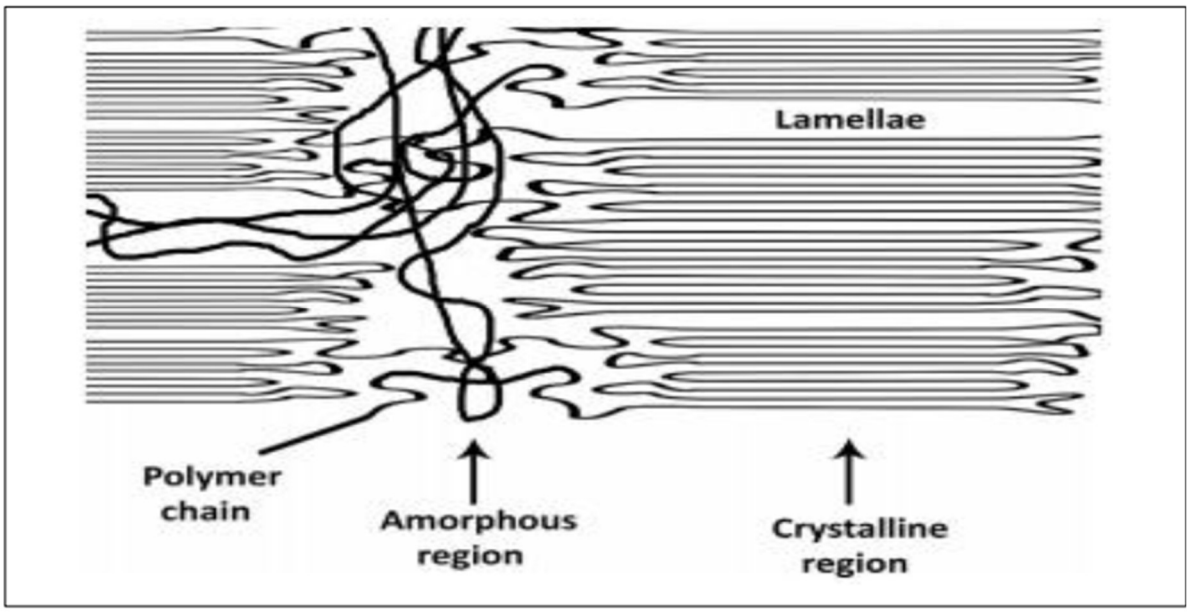

Figure (2-2). The crystallinity region in the polymers [37]**.**

Layered crystalline structures develop in precise systems with strongly interacting functional groups even at high melt temperatures, and they play a role in self-assembly, which affects their uniaxial tensile deformation behavior [38].

2.3 Nanomaterial's

The field of nanotechnology has substantially developed throughout the last century. Nowadays, nanotechnology is a major topic in a wide variety of study fields. The development, production, characterization, and use of materials and devices by changing their size and shape at the nanoscale can be classed as nanotechnology [39] .

Every flow uses the prefix "nano" as a term, even in product advertising. Due to the fact that nano is a combination of physics, chemistry, materials science, solid-state, and biological sciences, and that the name "nano" is derived from the Greek

Nanotechnology has many uses in both science and technology. Nanotechnology is intriguing, although the general some is unaware of its existence in practically all disciplines of engineering.it has broad application in medicine, the environment, electronics, defense, and security. Although a lot of work has been done using this technology, there is still room for the development of new nanomaterials in various fields for the advancement of mankind [40].

2.4 Nanocomposites

A nanocomposite is a polyphase solid substance with one, two, or three dimensions of less than 100 nm in one of the phases. Nanocomposites have a high surface-area-to-volume ratio. The physicochemical qualities may vary depending on the size and shape. Nanocomposites come in a variety of forms, including nanomaterials [40]. The three primary forms of nanocomposites are polymer matrix nanocomposites (PMNC), metal matrix nanocomposites (MMNC), and ceramic matrix nanocomposites (CMNC). The nanoparticles characterize nanomaterials by exhibiting various physicochemical features. As their size and even a tiny dimension at the nanoscale changes, they display shifting properties [17] .

In order to determine the properties of nanoparticles, they must be characterized using a variety of tools, including a UV spectrophotometer, Fourier transform infrared (FTIR) spectroscopy, atomic force microscopy (AFM), transmission electron microscopy (TEM), scanning electron microscopy (SEM), vibrating sample magnetometer (VSM), energy dispersive x-ray spectroscopy (EDS), XRD photoelectron sect (T_g) [40] , etc. Due to their small size and correspondingly higher surface area, nanoscale fillers differ from bulk materials and traditional micronize fillers. The incorporation of nanoparticles into polymers is anticipated to result in a previously unheard-of level of control over the electrical

characteristics of filled polymers [41]. One-dimensional nanotubes and nanowires, two-dimensional nano clays and silicon and three-dimensional spherical and cubical nanoparticles are the three categories into which nanofillers fall [42].

2.5 The Raw Materials

2.5.1. Polyacrylamide (PAAm)

The molecular weight of polyacrylamide (PAAm) is about 71.07 g/mol which is a water-soluble polymer, this polymer stands out because it is distinct from a monomer, non-toxic due to the 19.7 % nitrogen content, and the 3.6 % of molecules are hydroxyl groups[43].

It is a chemical substance that takes on the shape of a gel and has a high-water absorption rate. Because it has a high water absorption rate, it is typically employed in the production of soft contact lenses to raise the viscosity of water (i.e., making the solution thicker)[44]. This polymer can be used in a variety of applications, including water treatment, mining, and oil recovery. Recently, it has been used in surface grafting polymerization. Also, PAAm is used as a thickening agent for materials and as a flocculant. In the field of soft tissues and artificial corneas, and in the manufacture of tissues for covering burn [37]. Figure (2-3) shows the chemical formula of polyacrylamide. and there are some physical and chemical properties as shown in Table (2-1) [43].

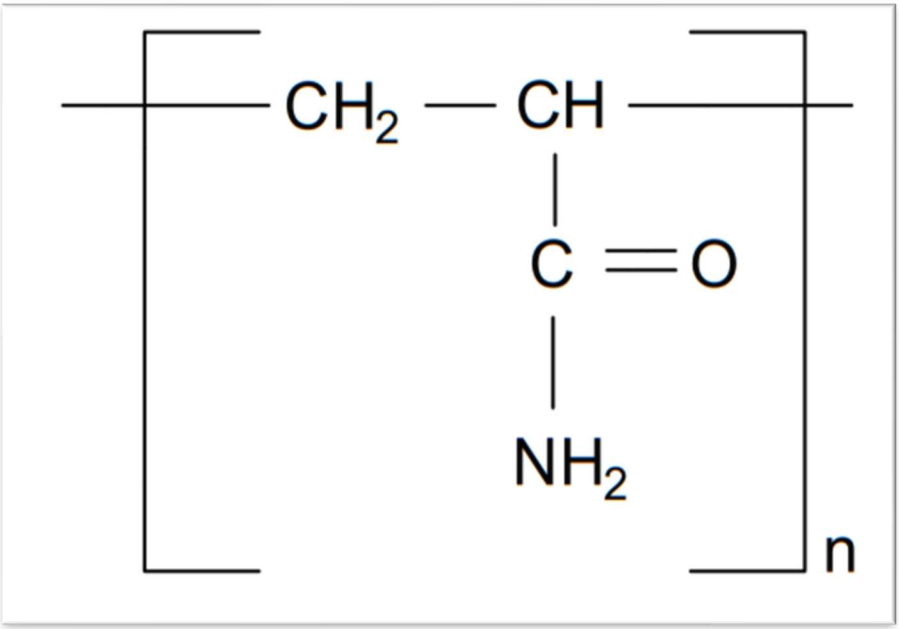

Figure (2-3). The chemical formula of polyacrylamide(PAAm)[44]**.**

Table (2-1). Physical and chemical properties of Polyacrylamide (PAAm) [43]

Property	Value
Appearance	crystal granular
Glass transition temperature (T_g)	161 C^o
Molecular formula	$(C_3H_5NO)_n$
Solution pH	3.5 - 6.8
Density	1.13 g/cm^3
Refractive index	1.45
Solubility	Stable. Incompatible with strong oxidizing agents
Melting temperature (T_m)	237 C^o

2.5.2 Polyvinyl pyrrolidone (PVP)

Polyvinyl pyrrolidone (PVP), commonly called poly Vidone or povidone, is a water-soluble polymer and polar solvents [46]. PVP is a biocompatible, compatible synthetic polymer that has been used as a biomaterial for many years. PVP is notable for its ability to interact with a wide range of hydrophilic and hydrophobic materials, and its pyrrolidone structure gives it capabilities comparable to those of a protein. This substance has a low immunogenicity, antigenicity, and toxicity. PVP has the formula $(C_6H_9NO)_n$ as shown in Figure (2-4) [47]. and has some physical and chemical properties as shown by the Table (2-2).

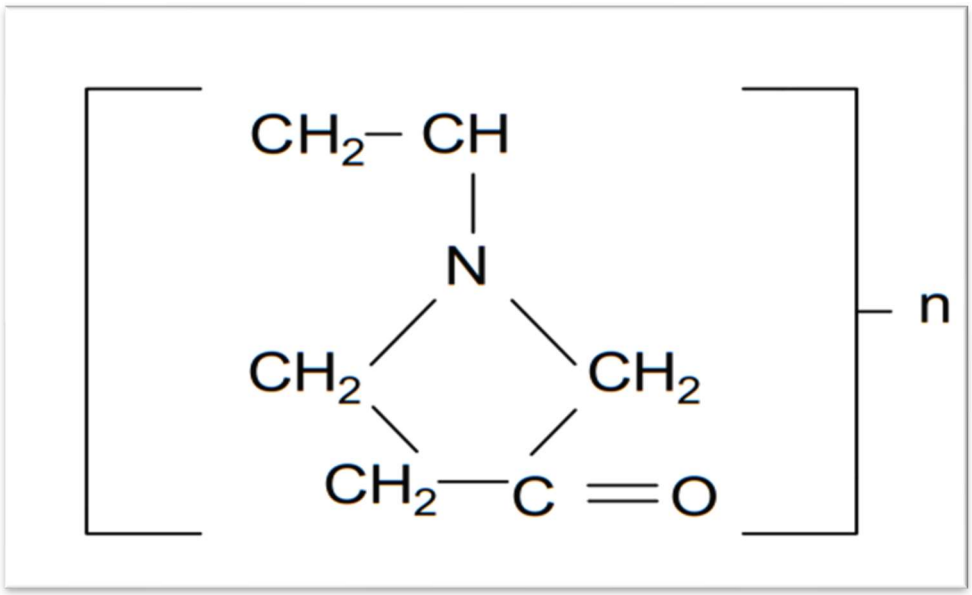

Figure (2-4). The chemical structure of polyvinyl pyrrolidone (PVP) [47]

PVP is amorphous and possesses an elevated glass transition temperature (T_g) due to the presence of the rigid pyrrolidone group, which is known to form various complexes with inorganic salts [46,47].

Table (2-2). Physical and chemical properties of polyvinyl pyrrolidone(PVP)[47]**.**

Property	Value
Appearance	White to creamy-white
Glass transition temperature (T_g)	109 C^o
Molecular formula	$(C_6H_9NO)_n$
Solution pH	3 -7
Density	1.25 g/cm^3
Refractive index	1.53
Solubility	Soluble > 10%, Insoluble < 1%
Melting temperature (T_m)	150-180 C^o

2.5.3 Polyvinylalcohol (PVA)

Polyvinylalcohol is a synthetic polymer that comes in the form of a white or cream-colored granular powder that is odorless, clear, and tasteless [50] .It is one of the oldest and most commonly used polymers, with uses in a wide range of fields, including semiconductors. formula is $(C_2H_4O)_n$, as shown in Figure (2-5) [51]. Polyvinylalcohol, may be combined in water. that the benefit of being resistant to solvents and oils, as well as having outstanding characteristics [52]. Polyvinyl alcohol is semi-crystalline and has a good visible light transmission. PVA polymeric compounds are well-known for their importance in a variety of technical applications [53]. It's made commercially by hydrolyzing polymers (vinyl acetate). Many researchers have investigated PVA for usage as fillers or crosslinking products, and it has also been widely used as a thermoplastic

polymer in living, non-toxic, and innocuous tissues, among other things [54].Furthermore, it is very easy to produce the film, making it a good choice for mixing natural and synthetic polymers [55,39]. PVA is most commonly used for paper packaging as well as in textile sizing due to its biodegradable receptor [56]. PVA is used in many applications because it is an incompatibility structure with capacity and aqueous properties that help improve the mechanical properties of membranes [57,58]. In addition, nanoparticles can be physically entangled or chemically bound to PVA [45]. They are widely used in papermaking, textiles, and manufacture of oxygen-retardant films, and the coating of photographic film [52]. and the coating of photographic films [45]. and there are some physical and chemical properties as shown in Table (2-3).

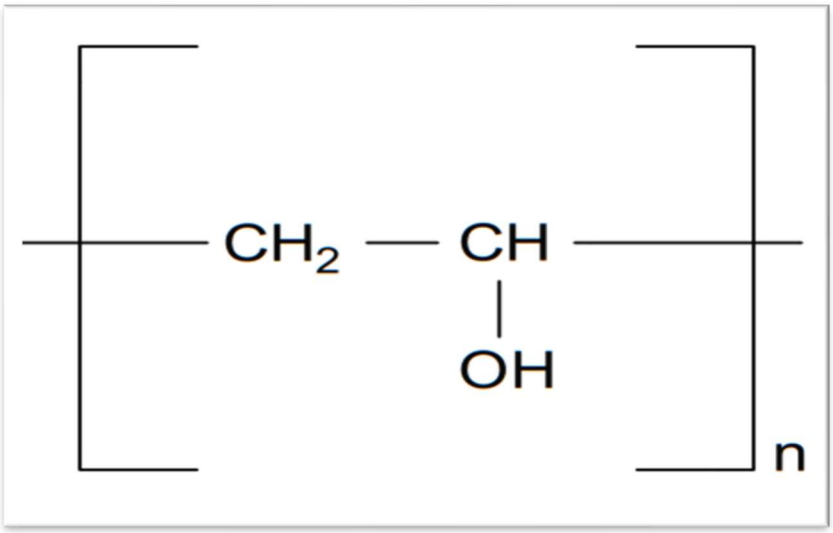

Figure (2-5). The chemical structure of Polyvinyl alcohol(PVA)[51]**.**

Table (2-3). Physical and chemical properties of Polyvinyl alcohol(PVA)[51]**.**

Property	Description
Appearance	White to ivory white granular powder
Molecular formula	$(C_2H_4O)_n$
Density	(1.19 - 1.31) $g.cm^{-3}$
Solution PH	5- 6.5
Refractive index	1.55
Glass transition temperature (T_g)	75-85 °C
Melting temperature (T_m)	180 – 190 °C

2.5.4 Silicon dioxide (SiO_2)

Silicon dioxide (SiO_2) is widely distributed in the environment, and is present in the form of sand on all beaches and deserts. It is the starting material for the production of silicate glasses and ceramics [59]. It may occur in crystalline or amorphous form, and is found naturally in impure forms, such as sandstone, silica sand or quartz. It is specific gravity and melting point depend on the crystalline structure [60].

Silicon dioxide is not only one of the most abundant materials on earth as mentioned, but also a critical material component of considerable technological importance [61]. Today's, modern electronics greatly depends on silicon dioxide for the manufacture of semiconductors and microelectronic devices, besides crystalline Silicon – properties and uses it is the basic material of which the most of common communication optical fibers that are presently made [62]. It is high

melting temperature (≈1700 °C) and it is chemical stability make it an excellent thermal and electrical insulator and hence the principal dielectric in silicon electronic technology [63].

the reduction of the silicon dioxide diameter to nanometric size produces the formation of minibands with consequent enlargement of the effective band gap [64]. The nanoparticles are formed by depositing a silicon rich material, and then inducing the precipitation of the excess silicon by thermal treatments[65]. The control of the phenomenon is strictly subordinated to the control of the nanoparticle size, which is normally achieved using the multilayer approach [66]. formula is (SiO_2), as shown in Figure (2-6). and there are some physical and chemical properties as shown in Table (2-4).

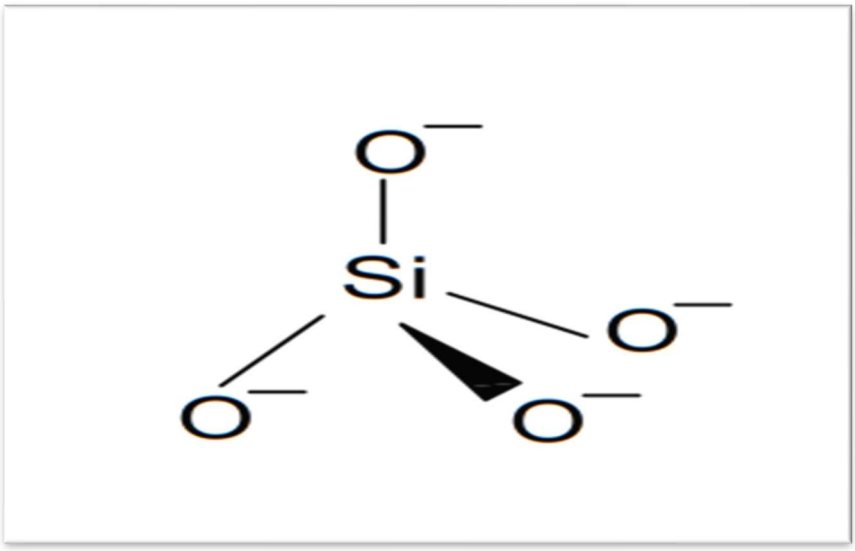

Figure (2-6). The chemical structure of Silicon dioxide (SiO_2)[59]**.**

Table (2-4). Physical and chemical properties of Silicon dioxide[59]**.**

Property	Description
Appearance	White powder
Molecular formula	SiO_2
Grain size	20-30 nm
Solubility	widespread
Toxicity	non-toxic

2.6 Silicon dioxide Nano practical -Based Polymer Nanocomposites

Silica is identical in chemical composition, but with different atomic arrangements. All forms of silica are odorless solids composed of silicon and oxygen atoms. Silica particles become suspended in the air and form non-explosive dust [67]. The development of minibands and subsequent widening of the effective band gap result from the reduction of silicon dioxide diameter to nanometric scale. A silicon-rich substance is deposited to create the nanoparticles. sophisticated practical materials that are widely included in rubbers, plastics, and polymers [6].

2.7 Characterizations

2.7.1 Fourier Transforms Infrared Spectroscopy (FTIR)

More complex molecules have more than one bond and different types of vibrations may occur. Vibrations fall into the two main categories of stretching and bending.

1. Stretching vibrations

In this type of vibrations, the bond length is increased or decreased at regular intervals. There are two types of stretching vibrations. Symmetrical stretching and asymmetrical vibration, as shown in Figure (2-7) [68].

a) Symmetrical stretching: in this type of stretching, bond length increases or decrease symmetrically.

b) Asymmetrical stretching: in this type of stretching, the length of one bond increases and the other one decreases.

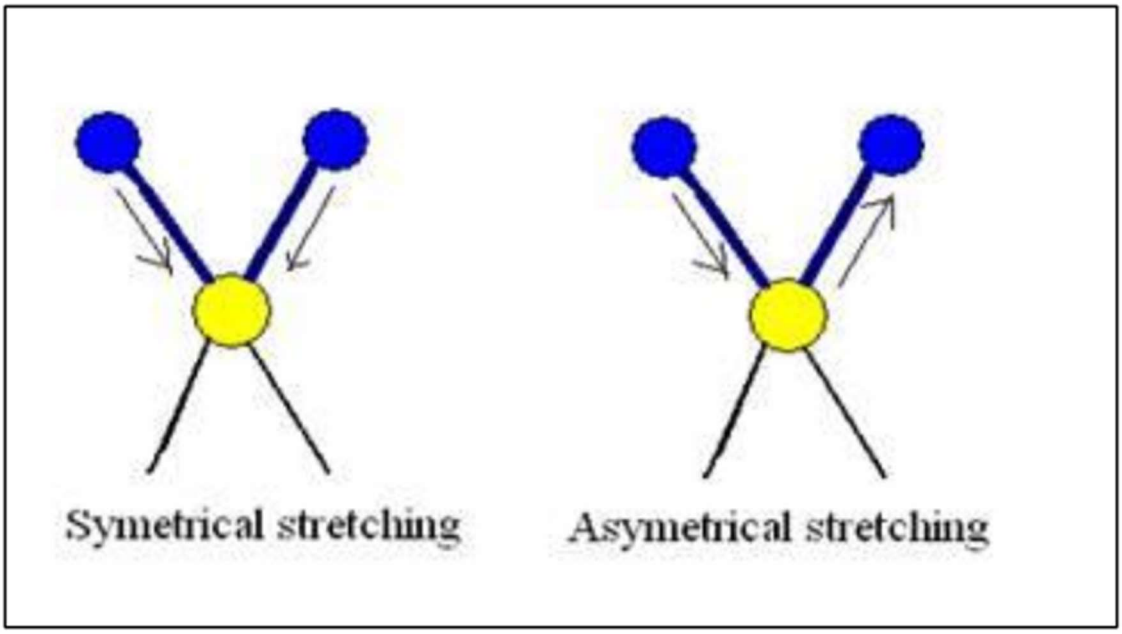

Figure (2-7). Types of stretching vibrations [68].

2. Bending Vibrations

In this type of vibrations, a change in bond angle occurs between bonds with a common atom, or there is a movement of a group of atoms with respect to the remainder of the molecule without movement of the atoms in the group with respect to one another. The bending vibrations are also called as deformation vibrations. Deformation vibrations are two types, as illustrated in Figure (2-8) [69].

a) In-Plane Bending Vibrations

In this type of vibrations, there is a change in bond angle and takes place within the same plane. In-plane bending, there are two types:

I. Scissoring: in which bond angle decreases.

II. Rocking: in which the bond angle is maintained but both bonds move within the same plane [69].

Out of Plane Bending Vibrations

This type of bending takes a plane outside of the plan of the molecule.

I. Wagging: in which both atoms move to one side of the plane.
II. Twisting: in which one atom is above the plane and the other is below the plane [69].

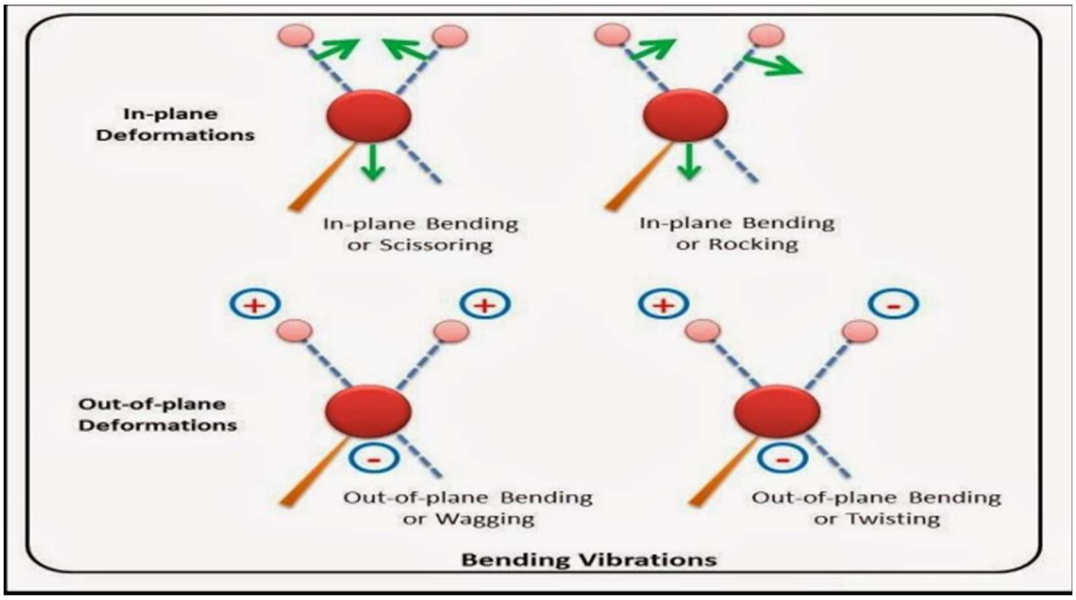

Figure (2-8). Types of bending vibrations [69].

FTIR spectroscopy is a powerful tool for identifying types of chemical bonds in a molecule applying to produce an infrared absorption spectrum as a molecular "fingerprint" the principle of this technique is that molecular bonds vibrate at various frequencies. Molecular bonds vibrate at various frequencies depending on the elements and the type of bonds. Since FTIR provides information about the chemical bonding or molecular structure of materials without causing destruction, it could be used to identify unknown materials, detect the organic and some inorganic additives at the level of a few percent, also characterize the chemical structure change and solvent residue [68].

2.7.2 X-Ray diffraction (XRD)

Apply to XRD investigate the crystallization process, unit cell lattice parameter detail, crystal structure, crystal orientation, and crystallite size, which is a fast and effective approach. The constructive interference of a monochromatic beam of X-rays is used to produce the XRD peaks after scattered of each set of lattice planes in the sample at specific angles, where the distribution

of the atoms determines the peak intensities within lattice. Therefore, the periodic atomic fingerprint of materials is represented by XRD pattern [70].

The sample holder, X-ray tube, and X-ray detector are the three basic components of an X-ray diffractometer. The cathode ray tube is responsible for creating X-rays by burning the filament to create electrons, which are subsequently driven toward a target by a voltage and attack the target substance. When electrons with sufficient energy displace inner shell electrons of the target material, X-ray spectra are produced [71]. When X-ray light of wavelength (λ) is projected at an angle (θ) onto a crystal lattice, the incoming X-rays interact constructively with the sample if the circumstances meet Bragg's law, as shown in Figure (2-9) [72].

$$2d \sin\theta = n\lambda \qquad (2.1)$$

Where:

θ: is Bragg diffraction angle (degree) and λ: is wavelength forncident X-ray beam (Å). d: is distance, n : is Diffraction rating

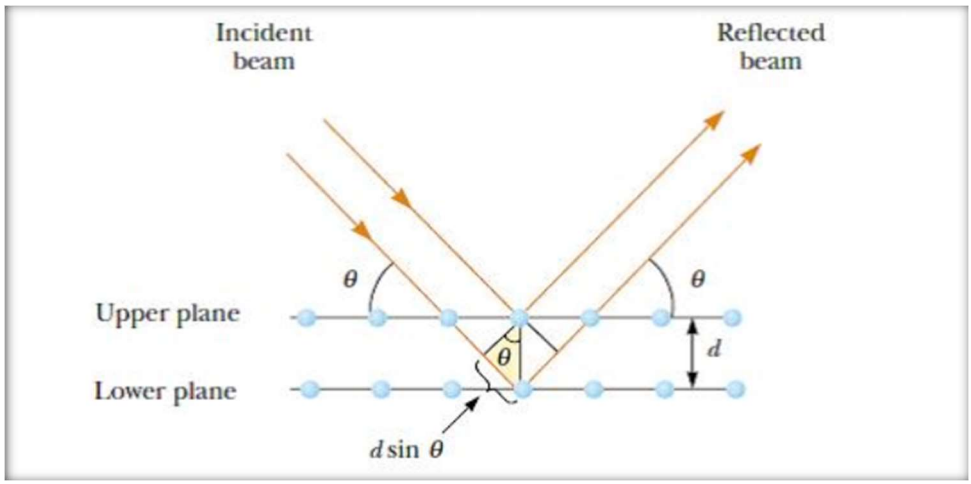

Figure (2-9). Bragg's Diffraction [72].

The structural factors of any material are determined by X-ray diffraction, which is crucial in explaining many of the material's physical properties. In the case of the cubic structure, which represents the dominant pattern of the structure (SiO_2), (a) represent the lattice constants, and thus it is calculated using the equation (2.2) [70].

$$a = \mathrm{d}\sqrt{h^2 + k^2 + l^2} \qquad (2.2)$$

where (h, k, l) represents Miller's coefficients.

The lattice constant can be extracted from the following equation [73].

$$\frac{1}{\mathrm{d}_{\mathrm{hkl}}^2} = \frac{h^2}{a^2} + \frac{k^2}{b^2} + \frac{l^2}{c^2} \qquad (2.3)$$

The size of the crystal (D nm) was calculated using the Schrrer formula (2.4) [74].

$$\mathrm{D} = \mathrm{k}\lambda/\beta\cos(\theta) \qquad (2.4)$$

D: means The size of the Crystal, β: the complete breadth at half the highest point (FWHM)and (k = 0.9), The lattice strain (ε) can be calculated using Equation (2.5) [74].

$$\varepsilon = \beta/4\tan(\theta) \qquad (2.5)$$

2.7.3 Field Emission Scanning Electron Microscope (FE-SEM)

Field emission scanning electron microscope (FE-SEM) is a type of electron microscope that uses electron beem to produce images. Light is replaced by electrons in an iron microscope (negatively charged particles). An emission source of electrons is used. In a zigzag pattern, electrons scan the element [75].

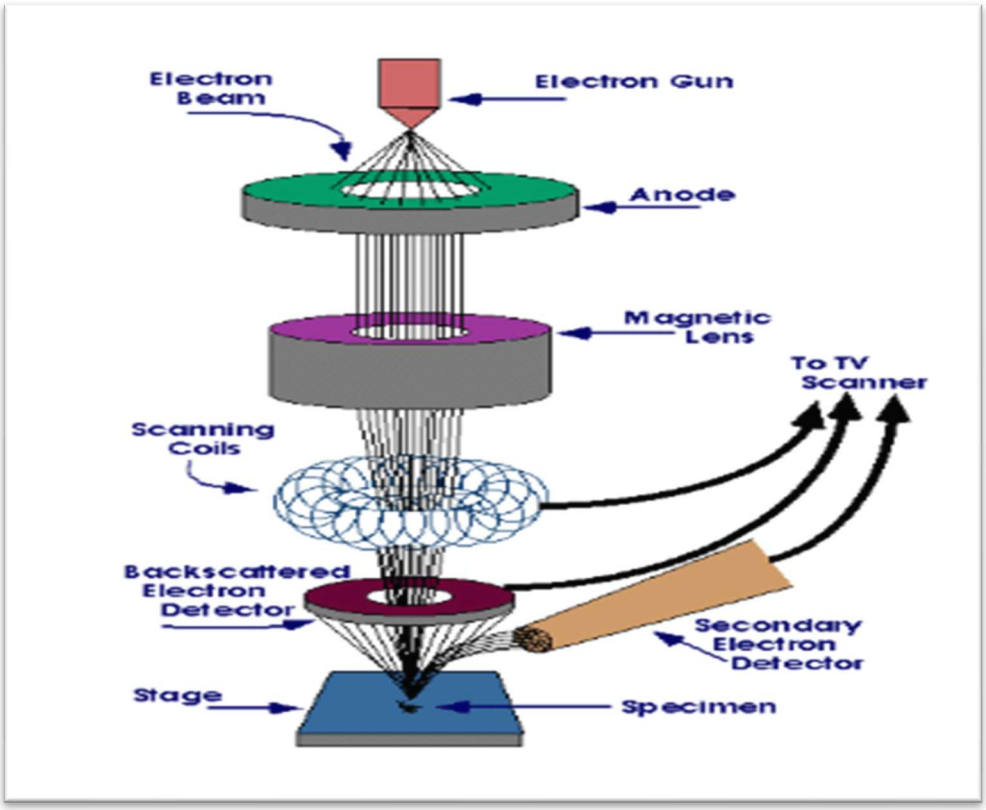

Figure (2-10). Ray Diagram for a system of FE- SEM [75].

2.8 Properties

2.8.1 The Optical Properties

The optical properties of materials composites are being investigated in order to better understand the kind of internal structure of polymer and the nature of bonds; as well as to expand the spectro of polymer applications. Knowing a polymer composite's absorption and transmittance spectrums can help detect a variety of optical qualities over a wide range of wavelengths. determine the type of bonds, orbits, and energy beams by examining them in the ultraviolet spectrum. The visible spectrum research gives enough knowledge about a matter's behavior for solar applications. The infrared spectrum is crucial for understanding the overall structure of polymer composites and the constituents that make up their chemical composition [76].

2.8.1.1 Absorbance (A)

In order to get good absorption, the optical depth should be high for energies above the band gap, and reflectivity should be small. Absorbance is defined as the ratio of absorbed light intensity (I_A) to incident light intensity (I_o) depending on the kind of material [77].

$$A = log \frac{1}{T} \quad (2.6)$$

2.8.1.2 Transmittance (T)

The formula for calculating transmittance (T) to split the intensity of rays transmitting from the film (I_T) by the intensity of incoming rays on it (I_o) [78] .

$$T = \frac{I_T}{I_o} \quad (2.7)$$

2.8.1.3 Absorption coefficient (α)

The absorption coefficient is the decrease in energy in the flow of incident ray in the direction of wave propagation in relation to the distance unit. (α) depends on the photon energy (*hv*), material characteristics, and forbidden band gap. Photon energy is taken from the following Equation (2.8) [79].

$$E = hv \quad (2.8)$$

The frequency is (ν), while the Planck constant is (h).

The photon will be transmitted if the incident photon energy is smaller than the forbidden band gap, and transmittance is given by Equation (2.9) [80].

$$T = (1 - R)^2 . e^{-\alpha t} \quad (2.9)$$

Where, T is transmittance, R, is the reflectance, α means the absorption coefficient. The intensity of incident photons is expected to be (dI) in direct proportion to both intensity (I) and thickness dt, as shown by Equation (2.10) [81].

$$dI = -\alpha I dt \quad (2.10)$$

If the incidence ray's intensity (I_o) is incident on a material with thickness (t) and transmittance ray's intensity (I_T)

$$\int_{Io}^{I_T} \frac{dI}{I} = \int_{\circ}^{t} -\alpha dt \quad (2.11)$$

$$\ln I_T \_ \ln I_o = -\alpha t \quad (2.12)$$

$$\frac{I_T}{I_o} = e^{-\alpha t} \quad (2.13)$$

$$T = e^{-\alpha t} \quad (2.14)$$

$$\frac{1}{T} = e^{\alpha t} \quad (2.15)$$

$$2.303 \log \left(\frac{1}{T}\right) = \alpha t \quad (2.16)$$

$$A = \log \left(\frac{1}{T}\right) \quad (2.17)$$

$$2.303.A = \alpha t \quad (2.18)$$

$$\alpha = \frac{2.303 \, . \, A}{t} \quad (2.19)$$

2.8.1.4 The fundamental absorption edge

The basic absorption edge is a sudden increase in absorbance that occurs when the amount of absorbed energy radiation is about equal to the band energy gap; the basic absorption edge shows the energy differential between the up point of the valance band and the bottom point of the conduction band. Figure (2-11) shows three types of absorption zones [80].

A. High absorption region

Magnitude (α) in the part A is greater than or equal to 10^4 cm^{-1}. The Magnitude of the prohibited optical band gap (E_g^{opt}) can be introduced from this area [80].

B. Exponential region

The value of (α) in component B is in the range 1 cm^{-1} < α < 10^4 cm^{-1}. It refers to the transition from extended levels at the top of the valence band to localized levels in the conductive band and vice versa, from local levels in (V.B.) to extended levels at the bottom of the conductive band and vice versa (C. B) [80].

C. Low absorption region

Value of (α) in component C is relatively tiny. it's around α < 1 cm^{-1}. The transition happens in this area as a result of structural faults causing state density inside space motion [80].

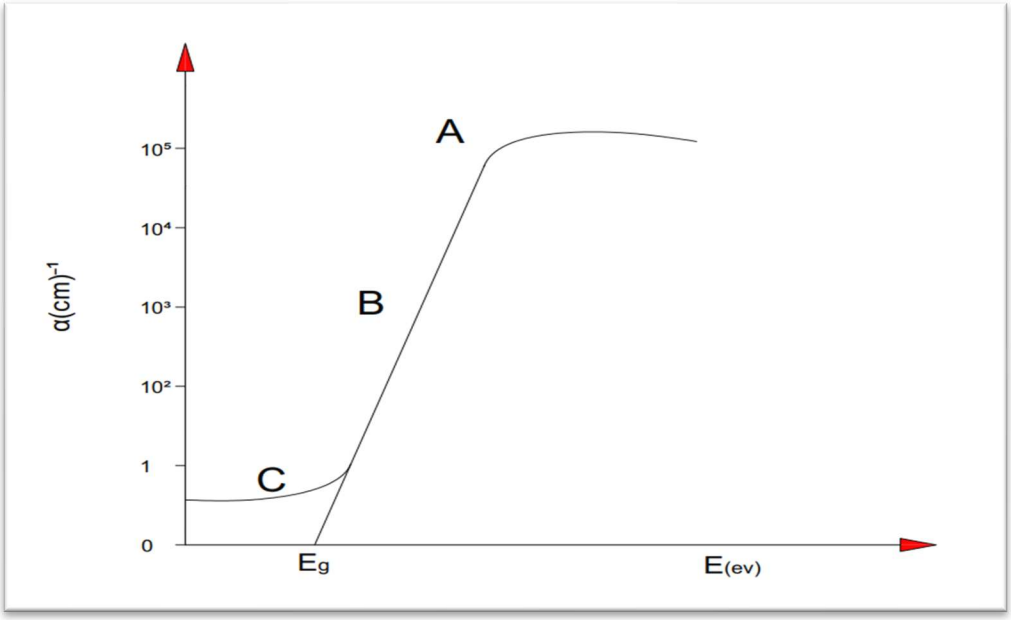

Figure (2-11) Absorption edge variation with absorption regions [80].

2.8.1.5 The Electronic transitions

Electronic transitions are divided into two categories.

2.8.1.5.1 Direct transition

In semiconductors, this transformation occurs where the bottom of (C.B.) is precisely above the top of (V.B.), indicating that they have the same wave vector K i.e., ΔK= 0. The absorption appeared in this state when $h\upsilon \geq$ Eg. This transition type required of the Law's conservation in energy and momentum, and has two types [82].

A. Allowed Direct transition.

This transition happens between the top points in the (V.B.) to the bottom point in the (C.B.), as shown in Figure (2-12. a) [83].

B. Direct forbidden transition.

This transition happens between near top points of (V.B.) and bottom points of (C.B.), as shown in Figure. (2-12. b) [83].

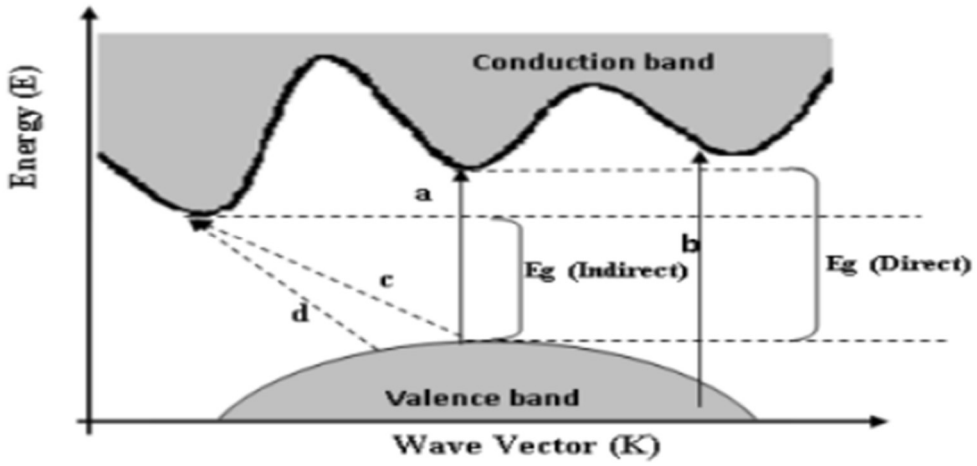

Figure (2-12) The Electronic Transitions Types of (A) Allowed Direct Transition (B) Forbidden Direct Transition (C) Allowed Indirect Transition and (D Forbidden Indirect Transition [83]**.**

2.8.1.5.2 The indirect transitions

Conduction band (C.B) does not have a bottom that is higher than the top of valence band (V.B) in an indirect band gap, in other words, the maximum of the V.B is found at different k-vectors than the minimum of the C.B. In this case, ($\Delta K \neq 0$), and this transition type must include the absorption or emission of a phonon, for the energy and momentum conservation laws Indirect transitions are divided into two categories [84].

C. Allowed indirect transitions

As illustrated in Figure (2-12. c), these transitions occur between the highest point of the efficiency band and the lowest point of the conduction band in a distinct area of K–space.

D. Forbidden indirect transitions

As illustrated in Figure (2-12. d), these transitions happen between the near points at the top of the valence band and the near points at the bottom of the conduction band, these transitions happened. To travel in the direction of phonon absorption, the absorption coefficient is given by Equation(2.20) [83].

$$\alpha h\nu = B\,(h\nu - E_g^{opt} \pm E_{ph})^r \qquad (2.20)$$

Where (B) is constant depending on the type of material, (E_{ph}) denotes phonon energy, (-) denotes phonon absorption, (+) denotes phonon emission, (r) denotes the exponential m transition, and (r) = 2 denotes permitted indirect transition while(r) = 3 indicates a forbidden indirect transfer.

2.8.1.6 Refractive index (n)

Dividing the speed of light in vacuum by the speed in light inside the material, the refractive index is computed. The following formulae are used to calculate the film's refractive index (n) [85].

$$n = \frac{1+\sqrt{R}}{1-\sqrt{R}} \qquad (2.21)$$

The reflectance (R) of the material.

2.8.1.7 Extinction coefficient (k_o)

As seen in the Equation (2.22) [86], the extinction coefficient is defined as the imaginary component of the complex refractive index(N).

$$N = n - iK_\circ \qquad (2.22)$$

where (n) is the real part of the refractive index. The extinction coefficient can be calculated using the following Equation (2.23) [86].

$$K_\circ = {}^{\alpha\lambda}/_{4\pi} \quad (2.23)$$

where (λ) is the incident ray's wavelength.

2.8.1.8 Dielectric Constant (ε)

The dielectric constant demonstrates matter's capacity to polarize; it may respond to numerous frequencies in a very difficult way, and electronic polarity dominates other forms of polarization. The real and imaginary dielectric constants may be computed using Equation (2.24) [87].

$$\varepsilon = \varepsilon_r - i\varepsilon_i \quad (2.24)$$

Where (ε_r and ε_i) are the dielectric constant's real and imaginary components. (n) and ($K_\circ$) numbers are proportional to the real and imaginary components of the dielectric constant [87].

$$\varepsilon = N^2 \quad (2.25)$$

$$(n - i\,K_\circ)^2 = \varepsilon_r - i\varepsilon_i \quad (2.26)$$

From equation (2.25), the dielectric constant's real and imaginary can be written as following [88].

$$\varepsilon_r = (n^2 - K_\circ{}^2) \quad (2.27)$$

$$\varepsilon_i = (2nK_\circ) \quad (2.28)$$

2.8.1.9 Optical Conductivity (σ_{op})

The optical conductivity (σ_{op}) depends directly on the refractive index (n), absorption coefficient (α) and (c) is the velocity light in vacuum following relate (2.29) [82] .

$$\sigma_{op} = {}^{\alpha nc}/_{4\pi} \quad (2.29)$$

2.8.2 Electrical Properties

The electrical properties of the material depend on the chemical composition, the arrangement of atoms in the solid and the presence of defects in the energy gap. In several ways, such as the annealing, this defect can be reduced. The electrical properties are also highly dependent on the preparation technique and the deposition conditions [89].

Matter can be classified according to its electrical conductivity into insulators, semiconductors and conductors. Conductivities for some polymers are (~ 10-17 $\Omega^{-1}cm^{-1}$) for polyethylene, (10-16 Ω^{-1} cm-^{1}) for polystyrene and (10-12 Ω^{-1} cm^{-1}) for polyamides. The electrical properties are designed to understand the number, origins, and actions of a charge. This includes the exact composition of the substance, the chemical composition, and the shape of the substance [90].

2.8.2.1 Alternating Current electrical conductivity

A.C conductivity differs from D.C conductivity in that the electric field frequency during D.C conductivity is constant, but the electric field frequency during A.C conductivity is variable. When an insulator is placed in a low frequency electric field, the newly created or permanent dipoles can follow the change of the applied electric field without leaving any residue, so the value of the dielectric constant becomes equal (ohmic conductivity is equal to zero).

At the other side, in more calculations, the frequency of the electric field is determined by the frequency of electric polarization; complex dielectric constants would be available [91]. The dielectric constant is the ratio of a capacitor's capacitance with an insulator material between its conducting plates to a capacitor's capacitance with a vacuum between the plates of the same size. When an alternating potential $V = V_m e^{iwt}$, is applied across a capacitor c filled with

an insulator, the current passing through the capacitor precedes the potential by a phase of π/2, as shown (2-13 A) [92].

$$I = i\omega C_P V \qquad (2.30)$$

where (**ω**) is the applied field's angular frequency (w = 2πf),(i) is an imaginary integer (i =$\sqrt{-1}$),(C_P) Capacity, (V) is the voltage and V_m is the voltage maximum [93].

$$I = I_P + iI_q \qquad (2.31)$$

This demonstrates that the electrical current is equal to the current's amount (I_p) in the same phase with (V) and (I_q) with a phase difference (π /2) that is. (I_P) is the capacitate current is short for capacitive charging current or better charging current of a capacitor and(I_q) is the conduction current in conductors due to flow of electron under applied electric potential.

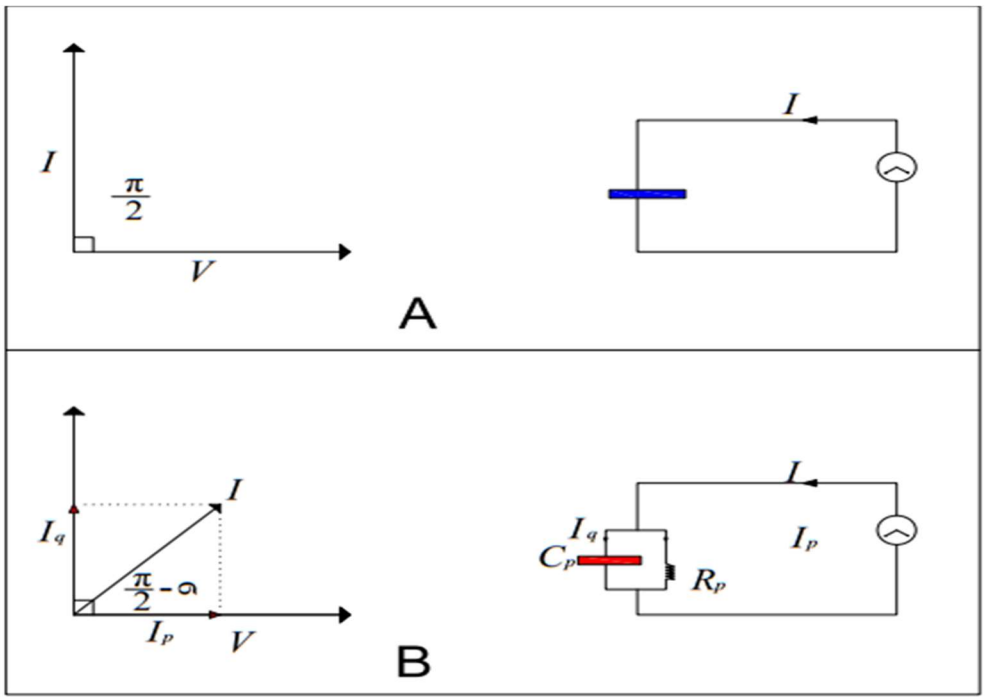

Figure (2-13) (A). The analogous circuit to a perfect capacitor, and(B). The analogous circuit to a non-ideal capacitor [91].

The Equation (2.33) defines the capacitance of a condenser made up of two parallel plates [94].

$$C_P = \varepsilon_{\circ}\frac{A_a}{\mathrm{d}} \qquad (2.32)$$

$(\varepsilon_{\circ})$ Vacuum permittivity,

(A_a) Area, (d)The distance between my widened plates Substituting Equation (2.30) in equation (2.28), you get.

$$\mathrm{I} = \mathrm{i}w\varepsilon\ \varepsilon_{\circ} V\, {A_a}/{d} \qquad (2.33)$$

The allowability (ε) has to be a complicated number. The electric current is a complicated variable because it has both real and imaginary components, as indicated in Equation (2.31) [95]

$$\varepsilon = \acute{\varepsilon} - \mathrm{i}\acute{\varepsilon} \qquad (2.34)$$

when ε ′′ is dielectric loss, acquire the following.

$$\mathrm{I} = \mathrm{i}\omega\varepsilon_{\circ}\frac{A_a}{\mathrm{d}}\ (\acute{\varepsilon} - \acute{\varepsilon})\mathrm{V} \qquad (2.35)$$

When we substitute the Equation (2.31) we get.

$$\mathrm{I_P} = \omega\acute{\varepsilon}\ \varepsilon_{\circ}\frac{A_a}{\mathrm{d}}\mathrm{V} \qquad (2.36)$$

$$\mathrm{I_q} = \omega\acute{\varepsilon}\varepsilon_{\circ}\ \frac{A_a}{\mathrm{d}}\ \mathrm{V} \qquad (2.37)$$

Figure (2.13 B) shows that the loss tan factor (tan δ) is given Equation (2.38) [89].

$$\tan\delta = \frac{I_P}{I_q} = \frac{\acute{\varepsilon}}{\acute{\varepsilon}} \qquad (2.38)$$

The electrical energy is lost in the insulator converted into thermal energy. In electrical applications, the significance of knowing the power factor is quite beneficial. In the high frequency insulator, excessive power factor will cause heat, resulting in a power outage [96].

The capacitor (C) can be represented by an ideal capacitor connected in parallel with a resistance Rp at low frequencies [90].

$$I = I_P + iI_q = \frac{V}{R_P} + i\omega C_P V \quad (2.39)$$

Obtain the impedance as a result of this [90].

$$1/Z = 1/R_P + i\omega C_p \quad (2.40)$$

(Z) Total Prohibition, Equations (2.35) and (2.36), can be written as follows [90].

$$R_P = d/\omega \ddot{\varepsilon}\varepsilon_\circ A_a \quad (2.41)$$

$$\ddot{\varepsilon} = \frac{1}{\omega R_P C_\circ} \quad (2.42)$$

$$C_P = \frac{\grave{\varepsilon}\varepsilon_\circ A_a}{d} \quad (2.43)$$

$$\grave{\varepsilon} = \frac{C_p}{C_\circ} \quad (2.44)$$

Dissipated strength in the insulator is expressed by the presence of an alternative conductivity ($\sigma_{a.c}$) [96].

$$\sigma_{a.c} = \omega \ddot{\varepsilon}\varepsilon_\circ \quad (2.45)$$

Alternative conductivity ($\sigma_{a.c}$) is a measure of the lost capacity, that is, a measure of the heat. It may be generated as a result of the rotation of the dipoles in their positions or the vibration of the charges by changing the direction of the

alternating field. Therefore, frequency is the basis on which alternating electrical conductivity depends [97].

2.9 Applications

2.9.1 Bacterial Isolates Utilized

2.9.1.1 Escherichia coli (E. coli)

E. coli is one of the most common gram-negative bacteria on the planet. E. coli is a facultative anaerobic bacterium, which means that it can live both with and without oxygen. Lactose fermentation is characterized by a non-spore forming, motile, rod-shaped bacterium [98]. E. coli is one of the most prevalent bacteria found in the human intestine, and it grows best in 37 °C [86]. At 37 °C, a pH of 6.0-7.0 is excellent for growing bacteria in a culture, with a minimum pH of 4.4 and a maximum pH of 9.0 required for growth [99].

2.9.1.2 Staphylococcus aureus (S. Aureus)

The term was changed to Staphylococcus aureus by Friedrich Julius Rosenbach, who was attributed under the official naming process at the time [100]. The gram-positive, round-shaped bacteria S. aureus (golden staph is another name for it) Gram –positive nonmotile, noncore-forming cocci with a diameter of 0.5 – 1.0 μm that appear alone, in pairs, and in clusters. It is a facultative anaerobe that can grow without oxygen and is typically positive for catalase and nitrate reduction. It may be found in the nose, respiratory system, and on the skin and is a normal part of the body's flora [101].

S. aureus causes a number of skins problems, including abscesses, respiratory infections, and food poisoning. Virulence factors such as powerful protein toxins and the synthesis of a cell-surface protein that binds and inactivates

antibodies are frequently produced by pathogenic strains to aid infections [102]. Pneumonia, meningitis, osteomyelitis, endocarditis, toxic shock syndrome, bacteremia, and sepsis are all symptoms of S. aureus, as are pimples, impetigo, boils, cellulitis, folliculitis, carbuncles, scalded skin syndrome, and abscesses, as well as pneumonia, meningitis, osteomyelitis, endocarditis, toxic shock syndrome. It's still one of the top five causes of hospital –acquired infections, and it is a leading cause of wound infections following surgery [103]. S. aureus causes a number of skin problems, including abscesses, respiratory infections, and food poisoning. Virulence factors such as powerful protein toxins and the synthesis of a cell-surface protein that binds and inactivates antibodies are frequently produced by pathogenic strains to aid infections [104].

2.9.1.3 Antibacterial Mechanisms of Nanoparticles

Nanoparticles should communicate with bacterial cells for performance antimicrobial effect. Electrostatic attraction [105], van der -Waals forces [106], receptor ligand interactions [107], finally hydrophobic interactions [108]. Nanoparticles enter the bacterial membrane and aggregate throughout the metabolic route, altering the cell membrane's shape and function. The NPs then interact with DNA, lysosomes, ribosomes, and enzymes in the bacterial cell, causing oxidative stress, heterogeneous modifications, changes in cell membrane permeability, electrolyte balance issues, enzyme inhibition, protein deactivation, and gene expression changes as shown in Figure (2-14) [109]. The most important mechanism of nanoparticles toxicity to bacteria is damage to cell membrane, besides cell membrane damage, generation of reactive oxygen species, disturbance in metal/metal ion homeostasis, protein and enzyme dysfunction and Geno-toxicity [109].

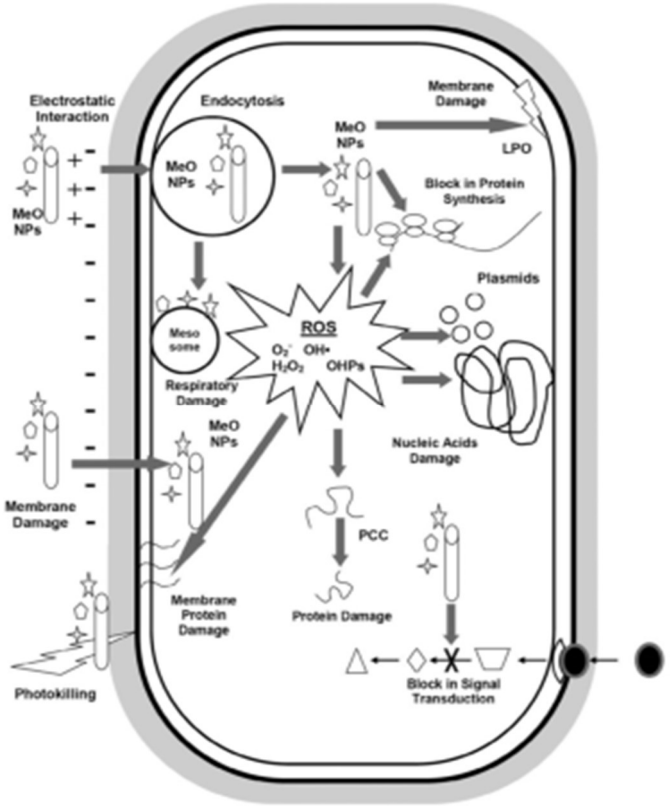

Figure (2-14) Overview of Antimicrobial Mechanisms by Metal Oxide Nanoparticles. ROS: Reactive Oxygen Species, LPO: Lipid Peroxidation [109]**.**

2.9.2 Radiation shielding

Ionizing radiation is composed of either particles or photons that have enough energy to ionize an atom or a molecule by completely removing an electron from its orbit, thus creating more positively charged atom. The ionization of matter can be divided into two processes, that is, indirect and direct ionization [110]. Electromagnetic radiations, such as x-ray and γ-rays, are termed indirect ionizing radiation because part or all the photon energy is transferred to the electrons in the cell's molecules, which, then, upon release produce the bulk of ionizations. Whereas, charged particles, such as high-energy electrons, protons, α-particles (a helium atom nucleus moving at a very high speed), α-particles (a high-speed electron or positron), and fast heavy ions, are termed direct ionizing radiation

because while they traverse the cell, they ionize numerous molecules by direct collisions with their electrons [111]. There are some basic principles for radiation shielding depending on distance and time. The type and amount of shielding required depend on the type of radiation, the activity of the radiation source and the dose rate. However, there are other factors for the choice of shielding material such as their cost and weight. An effective shield will result in a large energy loss in a small penetration distance without emission of radiation [112]. A number of experimental and theoretical works have been performed on radiation shielding which has large different application areas with different materials (e.g., concrete, semi- conductor, polymer, etc.) [107,108].

2.9.2.2 Gamma ray shielding

A study of absorption of gamma and neutron radiations in shielding materials is an important subject in the field of radiation physics. For instance, most of the previous studies have been concerned with photon attenuation coefficients [104,105].

There are two main methods for radiation shielding materials. First, shielding materials are furnished on the wall surface or directly in it (e.g., concrete). Second, these materials are covered around the radiation source. Any material can be used for radiation shielding, if it has a sufficient thickness to absorb the incident radiations to a safe level. In the field of shielding materials and the design of some research works have reported different types of glasses as new shielding materials [117]. The absorption coefficient in the lead of the gamma radiation from a given source [118].The attenuation coefficient μ is approximately proportional to the material density and only weakly dependent on the chemical composition of the material and its aggregation state (i.e., solid,

liquid, or gas). That is why the so-called mass attenuation coefficient, where (μ_m) is frequently used instead of (μ). The mass attenuation coefficient is obtained by dividing (μ) by the material density (ρ) [119].

$$\mu_m = \frac{\mu}{\rho} \qquad (2.46)$$

The value of (μ_m) is approximately constant for all materials. The absorption law for gamma particles can be written in the appropriate depending on the equation order [119].

$$N = N_o\, e^{-\mu x} \qquad (2.47)$$

where (N) is the number of photons passing through the thickness (x) of the absorber [118]. For radiation protection design, a commonly specified entity is the half-value thickness, which characterizes suitable materials for any particular type of radiation and the energy involved. As the name indicates, this number directly gives the thickness required to reduce the intensity of the incoming radiation by half. For calculations, the more fundamental attenuation coefficient) μ) is preferred, which of course, is related to the half value thickness Equation (2.46) [112].

$$x^{1/2} = \frac{\ln 2}{\mu} \qquad (2.48)$$

for the $x^{1/2}$,(μ) depends on the material of the absorber and the energy of the radiation [120].

Chapter Three

Experimental Part

3.1 Introduction:

The used materials, preparation process, devices, and measurement techniques were introduced in this chapter.

3.2 The Utilized Materials

3.2.1 Polyacryl amide (PAAm)

Poly acrylamide (PAAm) with molecular weight of (71.07) g. mol^{-1}color (white), appearance (crystal granular), molecular formula $(C_3H_5NO)_{n.}$ was supplied by Ntchito zomasulira sizikupezeka,

China.

3.2.2 Polyvinyl Pyrrolidone (PVP)

Poly Vinyl Pyrrolidone (PVP) is a white powder hygroscopic, molecular weight = (40.000) g. mol^{-1} molecular formula is $(C_6H_9NO)_n$. that was supplied by Alpha chemika company,

India.

3.2.3 Polyvinyl alcohol (PVA)

Poly vinyl alcohol (PVA) with molecular weight (160000 g. mol^{-1}), with Cas NO. (9002-89-5), molecular formula is $(C_2H_4O)_{n.}$ was supplied by Dindori, Nashik, India.

3.2.4 Silicon dioxide (SiO_2)

Silicon dioxide **(**SiO_2) nanoparticle (20-30) nm white color, purity of (99.8%) melting point of (1610-1728 C°), and boiling point range 2230 C°, was supplied from Hongwu inter National group ltd, China.

3.3 preparation of the nanocomposites

Polymers were dissolved, independently, and SiO_2 nanomaterials were distributed in distilled water (DW). The polymer mixture was fabricated using different proportions of polymers (0.45:0.10:0.45) for PAAm: PVA: PVP. Firstly, 0.10 wt.% of PVA/DW was added after dissolving in distilled water to 0. 45 wt.% of PAAm/DW and combining the mixture for two hours. where, PVA was added in this stage to increase the interaction between the polymers. It is considered a factor that strengthens the link between the polymers. Secondly, PVP/DW with 0.45 wt.% concentration was added to the PAAm-PVA matrix and blended for two hours to fabricate PAAm-PVA-PVP using the magnetic stirrer to achieve BP1. Thirdly, the nanocomposites were prepared following the same procedure by adding their different ratios of SiO_2 (0.01, 0.03, and 0.05) wt. %. Finally, the samples matrix was placed in a Petri dish (5 cm) and dried in the vacuum oven at 40 ^oC for 72 hours until fully dried. Samples were saved in the desecrator till characterizations were done. The samples were coded simply according to the nanomaterial's ratios, as shown in Table (3-1), and the procedure is presented in Figure (3-1).

Table (3-1) displays cods mixing weight percentages of samples.

Sample ID	Concentration wt. %			
	PAAm	PVA	PVP	SiO_2
BP1	0.45	0.10	0.45	0.00
NC2	0.45	0.09	0.45	0.01
NC3	0.20	0.07	0.70	0.03
NC4	0.70	0.05	0.20	0.05

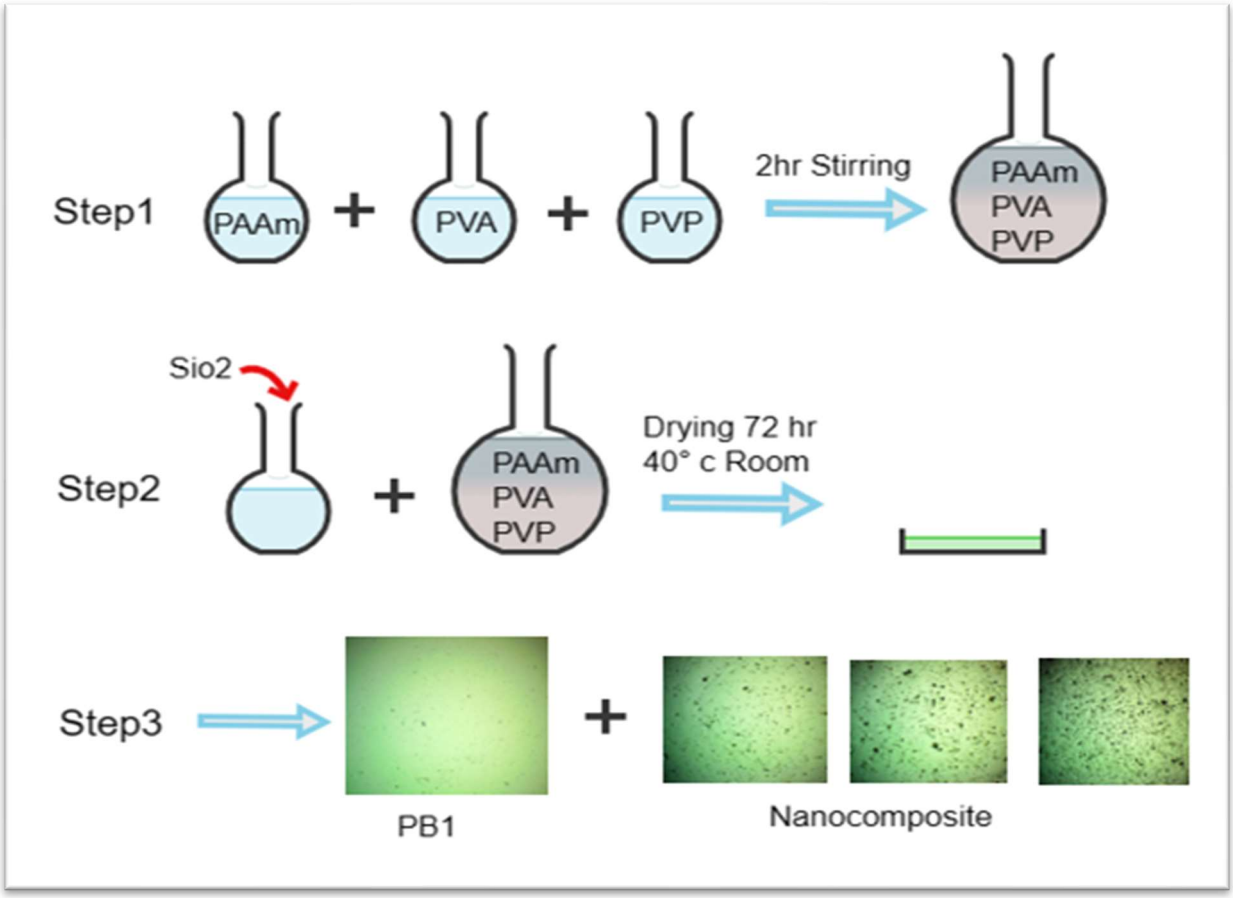

Figure (3-1). Scheme of the experimental work procedures of fabricated sample films.

3.4 Characterizations

3.4.1 FTIR Spectral

FTIR spectra were recorded by FTIR (Bruker Company, German origin, type vertex 70). FTIR was implemented at the University of Babylon /College of Education for Pure Sciences/Department of Physics. In this study, the considered wavenumber range is (400-4000) cm^{-1}, Figure (3-2), shows the diagram explain the machine of work of FTIR.

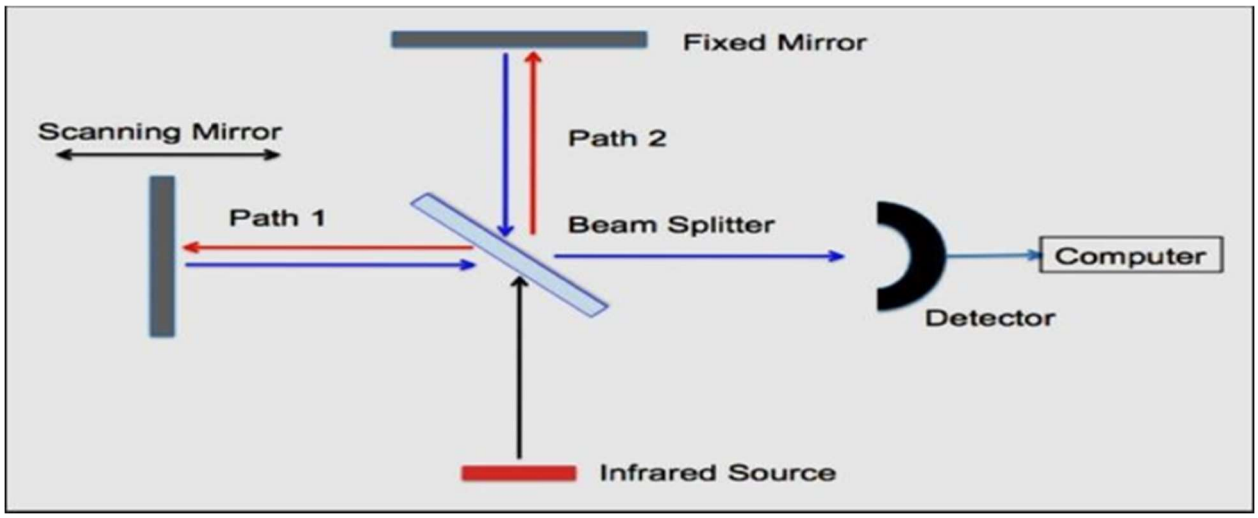

Figure (3-2). Fourier Transform Infrared (FTIR) Spectroscopy [121].

3.4.2 Optical Microscope (OM)

The change of surface morphology of blended polymers samples and its nanocomposites was observed applying the optical microscope. The use of OM was provided by Olympus (Top View, type Nikon-73346), Figure (3-3), shows the diagram explain the machine of work of OM. It is implemented at the University of Babylon /College of Education for Pure Sciences/ Department of Physics.

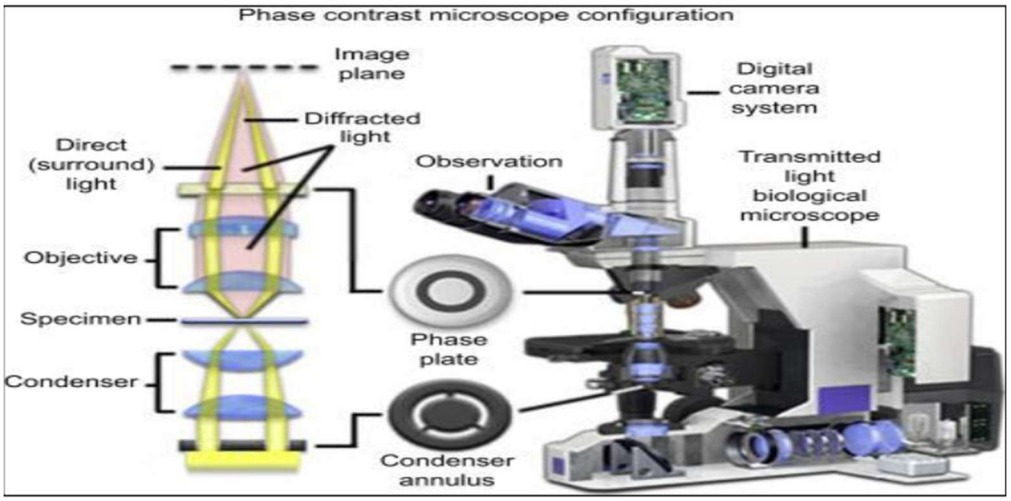

Figure (3-3). Optical Microscope [122].

3.4.3 X-Ray Diffraction (XRD)

All crystal structures of the polymeric preparations and nanocomposites were characterized using an XRD (6000) diffraction device. Manufacturing and country/ Tescan, France - Model/Xpert. X-ray diffraction (XRD) data were collected of (2θ) from (0º - 80º). It has the following characteristics, wavelength of 0.154 nm, voltage of 40.0 kv, current of 30.0 (mA), high power: 3 kv, target: copper, measurement temperature: 25 °C and the type of X-ray generation tube (copper, Bα). Figure (3-4), shows the diagram explain the machine of work of XRD

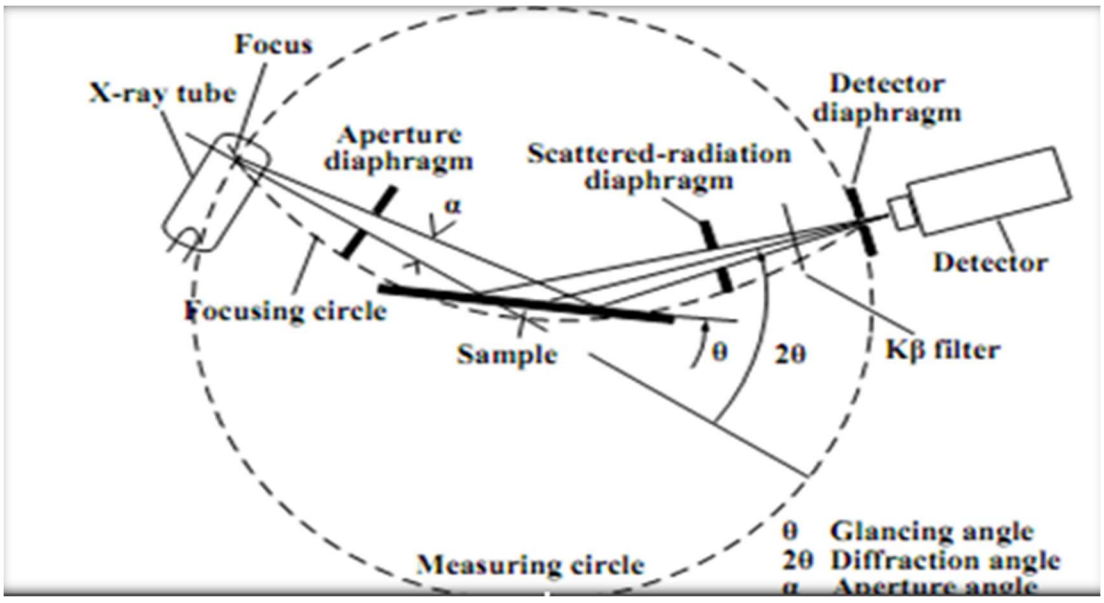

Figure (3-4). X-Ray diffraction Spectro sample [123]**.**

3.4.4 Field Emission Scanning Electron Microscope (FE-SEM)

the structural properties and nanoparticles size, shape and morphology of nanocomposites films were analyzed by field emission scanning electron microscope (FE-SEM) (TESCAN Mira3, Company TESCAN, Czech Republic), at Mashhad University of Medical Sciences.

3.5 Optical Properties Measurements.

The absorption spectrum of (PAAm-PVA-PVP/SiO_2) nanocomposites were recorded in the wavelength range (200-1100) nm using the double beam spectrophotometer (Shimadzu, UV-1800 Å). The absorption spectrum was recorded at room temperature. A computer program (UV Probe software) was used to get absorption. Implemented at Babylon university/college of education for Pure Sciences/department of physics.

3.6 Measurements of A.C. Electrical Conductivity

The A.C. electrical conductivity was measured by LCR meter type (HIOKI 3532-50 LCR Hi TESTER (Japan)) in university of Babylon / college of education for pure sciences/ department of physics. Figure (3-5) demonstrates a diagram for the system of A.C electrical measurement. Only (1 cm) from each one of the samples were taken and put between two electrodes and by different frequencies from (100Hz-6MHz) at room temperature. The capacity (C_P) and dissipated factor (D) were recorded for all samples. Dielectric constant, dielectric loss and conductivity was calculated from this data.

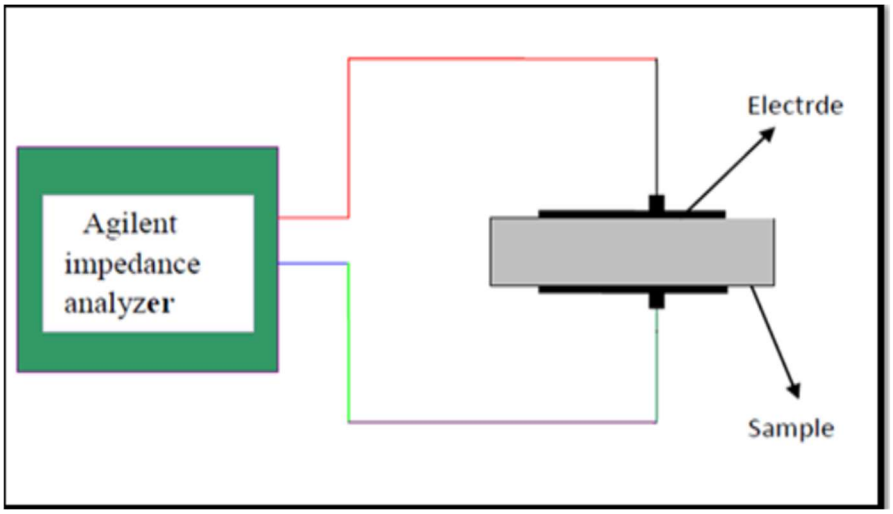

Figure (3-5). A.C electrical meter

3.7 Applications

3.7.1 Antibacterial Activity

3.7.1.1 The preparation of the bacterium inoculum

Four- five isolated colonies were selected from an 24h culture and diluted in Mueller Hinton broth to a turbidity like to 0.5 Mc Farland turbidity standard.

3.7.1.2 Antibacterial susceptibility test for nanocomposites

The antibacterial susceptibility test of synthesized Nanocomposites was made by Agar disk diffusion method. It is implemented at the University of Kufa /College of Science/ Department of Physics.

3.7.1.3 Agar disk diffusion method

Antibacterial activity of synthesized nanocomposites was performed by agar disk diffusion method. 20 mL of sterilized Mueller Hinton agar was placed in Petri dishes. After media solidification, 0.1 mL of each bacterial isolates were spread on the surface of media, the Petri dishes were left for 5 minutes, then 6 mm diameter disk from each NPs were placed in each Petri dish. The polymer blend pure was considered as negative control, the Petri dishes then incubated at 37 C^o for 24h. The zones of inhibition were measured and expressed as millimeter in diameter, the experiment was performed in triplicate.

3.7.2 Gamma Ray Shielding Application

Gamma ray attenuation measurements of blend polymer and nanocomposites were performed to investigate attenuation properties of gamma rays for the samples with different concentrations of SiO_2 nanoparticles. Test samples with different concentrations were arranged in front of a collimated beam emerged from gamma ray source (Cs-137, 5μC). The gamma ray source is positioned at distance (3) cm from the detector; the sample of nanocomposites is positioned at

distance (5) cm from the gamma ray source. The transmitted gamma ray fluxes through the samples are measured by the Geiger counter which were used to estimate the linear attenuation coefficients. The Geiger counter, would contain a Geiger-Müller tube, the element of sense that detects the radiation and the electronics that process and would provide the result. The Geiger-Müller tube is filled with a gas such as helium, neon, or argon at the pressure being the lowest, where there is an application of high voltage. There would be the conduction of the electrical charge on the tube when a particle or photon of incident radiation would turn the gas conductive by the means of ionization [124], as shown in Figure (3-6).

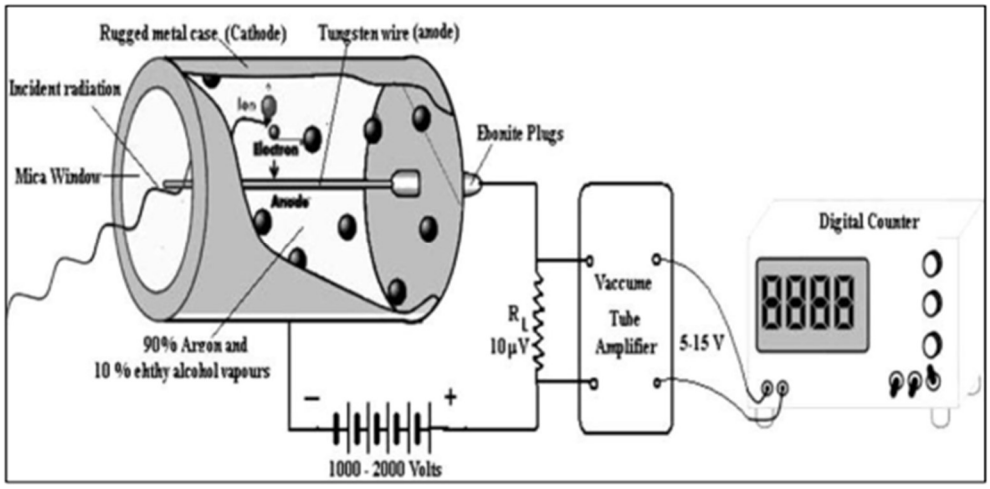

Figure (3-6). Geiger Counter [124]**.**

Chapter Four

Results and Discussions

4.1 Introduction

This chapter presents the findings and discussions on and SiO_2 nanoparticles on some morphology, optical, electrical properties, antibacterial and shielding of new blends polymers PAAm-PVA-PVP/SiO_2.

4.2 Structure and Morphology Properties

4.2.1 FTIR Measurement

FTIR spectroscopy is one of the main tools that provide information to help recognize the interconnections between the matrix functional groups and their interactions to identify the mixture and the nanoparticles at the intermolecular level. The FTIR spectrum in pure PAAm in Figure (4-1A), the broad bands observed at 3329 and 3182 $cm^{-1,}$ are linked to the asymmetric variation of NH_2 and symmetric vibration of NH_2. The two intense peaks at 2917 and 2355 cm^{-1} correspond to the CH_2 asymmetric stretching and strong O=C=O stretching vibration. The two peaks are 1651,1398 cm^{-1} and 1121 due to the C=O vibrational stretching and N-H bending [125].

In the FTIR spectrum for pure PVA in Figure (4-1A), the broad band observed at 3278 cm^{-1} is linked to the stretching O–H from intramolecular hydrogen bonds [126]. The two intense peaks at 2908 and 2358 cm^{-1} correspond to the CH_2 asymmetric stretching and O=C=O stretching vibration. The peak at 1711 cm^{-1} is due to the stretching C–O from the carbonyl group, and the peak at 1415 cm^{-1} corresponds to the C–H deformation vibration. The peak at 1244 cm^{-1} is attributed to the deformation stretching vibration of the C-N link. Moreover, the peaks observed at 1089 cm^{-1} could be attributed to the twisting vibration of the strong C-O stretching vibration band and medium C=C bending [129,130].

The FTIR spectrum of PVP in Figure (4-1A) had a peak at 3388 cm^{-1}, which indicates O-H stretching. The peaks at 2875, 2353, and 1638 cm^{-1} proved the existence of asymmetric stretching of CH_2, O=C=O stretching vibration, and stretching of C-O, respectively. The C-H bending and CH_2 wagging was observed at 1419 cm^{-1} and 1284 cm^{-1}, respectively [102].

In the FTIR spectrum in pure SiO_2 in Figure (4-1A), the broad band observed at 3569 cm^{-1} is linked to the stretching O–H from intramolecular hydrogen bonds. The two intense peaks at 2083 cm^{-1} correspond to the CH_2 asymmetric stretching and O=C=O stretching vibration. the peak at 1378 corresponds to the C–H deformation vibration and the peak at 1178 cm^{-1} is attributed to the deformation stretching vibration of the C-N link. Moreover, the peaks observed at 949 cm^{-1} could be attributed to the twisting vibration of the strong C-O stretching vibration band and medium C=C bending [129].

Figure (4-1B) shows the FTIR spectrum of the ternary blend polymers BP1 and NC films with (0.01.0.03.0.05) wt. % of SiO_2 in range (500-4500) cm^{-1} wavenumber. Several peaks were observed in the BP1 spectrum that observed peaks at 3343, 2959, 2384, 1648, 1505, 1421, 1288, and 1028 cm^{-1} and was connected with the expansion hydroxyl (O-H) group and methylene oscillations (C-H_2), strong O=C=O stretching vibration, (C=C) stretching, (N-O) stretching, (O-H) bending, (C-O) stretching, and (C-O) stretching. The results of the PAAm-PVA-PVP/SiO_2 vibration pattern (NC2) revealed the same peaks,

whereas some peaks were shifted to 3311 and 3183, 2960, 2384, 1649, 1509, 1421,1288, and 1009 cm^{-1}, in addition to present two peaks in the O-H area at 3311 and 3183 cm^{-1} than one abroad peak for BP1. Increasing the SiO_2 to 0.03 wt. % and change the ratios of polymers revealed shifting of the most peaks position to 3393, 2959, 1647,1422, 1288, and 1011 cm^{-1}. Additionally, it noted

one peak in the O-H area. The peaks at 2384 and 1509 cm^{-1} were dispersed, which could relate to increasing the PVP ratio of 70 wt. % as a higher ratio in this sample NC2. Increasing concentration of SiO_2 NPs to 5 wt. % and increasing the ratio of PAAm to 70 wt. % in the NC4 showed the same peaks of NC2. Most of the peaks were shifted to 2950, 1648, 1502, 1418, and 1019 cm^{-1}, respectively, compared with BP1.

Also, it is noted increasing the intensity of some peaks 2384 and 1502 cm^{-1} in NC4. The FTIR spectrum of these polymer nanocomposite films demonstrated the interfacial interactions between the miscible chain architectures and the SiO_2 nanoparticles and PAAm-PVA–PVP blend. The presented functional groups approved the fabrication of BP1 ternary blend polymers and NPs, whereas the loaded of SiO_2 exhibited changes in the position peaks and intensity of such as O-H, C-O, and C-H as a result of the network formed between SiO_2 and oxygenated groups of polymers. These results strongly agreed with other reports [5,131].

Figure (4-1) FTIR spectra of (A) pure polymer and SiO_2 and, (B) nanocomposites.

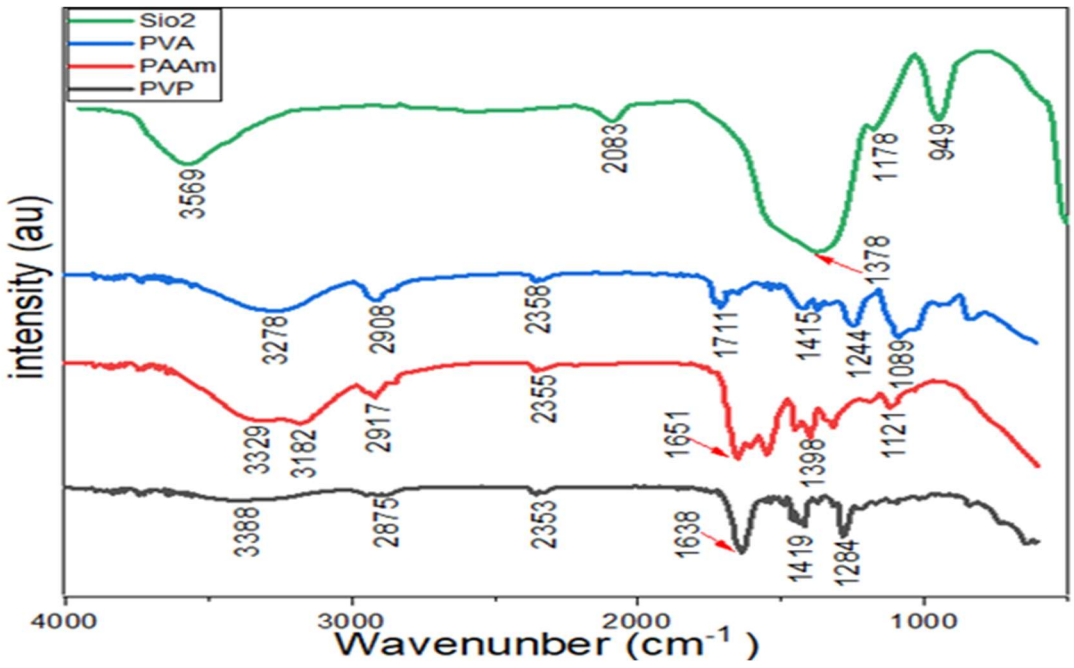

(A)

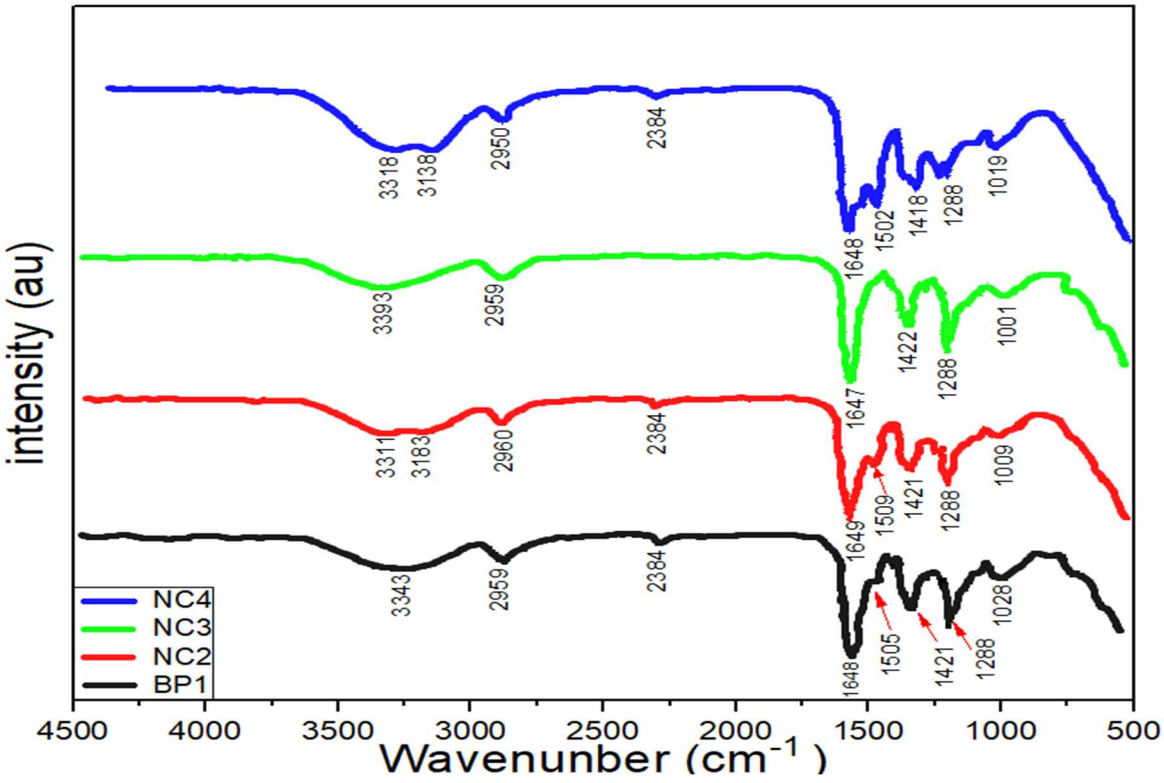

(B)

4.2.2 X-Ray Diffraction Measurement

The crystallographic structure of polymers and SiO_2 was determined using XRD patterns, as shown in Figure (4-2 A). PAAm spectra display an amorphous structure with a broad peak between 10 to 50°, where the higher intensity of the top peaks was at 2θ = 22° with other small features exhibited at 7°, 50.2°, 68.6° in agreement with the literature [130,132]. PVA spectra display an amorphous structure with a broad peak where the higher intensity of the top peaks was at 2θ =19° and other small features exhibited at 35.8°, 40.2°[133,134]. PVP spectra display an amorphous structure with a broad peak where the higher intensity of the top peaks was at 2θ =21°. Other small features were exhibited at 11.2° and 13°[134]. SiO_2 spectra display an amorphous structure with a broad peak where the higher intensity of the top peaks was at 2θ =21.8°. Other small features

exhibited at 31.8°, 42.4°,49.6°, 62.2°, 65° and 75.6° in agreement with other report [130].

The crystallographic structure of BP1 polymer blend and its nanocomposite films with different ratios of (1, 3, and 5) wt.% SiO_2 NPs were determined using XRD patterns, as shown in Figure (4-2B). BP1 spectra display an amorphous structure with a broad peak between 10 to 50°, where the higher intensity of the top peaks was at 2θ =22.2°. Other small features exhibited at 9.3, 14.2, 25.5, 33.1, and 54.3°.This behavior is similar to the PAAm-PVP behavior reported in the literature [136, 137]. PVA crystallite pattern at 19.9° disappeared, which could be overlapped in the abroad peaks, or the lower percentage could assist in this disappearing in agreement with the other reports [138,139]. NC2 showed the same behavior as BP1, but the contribution of SiO_2 exhibited shifting in the top abroad peaks from 2θ = 22.2° to 20.1°, and 10.0, 13.9, 25.6 and 30.1°, respectively. Whereas NC3 revealed a different behavior than BP1 and NC2, NC3 exhibited two main peaks at 9.6° and 19.8°. This behavior matched the behavior of pure PVP because it consists of 70 wt. % of PVP in strong agreement with the literature [139]. It showed a reduction or diapered in the SiO_2 peaks presented in the NC2. NC4 showed the same behavior as BP1 and NC2. The contribution of the increase in the SiO_2 nanoparticle concentration to 0.05 wt. % showed a shift of the main top peak back from 2θ =22.2° to 23.9°, in addition, another shifting of peaks from 9.3 to 11.9°, 25.5 to 26.1°, and 54.3 to 54.6°. Furthermore, it also revealed new small peaks at 2θ = 11.9, 36.2, 68.8, and 71.8° compared with BP1.

NC4 showed an increase in the number of peaks from 5 to 8 compared with NC2 and from 2 to 8 compared to NC3. The ratios of both polymers and nanoparticles showed important factors that affected the behavior of nanocomposites as that presented the general behavior turned with the specific behavior of the higher ratio of main consist of the polymer as presented in the NC3 and NC4. Notably,

incorporating SiO_2 nanoparticles considerably changes the crystallinity degree of BP1 blended polymers. In addition, presents the small features of crystalline peaks after increasing the concentrations of nanoparticles from 0.01 to 0.05 wt. %. This behavior is strongly agreed with other researchers who reported the impact of SiO_2 on the PAAm -PVA- PVP /SiO_2 membrane [135]. As the amount of SiO_2 nanoparticles in the sample structure, the crystal sizes (D) of the samples increased. D was raised from 0.834 to 1.253 nm at that site which was calculated from the equation (2.4). Furthermore, as shown in Table (4-1), the contribution of the nanoparticles.

Figure (4-2). XRD patterns of (A) Pure polymer and SiO_2 and (B) nanocomposites

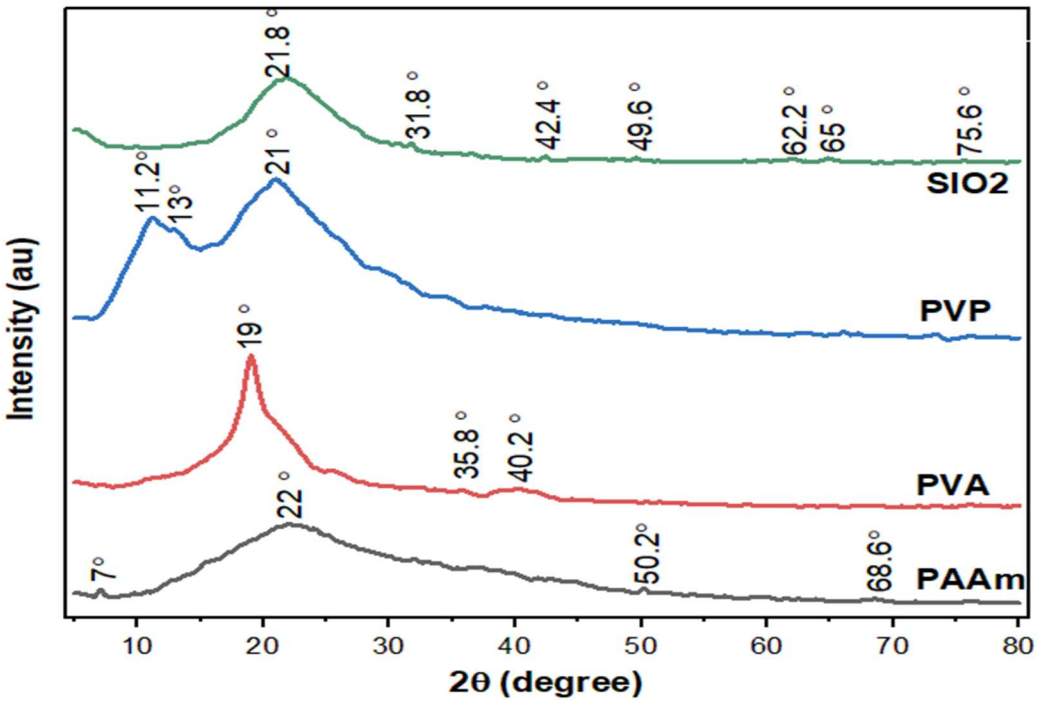

(A)

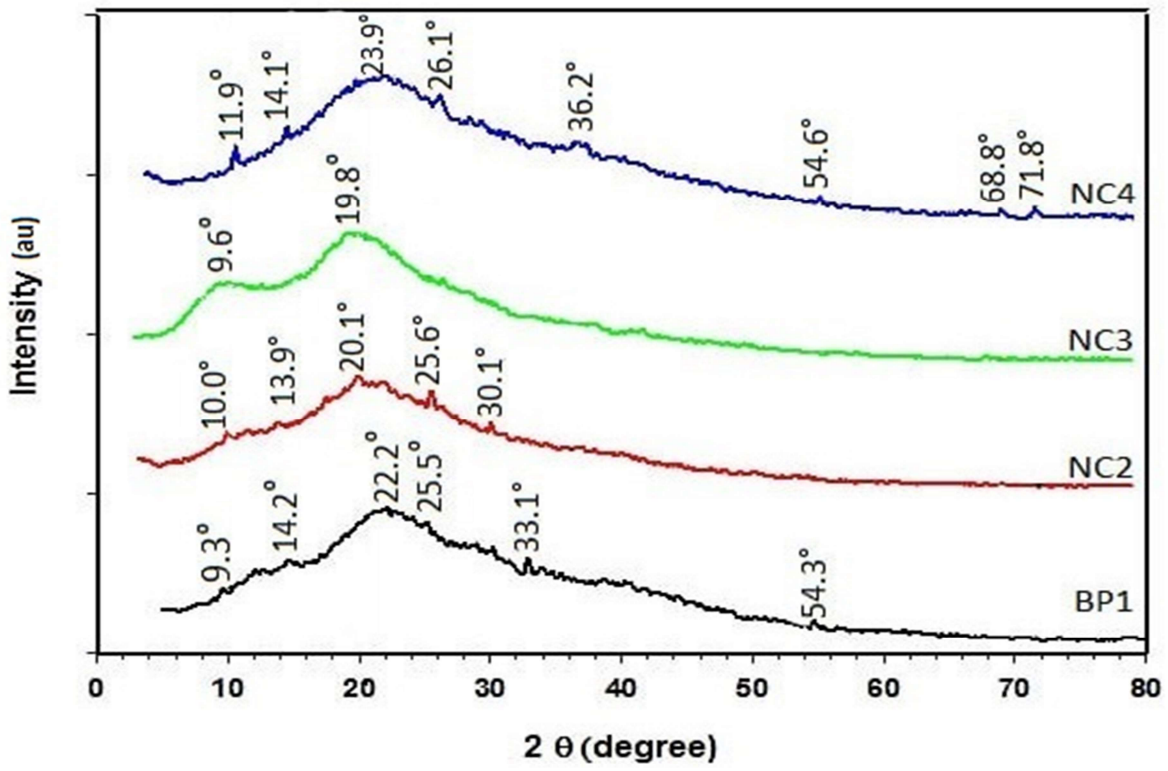
Intensity (au)
11.9°
14.1°
23.9°
26.1°
36.2°
54.6°
68.8°
71.8°
NC4
9.6°
19.8°
NC3
10.0°
13.9°
20.1°
25.6°
30.1°
NC2
9.3°
14.2°
22.2°
25.5°
33.1°
54.3°
BP1
0
10
20
30
40
50
60
70
80
2 θ (degree)

(B)

Table (4-1) summarizes the size of the crystallites, typically FWHM, diffraction angle, nanocomposite and mixed polymer lattice strain.

Samples	2θ (°)	d (nm)	β (°)	D (nm)	Average crystallite size average (nm)	Lattice Strain * 10^{-3}	Average Lattice Strain * 10^{-3}
BP1	9.3	0.894	0.951	7.840	7.83	0.051	0.027
	14.2	0.586	1.439	5.158		0.050	
	22.2	0.376	1.087	6.753		0.024	
	25.5	0.328	0.765	9.538		0.014	
	33.1	0.254	1.306	5.491		0.019	
	54.3	0.158	0.786	8.470		0.006	
NC2	10	0.832	0.822	9.066	10.5	0.040	0.024
	13.9	0.599	0.846	8.777		0.030	
	20.1	0.415	0.689	10.691		0.016	
	25.6	0.327	1.502	4.856		0.028	
	30.1	0.279	0.649	11.131		0.010	
NC3	9.6	0.866	1.125	6.626	7.16	0.058	0.040
	19.8	0.421	0.956	7.708		0.023	
NC4	11.9	0.699	0.53	14.038	7.62	0.022	0.018
	14.1	0.590	0.942	7.881		0.033	
	23.9	0.370	1.087	7.592		0.021	
	26.1	0.321	1.011	7.208		0.019	
	36.2	0.233	1.581	4.497		0.021	
	54.6	0.158	1.494	4.450		0.012	
	68.8	0.128	1.339	4.610		0.008	
	71.8	0.123	1.792	3.382		0.010	

4.2.3 Optical Microscope

The optical images of PAAm-PVA-PVP blended polymers and PAAm-PVA-PVP/SiO_2 at magnification 40X are shown in Figure (4-3). These images demonstrate the good homogeneity of BP1 polymers. These images illustrated good homogeneity and the distribution of SiO_2 with some aggregations into the polymer blend, which means a good procedure for preparing the blended polymers and PAAm-PVA-PVP/SiO_2 nanocomposites. Nanocomposites showed a noticeable alteration with an increase in the SiO_2 ratios. The influence of SiO_2 revealed several changes in all of these films, with some aggregates in the films without effects on the films' transparency, as shown in the inset images in Figure (4-3), in agreement with others finding [141,142].

Figure (4-3) Optical Microscopy Images of (40X) and inset images for samples.

BP1 **NC2**

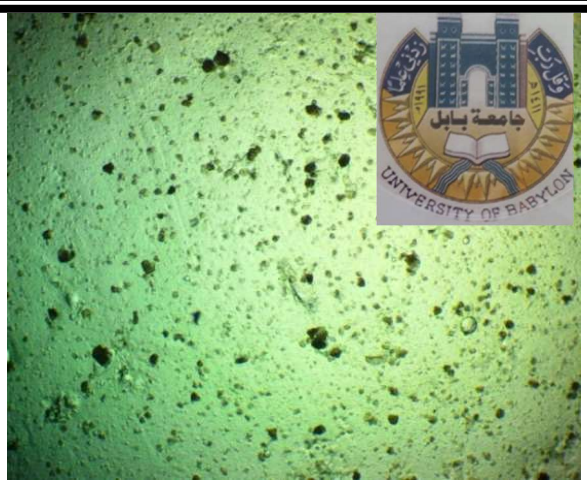

NC3

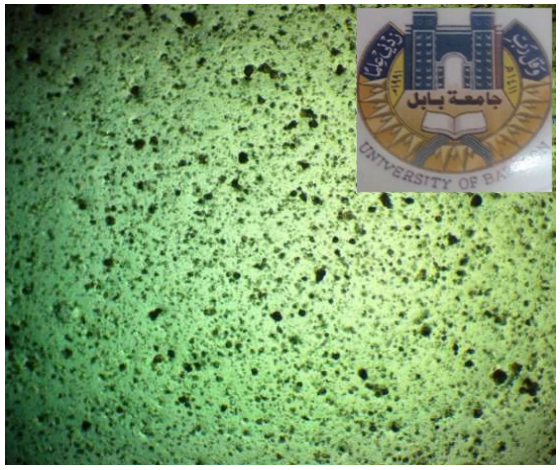

NC4

4.2.4 Field emission scanning electron microscopes (FE-SEM)

The FE-SEM was used to examine the surface morphology and dispersion of the nanoparticles in the polymer matrix, as shown in Figure (4-4). Samples presented the nano communications polymers viewed on the sample's surface (left side) with micron-size (right side) nano size images, as shown in Figure (4-4) [142]. Bland polymer films (BP1) (left side) showed homogeneous, grainy, coarse surface shapes. The right side shows that the surface suffers from some cracks and that the polymer crystals. On the left side, SiO_2 nanoparticles with 0.01 concentration in the NC2 revealed affected the polymer matrix and showed good dispersion and granular structure without assemblies. (right side) revealed that the surface was rough and homogeneous, but the crack still appeared. Increasing the loading ratio of SiO_2 nanoparticles to 0.03 and 0.70 wt. % of PVP represented the grainy surface of the NC3 (left side). Meanwhile, on the (right side), crack numbers and size were generally reduced. The incorporation of increasing nanoparticles to 0.05 wt. % and PAAm 0.70 wt. % in the NC4, FE-SEM images on (the left side) showed a rough, coarse surface. Interestingly, the cracks in the NC4 surface were significantly reduced too difficult to recognize and became very smooth compared with other samples. Moreover, the surface of

the NC4 showed the type of specific shape order or type of semi-crystalline shape of polymer particles existing on the surface. This supported the existence of crystalline peaks in the NC4 compared with other samples. Another observed the SiO_2 appeared on the surface of the samples that started reducing in NC3 and diapered in NC4. This could referee good adhesions and stronger interfacial interaction of the NC4 in agreement with FTIR results that showed a change in the functional peaks and XRD results [143].

Figure (4 -4). Field emission scanning electron for samples

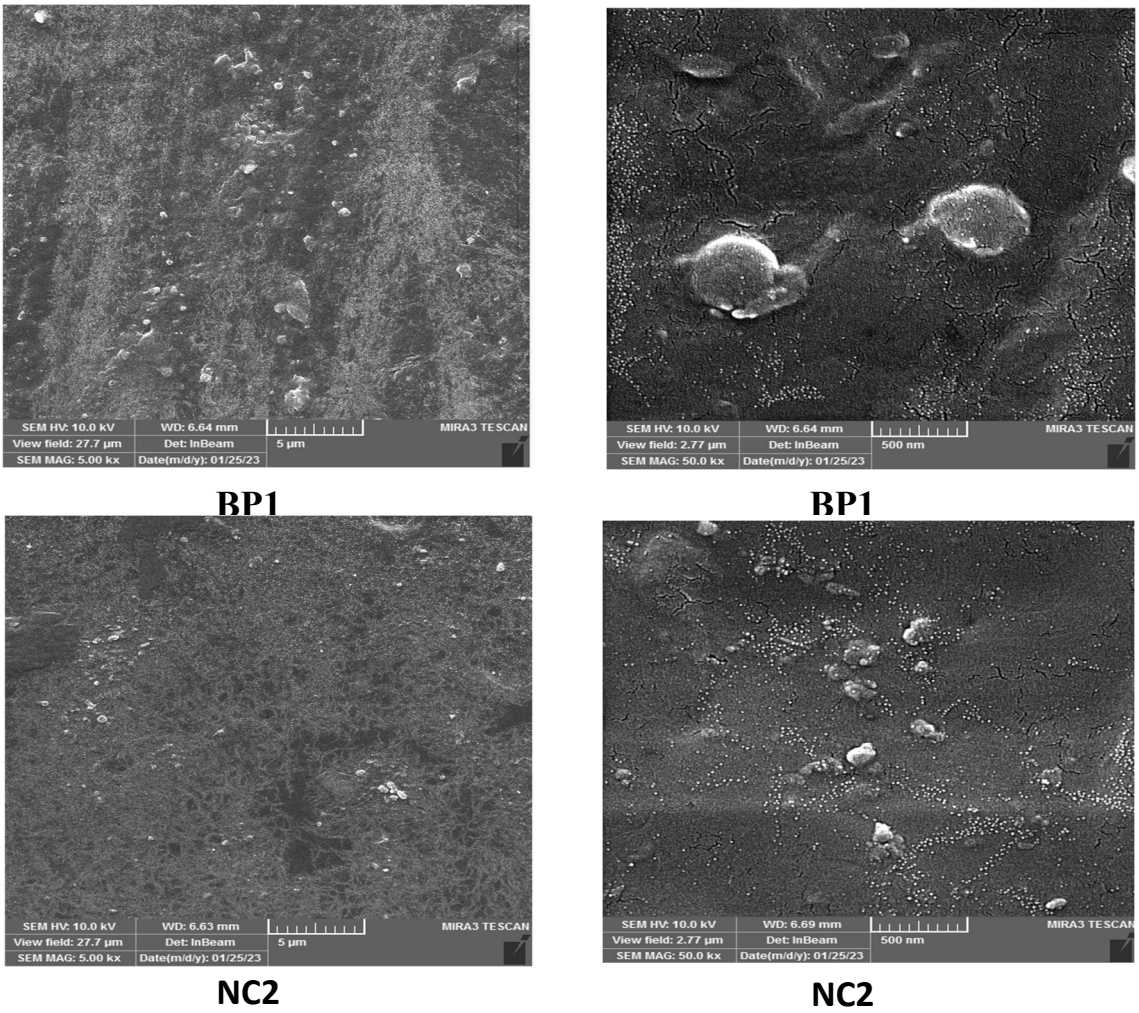

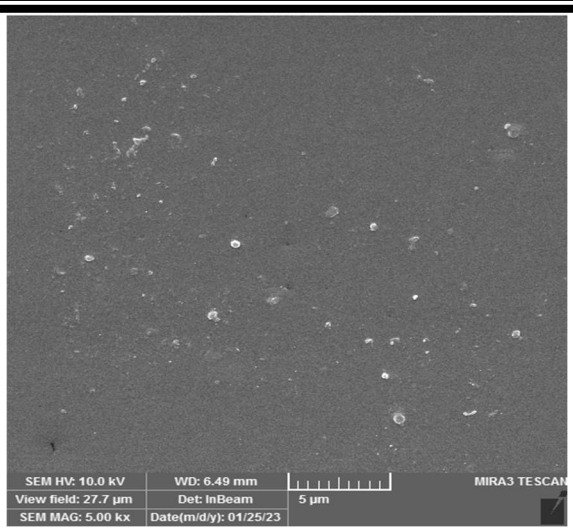

NC3

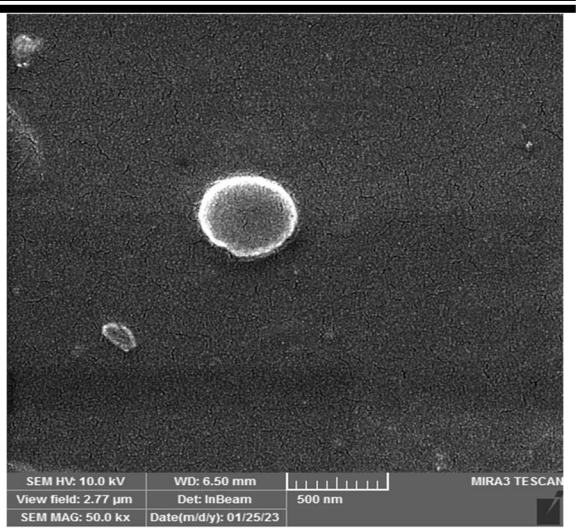

NC3

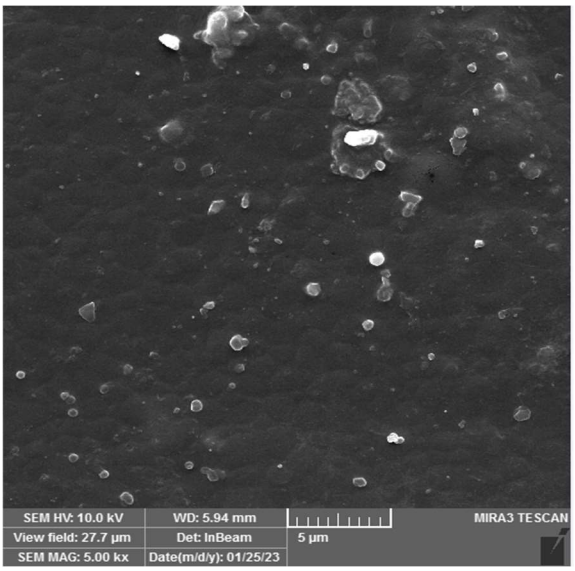

NC4

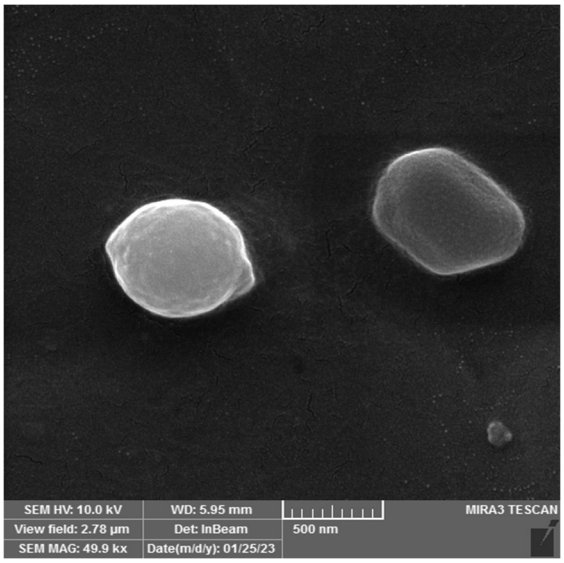

NC4

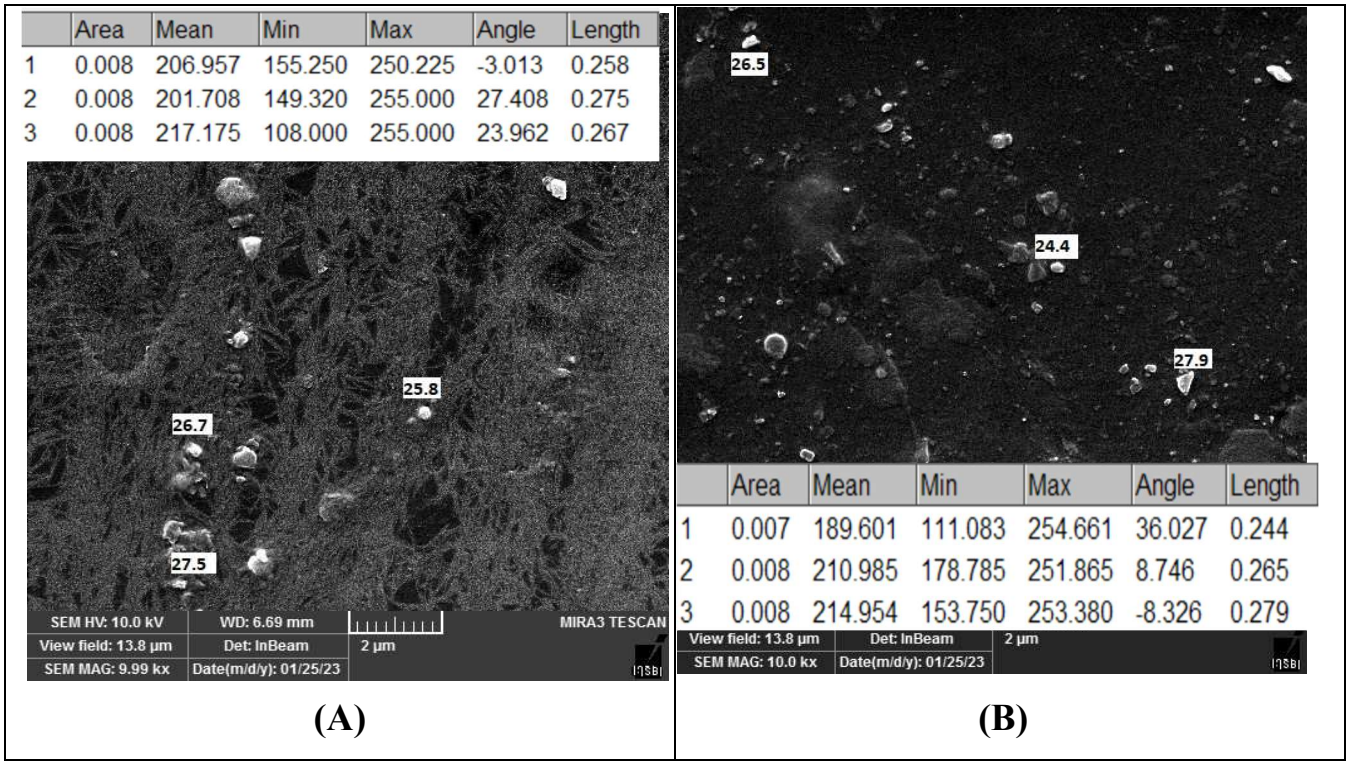

Figure (4 -5). Nanoscale silicon dioxide using image software

4.3 The optical properties

4.3.1 Absorbance

The optical absorption in the range of wavelength samples (200-1100) nm increases and the Figure (4-6) shows this. All samples had higher absorbance values in the UV band. The donor electrons were conduction band excitations at high energies by taking in a photon with known energy. The donor electrons were excited energy level increased from lower to higher. Additionally, the outcomes demonstrated a strong photon absorbance by the samples in the UV area. This resulted in these photons having sufficient to exert energy on atoms, especially at 200 nm. At high energies (200 nm), the sharp absorption peak could relate to the transition of plasmonic π-π* stacking (C=C) or the covalent bonding that indicated the interaction between the component's matrixes. This result matches the functional group with strong (C=C) vibration at 1648 cm^{-1}.

Where increasing the contribution of the loading ratio of nanoparticles from 0.01 wt. % to 0.0 5 wt. % SiO_2 NPs and PAAm from 20 wt. % to 70 wt. % revealed an enhancement in the absorbance from 0.73 to 0.91 with 25 %. Whereas, at higher wavelength between (340 and 1100 nm), the absorbance values were also improved from 0.013 to 0.113 at 1100 nm. Additionally, the case that the growing width of the absorption peak increased absorption from 260 nm to 320 nm.. This may be connected with the incident photons' inability to interact with atoms because they lack sufficient energy and the transmitted photon at high wavelengths. These findings agreed with the literature [24,143].

SiO_2 nanoparticles exhibit an abrupt reeducation in the (0–400 nm) low UV region suggesting strong electron transition within the bandgap [26]. The red shift toward high wavelengths suggests an electronic transition from n → π* and confirms the complexation process between ternary blend polymers and SiO_2 nanoparticles [128]. Ternary blend polymer concentrating does not show a strong effect on the results. At the same time, the results demonstrated reduced results with boosting the amount of SiO_2 in the matrix. Increasing the nanomaterials could increase light absorbance [145]. Additionally, the shift indicates an increase in the conjugation lengths of the polymers in agreement with the other finding [2]. Despite increasing the absorption of light amount, this did not impact the transparency of the samples, as shown in the inset optical images in Figure (4-3).

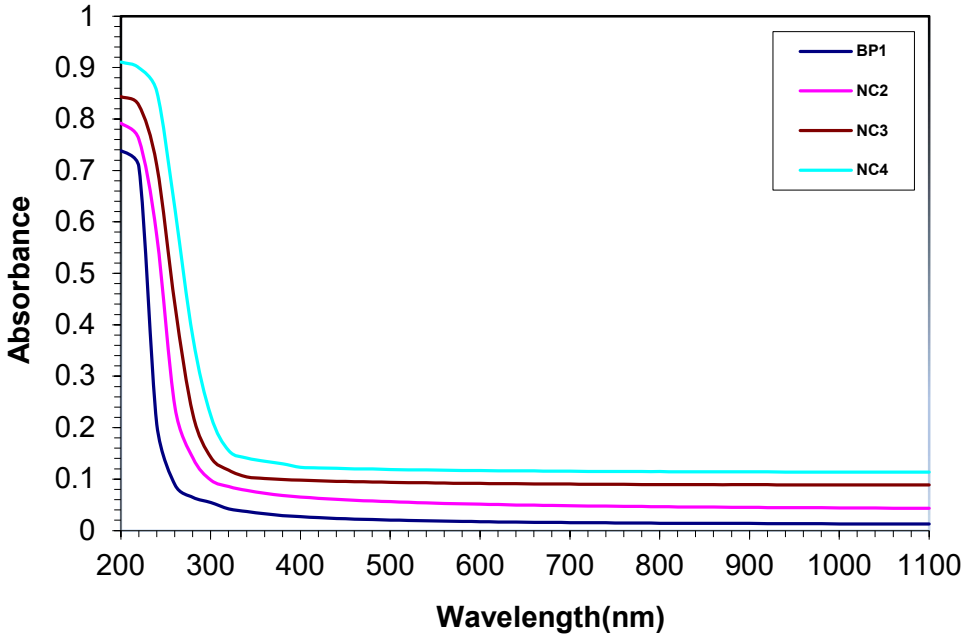

Figure (4-6). Absorbance spectra with a wavelength of the sample.

4.3.2 Transmittance

The transmittance was calculated from Equation (2.7). Figure (4-7) shows the transmittance (T) spectra with the samples' wavelength. The transmittance behavior for all samples was rapidly increased with increasing the wavelength at about 240 nm, and it was steady after 340 nm. Polymer concentrating does not show a strong effect on the results. Whereas the results demonstrated reduced results with boosting the amount of SiO_2 in the matrix, increasing the nanomaterials could increase light absorbance while decreasing transmittance [137].

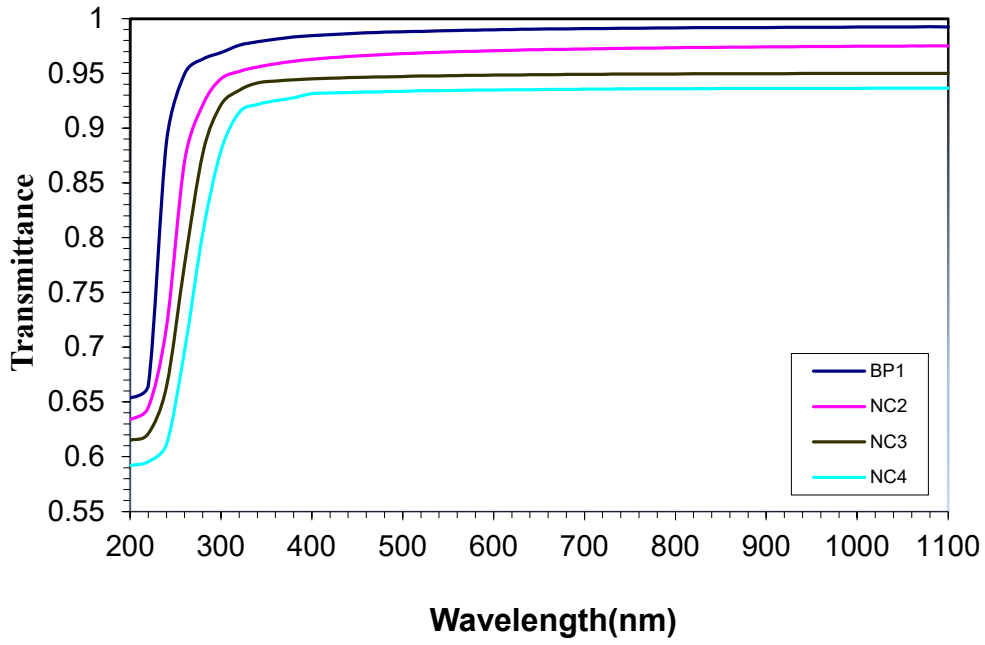

Figure (4-7). Transmittance spectrum with a wavelength of samples.

4.3.3 Absorption Coefficient

Figure (4-8) displays the impact of SiO_2 nanoparticles on the absorption coefficient (α) of sample films with photon energy. The absorption coefficient (α) was calculated using Equation (2.19). The behavior of the absorption coefficient showed a constant increase in values with increasing photon energy to about 4 ev of most samples. This may be connected to the electron's lower transition, where to transfer from the electron of the conduction band to the valence band, more input photon energy was required. In contrast, the absorption coefficient rapidly increases after 4.6, 4.2, 4, and 3.8 eV of BP1, NC2, NC3, and NC4 to reach 340, 362, 388, and 420 cm^{-1} at 6.2 eV, respectively. Increasing the SiO_2 nanoparticles in the polymer matrix is associated with increases in the absorption amount; at lower energy (1 to 4 eV), the absorption coefficient enhanced from 23.3 to 53.6 % and at higher energy (4 to 6.4 eV) 340.2 to 419.4 cm^{-1}. The increasing outcomes result from the strong electron transitions in the conductive band [145,131].

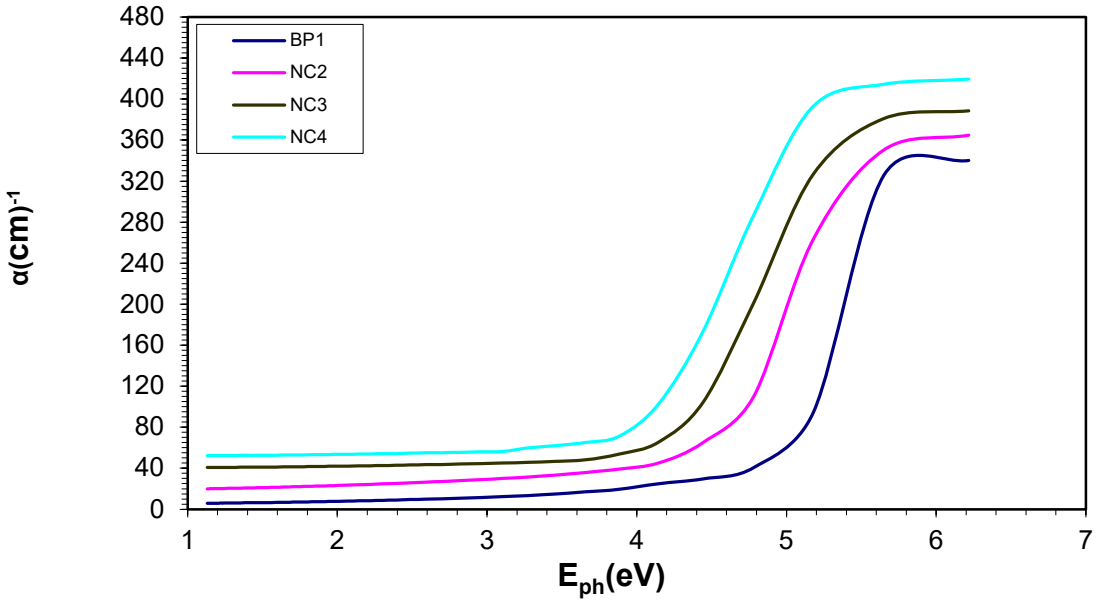

Figure (4-8). Absorption coefficient with the photon energy of samples.

4.3.4 Optical Energy Gap

Figures (4-9 and 4-10) exhibit the indirect band gap of permitted $(\alpha hv)^{1/2}$ and prohibited $(\alpha hv)^{1/3}$ of PAAm-PVA-PVP and PAAm-PVA-PVP/SiO_2 with the power of photons. These values were estimated using the formula (2.20) with $(\alpha hv)^{1/2} = 0$. Using the intercept of the extrapolated linear portion. To calculate the energy gap, draw a straight line from the upper portion of the curve in Figures (4-9 and 4-10). This Figures shows that the energy gap significantly reduced with increasing concentration of SiO_2, as shown in Table (4). It is reduced from 4.8 eV for PAAm-PVA-PVP blended polymers to 3.4 eV for PAAm-PVA-PVP/SiO_2 nanocomposites for the allow band gap. The forbidden band gap exhibited a reduction in the value from 4.2 eV for PAAm- PVA-PVP to 3.1 eV polymer mix for PAAm-PVA-PVP/SiO_2, as a result of polymer ratio manipulation and increased load ratio from 0.01 to 0.05 wt.%. The contribution of SiO_2 NPs was displayed as an important factor in the adjustable range gap. Additionally, raising the load ratio of SiO_2. This led to a significant reduction in the energy gap values

in non-communications. The energy gap decreases as the concentration of nanomaterials increases. This is because of the rise in the positioning levels between the parity and delivery packages. In this scenario, the electron moves from the parity package to the positioning levels and then to the two stages. The positioning levels to the connectivity package [146].

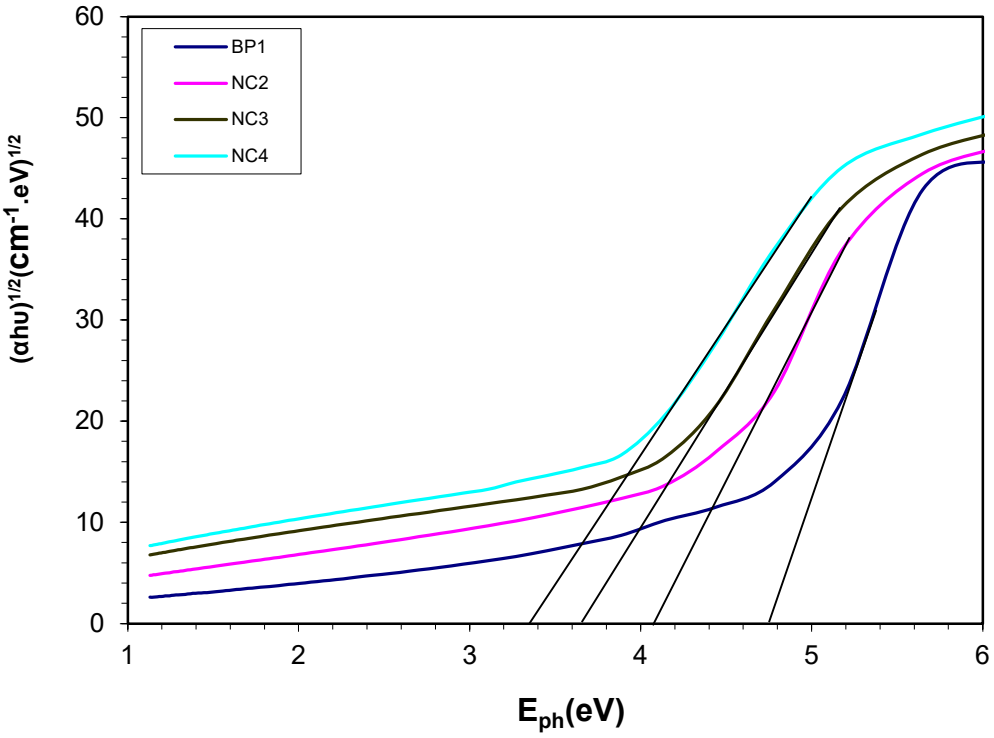

Figure (4-9). Tauc optical energy gap of the allowed indirect transition with the photon energy for samples.

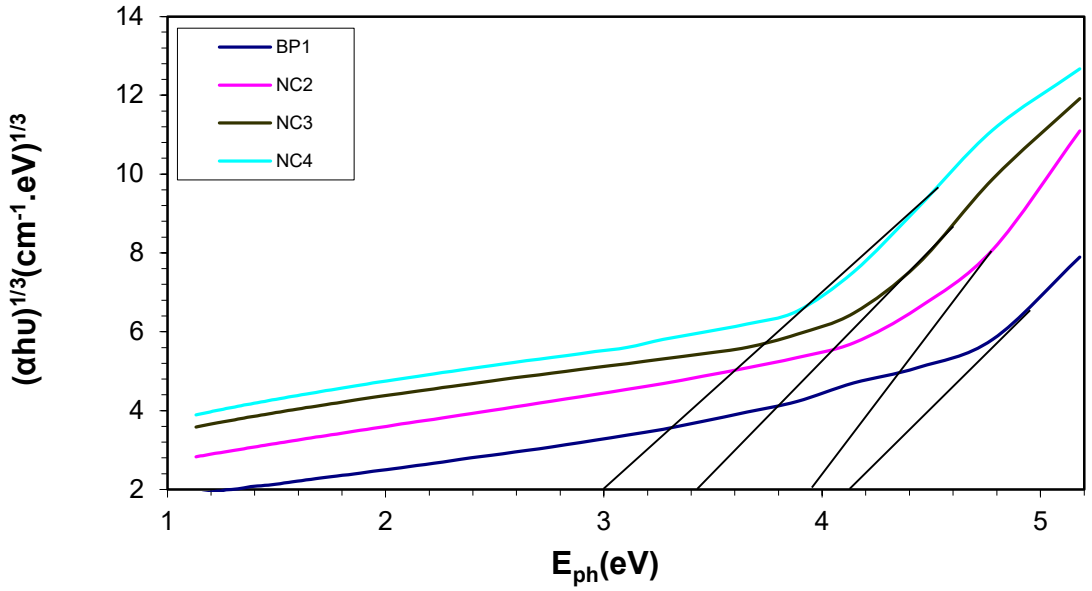

Figure (4-10). Tauc optical energy gap of the forbidden indirect transition with the photon energy of samples.

Table (4-2). The optical energy gap of samples.

Samples	E_g of Allowed Indirect (eV)	E_g of Forbidden Indirect (eV)
BP1	4.8	4.2
NC2	4.1	3.9
NC3	3.6	3.5
NC4	3.4	3.1

4.3.5 Refraction index

Figure (4-11) demonstrates the refraction index curves of samples with the desired wavelength. The refraction index (n) was calculated from relation (2.21). The refraction index presented a high value at a lower wavelength, which was reduced gradually with increasing the wavelength. The loading of SiO_2 to the NPs nanocomposites increased the samples' refractive indices. The density of

nanocomposites may be increasing, which could explain this phenomenon in agreement with other finding [147].

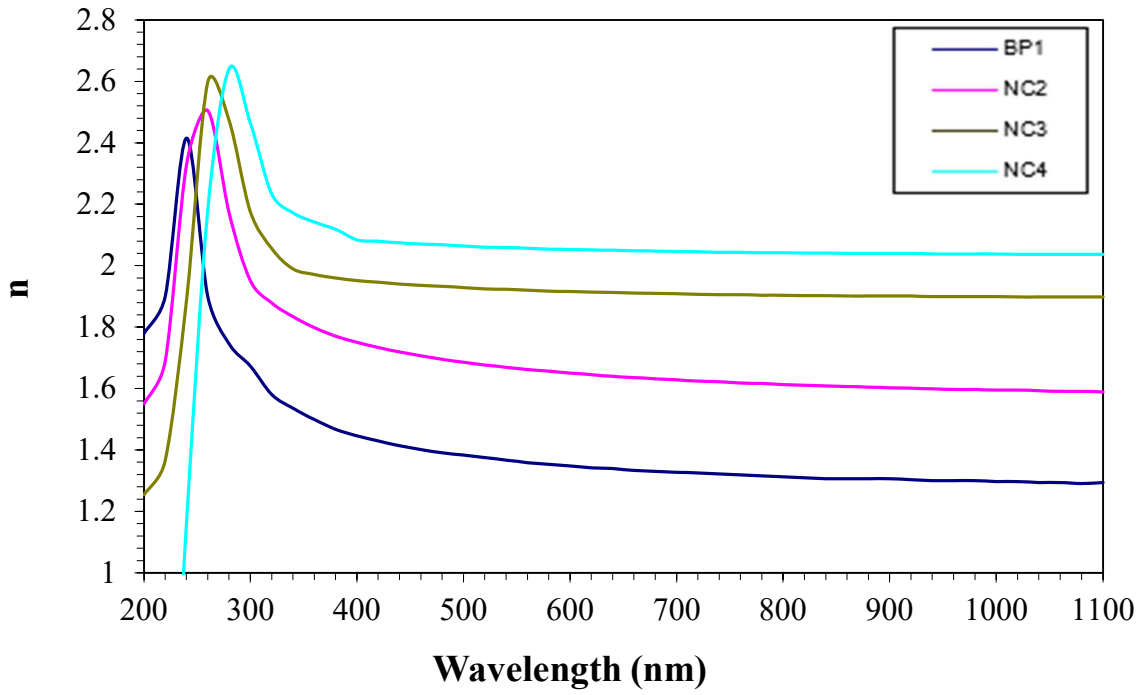

Figure (4-11). Refractive index against wavelength samples.

4.3.6 The Extinction coefficient

Figure (4-12) illustrates the samples' wavelength-based extinction coefficient (K). The extinction coefficient (K) was calculated from the relation (2.23). In the UV area, nanocomposites revealed a greater extinction coefficient value, connected to the high absorption for every nanocomposite. The same effect also exhibits in the visible and near-infrared spectrums. These findings showed that adding SiO_2 NPs to the polymer mixture considerably improved the behavior of the nanocomposites.

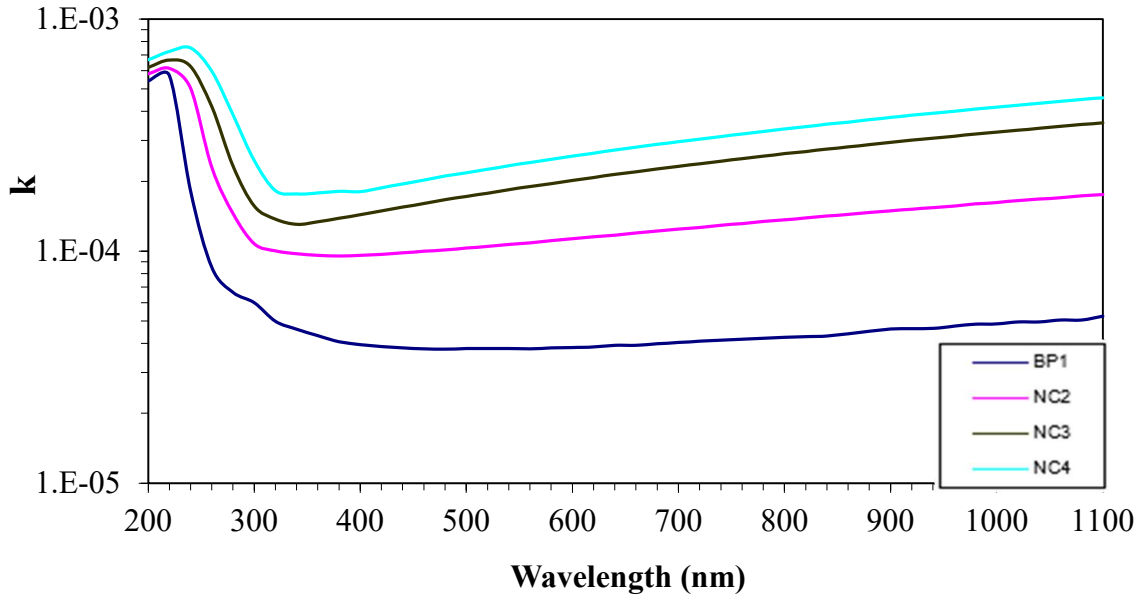

Figure (4-12). The extinction coefficient against wavelength of samples.

4.3.7 The real and imaginary dielectric constant

The real and hypothetical dielectric constant was calculated from relation was calculated using Equation (2.27) and (2.28). The relationship between the wavelength and the actual and imaginary dielectric constant of the PAAm-PVA-PVP/ SiO_2 nanocomposites is illustrated in Figures (4-13 and 4-14). These graphs demonstrate how raising the ratio of SiO_2 to NP concentration enhanced both portions' real and fictitious dielectric constants. The nanocomposites ' increased electrical polarization is to blame for this.

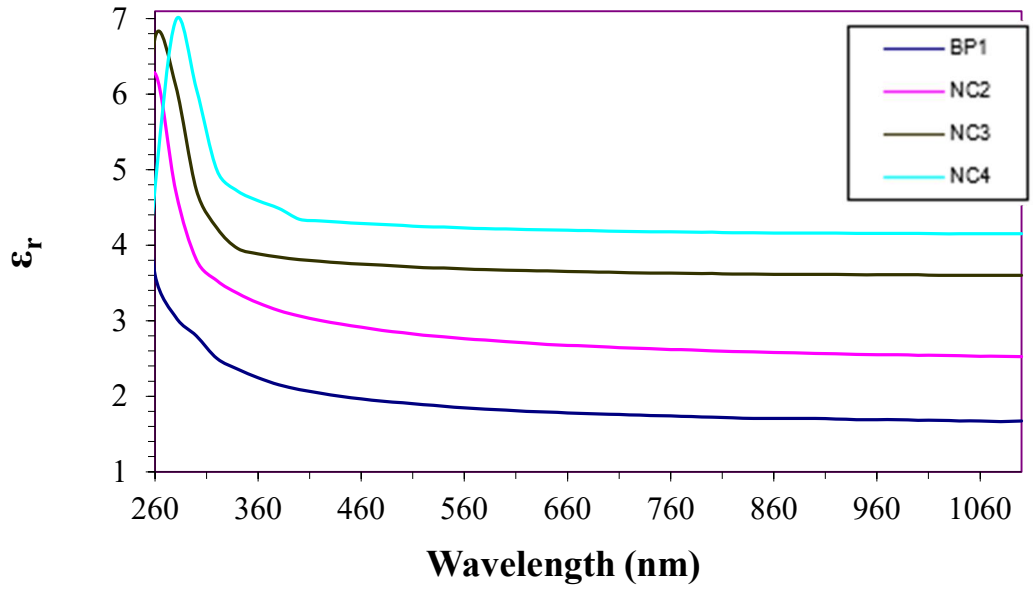

Figure (4-13). The real dielectric constant with wavelength for samples

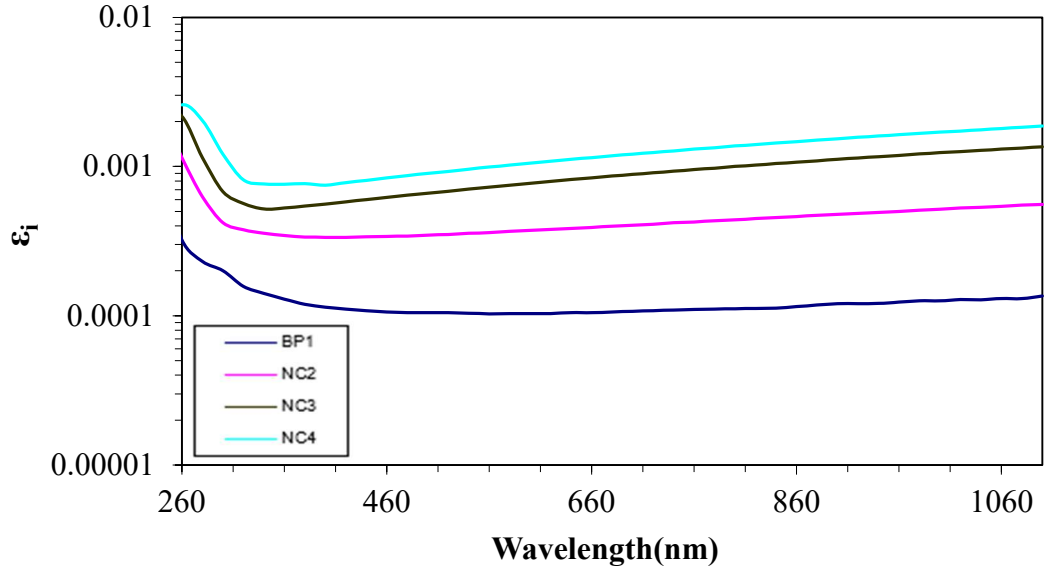

Figure (4-14). The imaginary dependence dielectric is constant with the wavelength for samples.

4.3.8 Optical conductivity

Optical conductivity was calculated using Equation (2.29). The σ_{op} for the samples with a wavelength are demonstrated in Figure (4-15). From this Figure,

the σ_{op} enhanced with increasing the content of SiO_2 NPs in the matrix, which is connected to the formation within the localized energy gap, rising nanoparticle content induced rise in the band structure's density of localized phases. Therefore, a higher absorption coefficient indicates a higher in σ_{op} of the nanocomposites ; This outcome is consistent with a previous study [148].

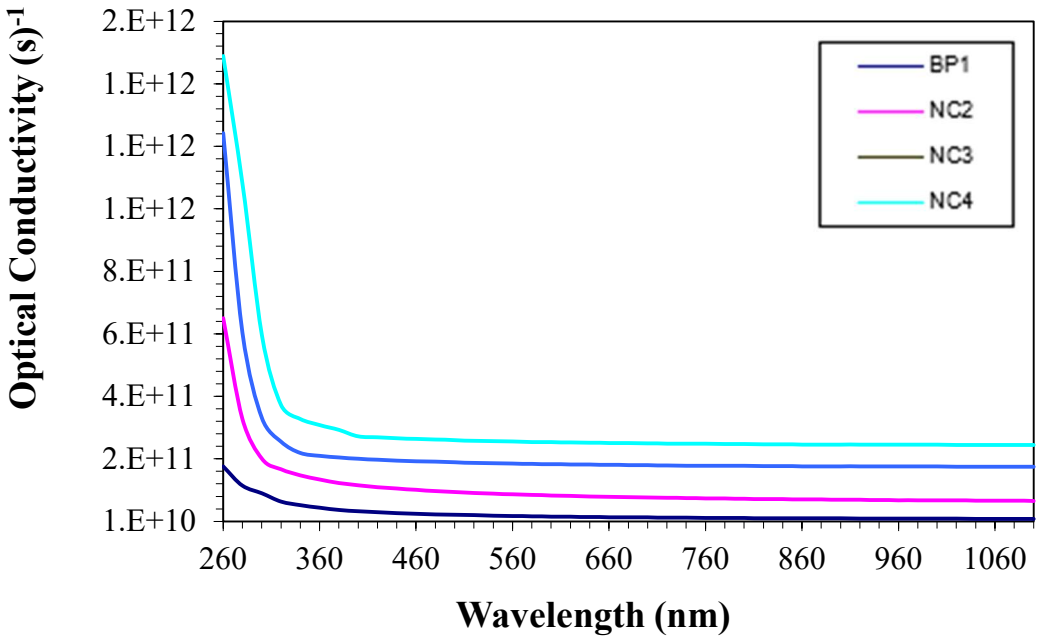

Figure (4-15). Variation of σ_{op} with the wavelength for samples.

4.4 The A.C electrical properties

4.4.1 Dielectric Constant

The dependence dielectric constant was calculated from Equation (2.44) for (PAAm-PVA-PVP/SiO_2) nanocomposites that are depicted in Figure (4-16 A). The graph indicates redaction in the dielectric constant values as the applied frequency rises. This could relate to the polarization of space charges relative to the total polarization decrease. Space charge polarization contributes more to the electric field at low frequencies and less to higher frequencies, which would cause the dielectric constant values for every instance for nanocomposites to drop as

the electric field's frequency increases [43]. Where Figure (4-16 B) displays constant dielectric changes with increasing the concentration of SiO_2 NPs. The weight percentages of SiO_2 NPs grow together with the dielectric constant, which causes the increase. Creating a continuous network of SiO_2 NPs ions inside the composite and the charge carriers. This action agrees with previous studies [5,149].

Figure (4-16). Dielectric constant variation with (A) frequency and (B) the concentration of SiO_2 NPs for samples.

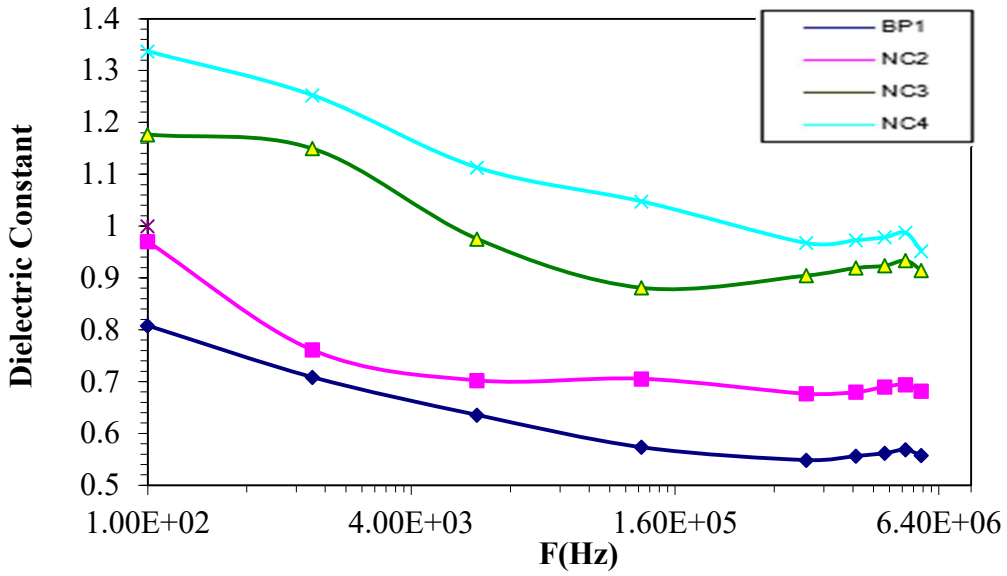

(A)

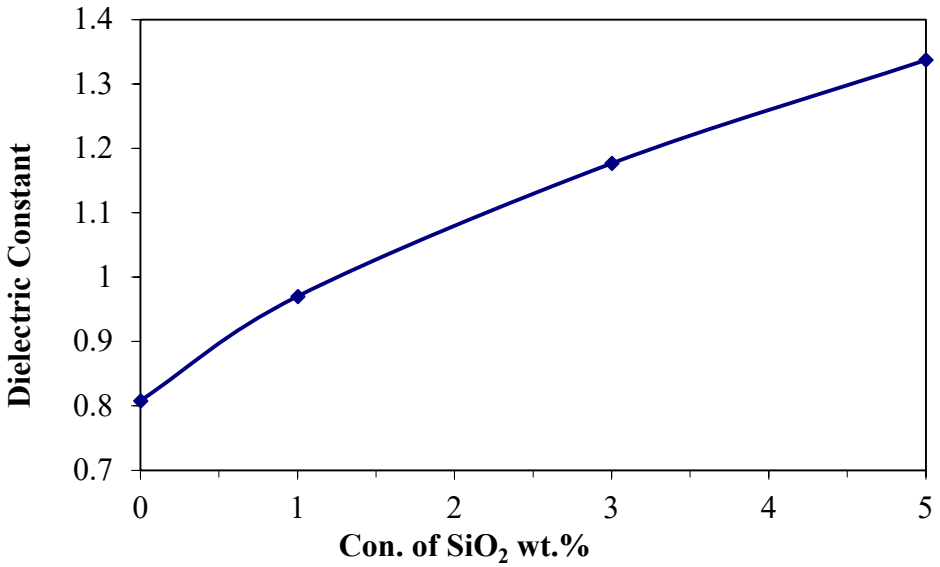

(B)

4.4.2 The Dielectric loss

The dielectric loss was, which is revealed in Figure (4-17 A). Figure (4-17 A) shows the relationship between dielectric loss for samples and frequency. The behavior values of dielectric loss showed a redaction with increasing frequency. This could be explained by the fact that the space charge polarization contribution decreased as frequency rise, where the highest value of the dielectric loss is presented at a low frequency of f=100Hz and then reduced with increasing frequency. This Figure shows an applied field's highest dielectric loss, or greatest absorption, at a particular frequency. Because the phases of nanocomposites have different dielectric constants and conductivities, the absorption occurs due to the Maxwell-Wagner phenomenon, which is brought on by A.C. current [150]. Figure (4-17 B) shows the correlation between silica content and dielectric loss. It is obvious from the Figure that the notable increase in values of the charge carriers was brought by an increase in SiO_2 NPs concentration. This behavior follows previous studies [151].

Figure (4-17). Relationship between dielectric loss with (A) frequency and (B) concentration of SiO_2 NPs for samples.

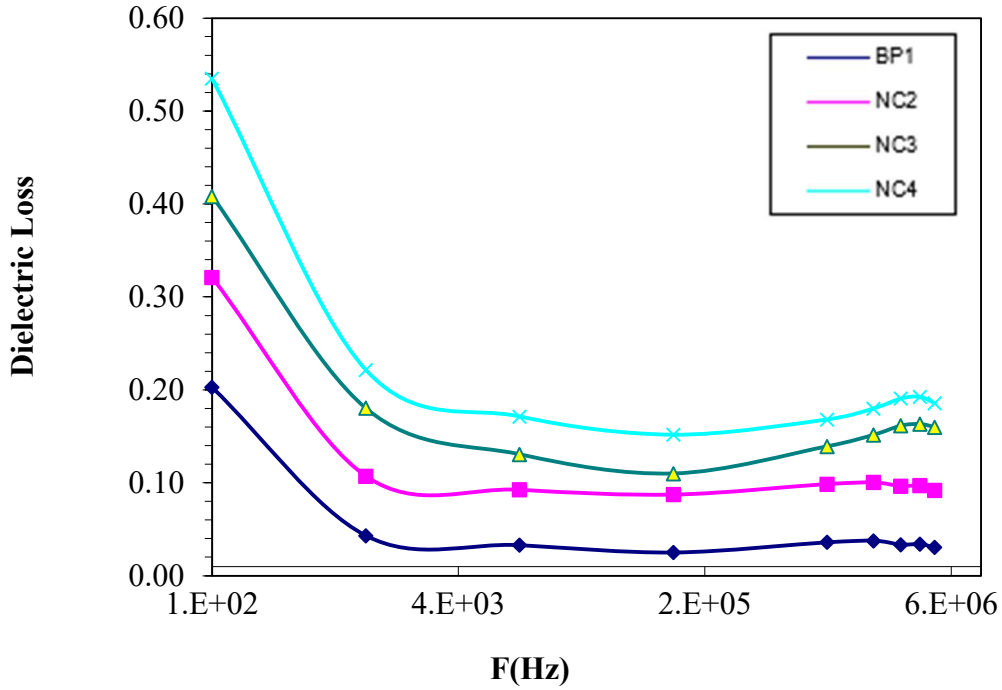

(A)

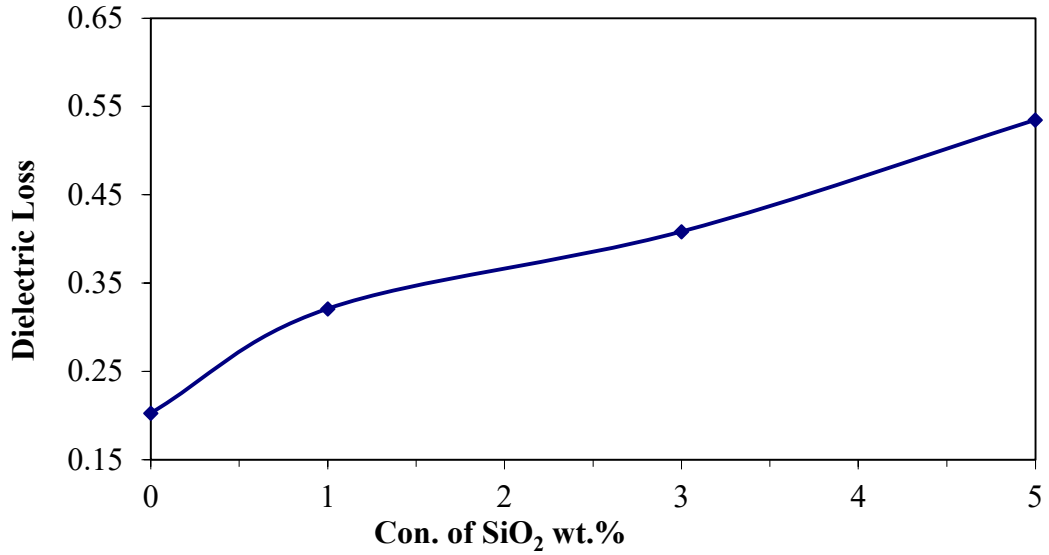

(B)

4.4.3 Electrical conductivity

The A.C. electrical conductivity was calculated from the Equation (2.45) and revealed in Figure (4-18 A) with frequency. As shown in the Figure, the space charge polarization at low frequencies and the migration of charge carriers due to the hopping process are responsible for the rise in AC conductivity. At high frequencies, the conductivity improved with increased SiO_2 NPs in the polymer matrix, as also presented in Figure (4-18 B). The electronic polarization and the charge carriers that move by the hopping process also increase, along with the A.C electrical conductivity. The impact of space fees is to blame for this increase and the formation of a continuous network from SiO_2 inside the (PAAm-PVA-PVP). This behavior is in agreement with previous studies [151] .

Figure (4-18). the dependence on A.C. electrical conductivity (A) with frequency and (B) the concentration of SiO_2 NPs of samples.

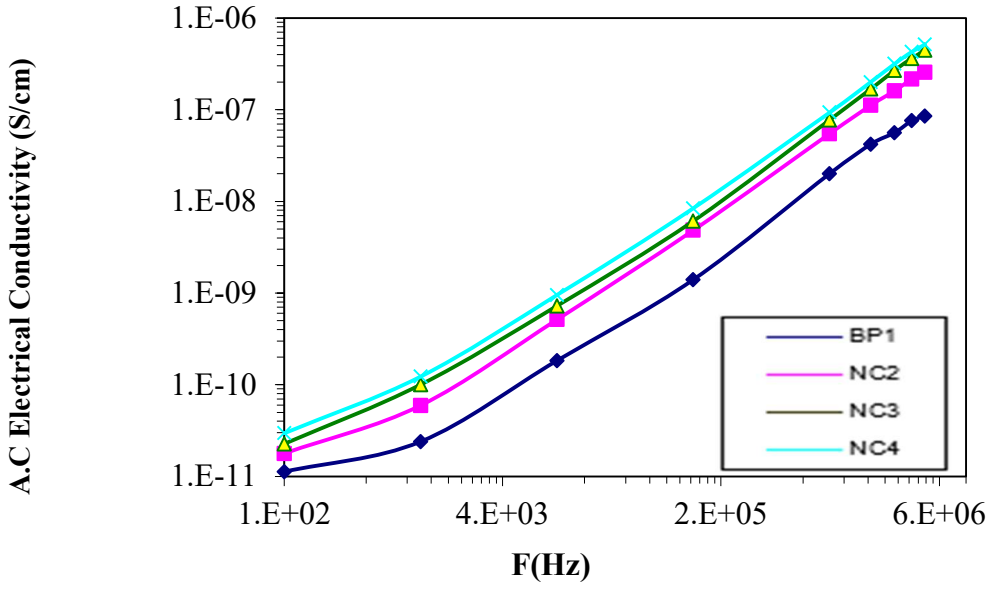

(A)

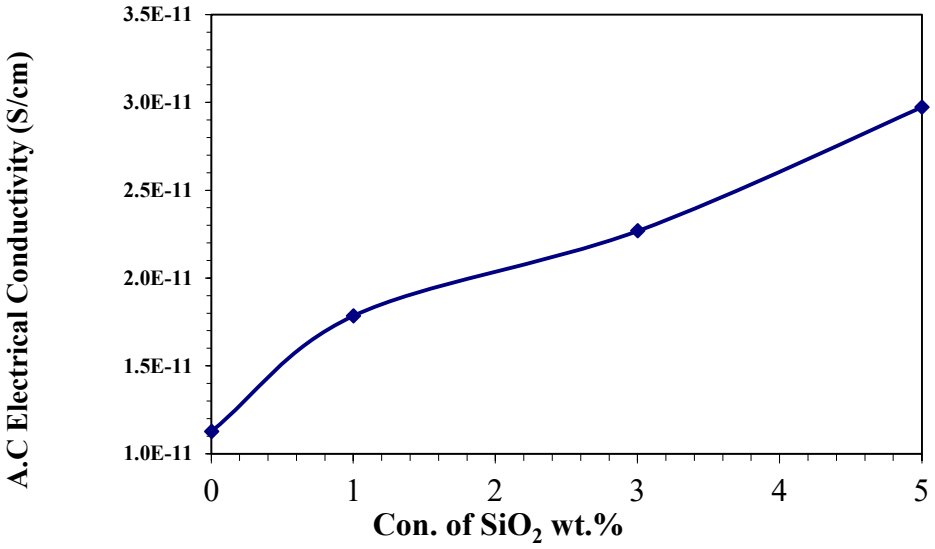

(B)

4.5 Applications

4.5.1 Antibacterial Activity

Figure (4-19) shows the image for inhibition zones of samples against the Escherichia coli and Staphylococcus aureus as gram-negative and positive bacteria, respectively. The BP1 revealed negative resistance and no killing bacteria for both bicriteria. This finding agrees with other researchers proved of these polymers, where PAAm exhibited a lack of biological activity [152]. Interestingly, the contribution of 0.01 wt. % of nanoparticles with the same polymer consecrations of NC1 revealed notable improvements of the antibacterial activity from 0 to 20 and 18 mm, respectively, compared to BP1.Meanwhile, increasing the SiO_2 loading to 0.05 wt. % revealed significant improving the inhibition zone up to 24 and 23 mm, respectively, shown in Figure (4-20). Reactive oxygen species (ROS) are produced by nanoparticles and cause the bactericidal action of nanostructures. The electrostatic interaction between the nanoparticles of nanocomposites and the bacteria causes the germs to oxidize and

die instantly since the nanocomposites contain positive charges, while the microbes have negative charges. Singlet oxygen (O_2) may be the culprit for destroying the DNA and proteins of bacteria, and ROS, which includes radicals like superoxide radicals, Hydrogen peroxide with hydroxyl radicals (OH) (O-2) (H_2O_2), is the primary mechanism causing the antibacterial activity of nanocomposites by the nanoparticles. Through the results, it was found that the polymer material did not show any activity to kill bacteria, and this activity increased with increasing concentrations, and these results show the susceptibility of these compounds to be used in the treatment and killing of bacteria as antiseptics, as well as biological sensors and other applications in this field [41,153].

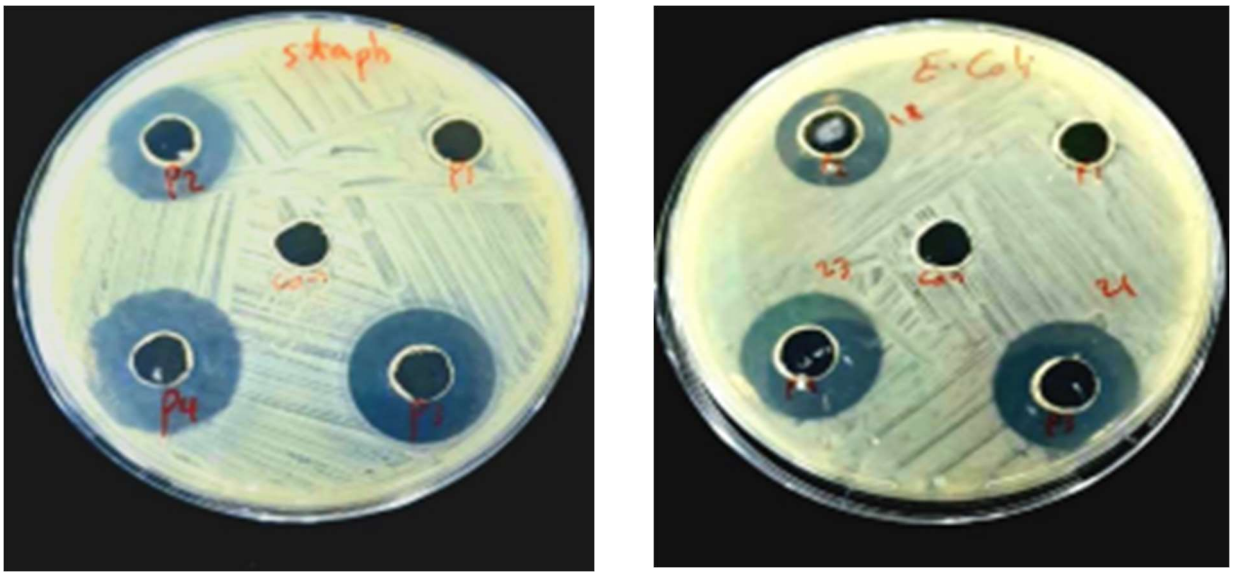

(A) **(B)**

Figure (4-19). Image for inhibition zones of (A) S. aureus and (B) E. coli for samples

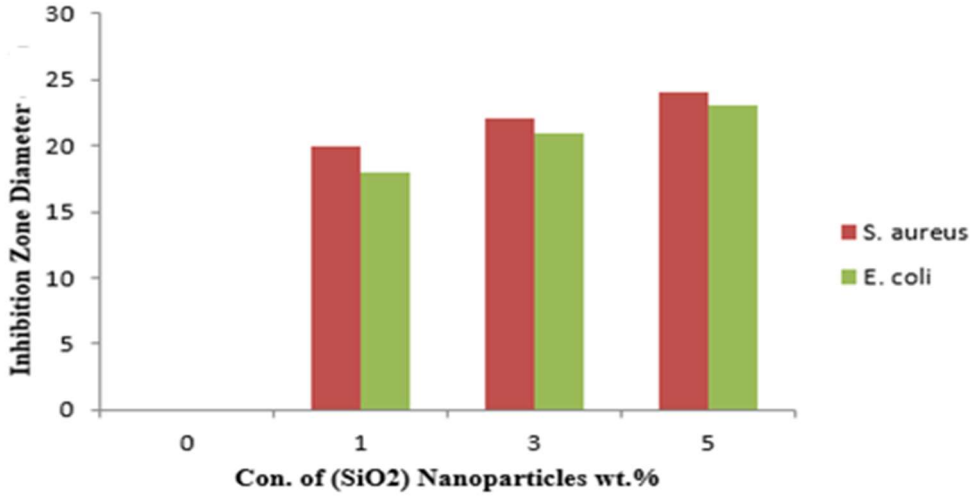

Figure (4-20). Antibacterial inhibition zones of S. aureus E. and coli. for samples as a function of SiO_2 nanoparticle concentrations.

4.5.2 The radiation ray Shielding

Absorption of mixed polymer radiation and effect silicon dioxide in this absorption is explained. The Figure (4-21) shows the absorption coefficient. Through it demonstrates the increased effect of the nanomaterial led to increased absorption (attenuation) compared with polymeric mixtures while Figure (4-22) shows the ratio between the radiation attenuation (N) with the number of radiation particles (N_o) as(N/N_o) calculated from Equation (2.48), which increases as the concentration of the nanomaterial increases. Figure (4-23) shows the attenuation coefficient of the source radiation (μ), which increases with the increasing concentration of the nanomaterial .From the results obtained, it turned out that the effect of the nanomaterial is important and led to an increase in the attenuation of the rays, and the best sample was NC4, and it can be used in shielding as suits for laboratory workers, the manufacture of special glasses, protective films and others This possibility led to radiation absorption through nano communications that have dropped dramatically compared to blended polymers. The scattered

shape of the two sides reduces the assimilation of Lambert's law [154].These results show promising absorption capacity of these ionizing radiation samples which opens the wide application in absorbing ionizing radiation.

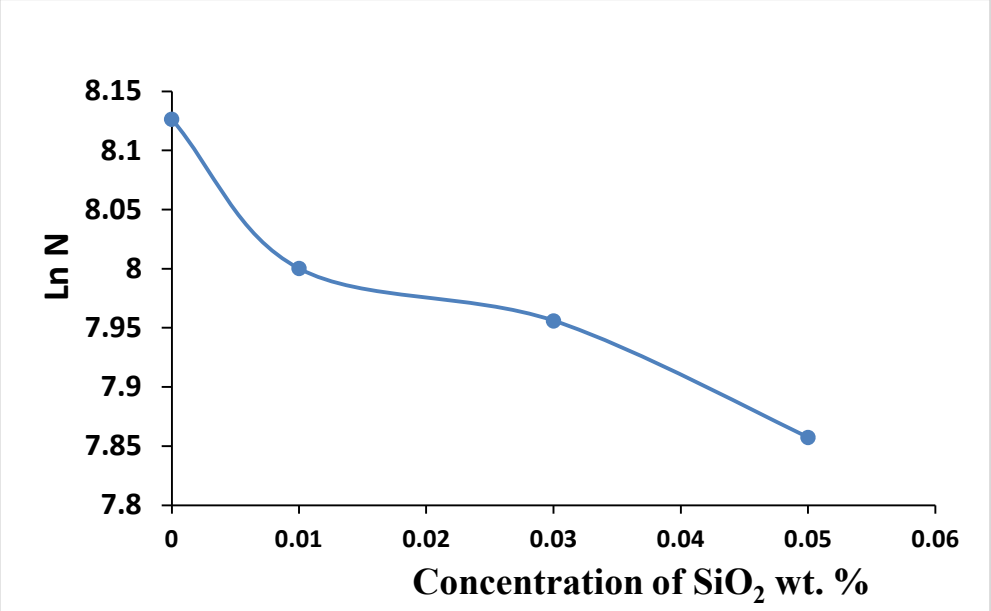

Figure (4-21). The Ln N of radiation attenuation (N) for samples

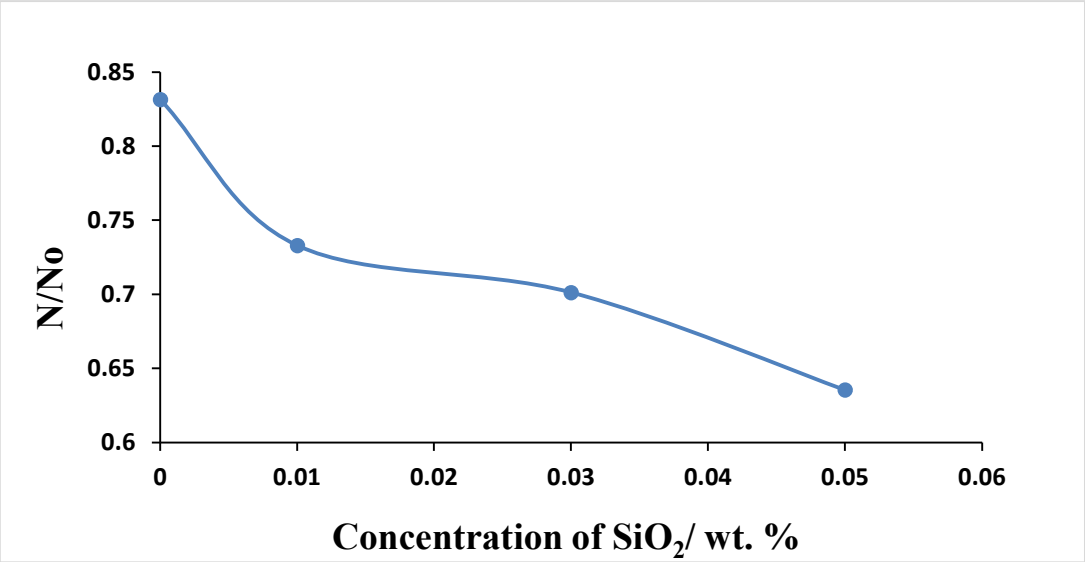

Figure (4-22). The relationship between the radiation attenuation (N) with the number of radiation particles (No) as (N/No) concentrations of SiO_2 for samples.

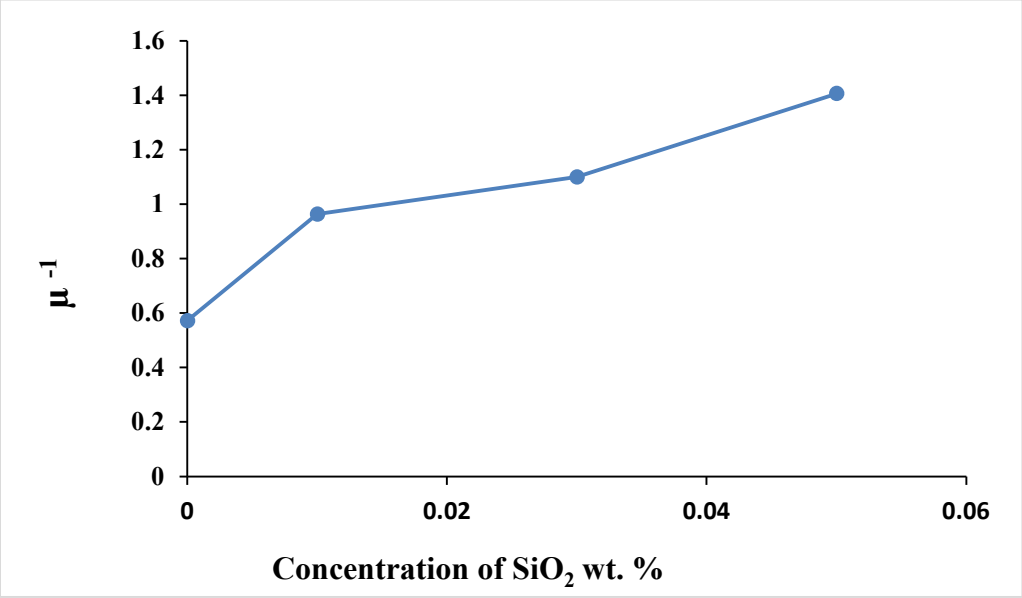

radiation (μ) and Concentration of SiO_2 wt. % for sample

Chapter Five
Conclusions and Future Works

5. 1 Conclusions

1-The following procedure successfully fabricated new nanocomposites using ternary blend polymers PAAm-PVA-PVP reinforced by SiO_2 NPs.

2- The FTIR and XRD present strong interfacial interactions. OM and FE-SEM images showed a homogeneous surface, and cracks were significantly reduced in the surface with increasing the nanoparticle concentrations.

3- From the optical properties of the nanocomposite, the absorption was improved increased from 0.73 to 0.91 at 200 wavenumber, the refractive index of the absorption coefficient, extinction coefficient, real and imaginary dielectric constant and optical conductivity improved with increasing concentration of SiO_2 NPS, while the permeability and indirect energy gap decreased with increasing concentration of SiO_2 NPS.

4-Dielectric constant improved from (0.20 to 0.53) Hz, loss constant improved for nanocomposites were reduced, whereas AC electrical conductivity increases for nanocomposites with the increase in the SiO_2 contained in the matrix.

5- Antibacterial activity for nanocomposites showed enhancement in the inhibition zone value from 0.00 to 24 mm of S. aureus and 23 mm of coli concentration of SiO_2 nanoparticles which may be used for antibacterial application.

6- gamma ray shielding applications for nanocomposites showed the transmission radiation decreased with the increasing of the SiO_2 concentrations. The attenuation coefficients from 0.5 to 1.4 increase with increase of SiO_2 nanoparticles concentration.

7- These nanocomposites are promising for various applications, such as solar cells, optoelectronic, biology applications. and gamma ray shielding.

5.2 Future Works

1- Studying the rheological properties of nanocomposites (PAAm-PVA-PMMA/SiO_2).

2- Studying the mechanical properties of nanocomposites (PAAm- PVA-PVP/SiO_2).

3- Preparation of nano communications (PAAm-PVA-PVP/SiO_2).and check their thermal properties.

4- Study the ability to predive soler cell and maser their efficacy.

References

References

[1] Y. Wang, J. Chen, H. Do Kim, B. Wang, R. Iriguchi, and H. Ohkita, "Ternary blend solar cells based on a conjugated polymer with diketopyrrolopyrrole and carbazole units," *Front. Energy Res.*, vol. 6, p. 113, 2018.

[2] B. Ali Al-Asbahi, S. M. H. Qaid, H. M. Ghaithan, and A. Alhamedi Alanezi, "Influence of SiO2/TiO2 nanocomposites on dual resonance Förster energy transfer in ternary hybrid thin films," *Results in Physics*, vol. 24. 2021. doi: 10.1016/j.rinp.2021.104142.

[3] L. Lu, W. Chen, T. Xu, and L. Yu, "High-performance ternary blend polymer solar cells involving both energy transfer and hole relay processes," *Nat. Commun.*, vol. 6, no. 1, p. 7327, 2015.

[4] K. M. Golant, "Bulk silicas prepared by low pressure plasma CVD: formation of structure and point defects," *Defects SiO 2 Relat. Dielectr. Sci. Technol.*, pp. 427–452, 2000.

[5] Z. Wan, S. Huang, M. A. Green, and G. Conibeer, "Rapid thermal annealing and crystallization mechanisms study of silicon nanocrystal in silicon carbide matrix," *Nanoscale Res. Lett.*, vol. 6, no. 1, pp. 1–7, 2011.

[6] M. Grayson, "Encyclopedia of composite materials and components," 1983.

[7] E. Al-Bermany, A. T. Mekhalif, H. A. Banimuslem, K. Abdali, and M. M. Sabri, "Effect of green synthesis bimetallic Ag@ SiO2 core–shell nanoparticles on absorption behavior and electrical properties of PVA-PEO nanocomposites for optoelectronic applications," *Silicon*, pp. 1–13, 2023.

[8] S. Choudhary, “Characterization of amorphous silica nanofiller effect on the structural, morphological, optical, thermal, dielectric and electrical properties of PVA–PVP blend based polymer nanocomposites for their flexible nanodielectric applications,” *J. Mater. Sci. Mater. Electron.*, vol. 29, no. 12, pp. 10517–10534, 2018.

[9] G. A. Kontos *et al.*, “Electrical relaxation dynamics in TiO2-polymer matrix composites,” *Express Polym Lett*, vol. 1, no. 12, pp. 781–789, 2007.

[10] M. A. Habeeb, A. Hashim, and B. H. Rabee, “Study the Electrical Properties of PS-CaO Composites,” *Am. J. Sci. Res.*, no. 72, pp. 5–9, 2012.

[11] G. A. Kontos, A. L. Soulintzis, P. K. Karahaliou, G. C. Psarras, and S. N. Georga, “CA krontiras, and MN Pisanias, Express Polym,” *Lett*, vol. 1, p. 781, 2007.

[12] S. Hossain, “Optical properties of polymers and their applications,” 2019.

[13] M. Naeimirad, A. Zadhoush, and R. E. Neisiany, “Fabrication and characterization of silicon carbide/epoxy nanocomposite using silicon carbide nanowhisker and nanoparticle reinforcements,” *J. Compos. Mater.*, vol. 50, no. 4, pp. 435–446, 2016.

[14] A. J. Crosby and J. Lee, “Polymer nanocomposites: the ‘nano’ effect on mechanical properties,” *Polym. Rev.*, vol. 47, no. 2, pp. 217–229, 2007.

[15] R. Kochetov, “Thermal and electrical properties of nanocomposites, including material properties,” 2012.

[16] J. Jagur-Grodzinski, “Modification of polymers under heterogeneous conditions,” *Prog. Polym. Sci.*, vol. 17, no. 3, pp. 361–415, 1992.

[17] C. Sun, *Controlling the rheology of polymer/silica nanocomposites*. 2010.

[18] M. Shahbazi, A. Bahari, and S. Ghasemi, "Structural and frequency-dependent dielectric properties of PVP-SiO2-TMSPM hybrid thin films," *Org. Electron.*, vol. 32, pp. 100–108, May 2016, doi: 10.1016/j.orgel.2016.02.012.

[19] Z.-K. Li, W.-Z. Lang, W. Miao, X. Yan, and Y.-J. Guo, "Preparation and properties of PVDF/SiO2@ GO nanohybrid membranes via thermally induced phase separation method," *J. Memb. Sci.*, vol. 511, pp. 151–161, 2016.

[20] S. Z. Haeri, B. Ramezanzadeh, and M. Asghari, "A novel fabrication of a high performance SiO2-graphene oxide (GO) nanohybrids: Characterization of thermal properties of epoxy nanocomposites filled with SiO2-GO nanohybrids," *J. Colloid Interface Sci.*, vol. 493, pp. 111–122, 2017.

[21] P. Paik, K. S. Kumar, M. Das Modak, K. Kumar, and S. Maity, "UCN–SiO 2–GO: a core shell and conjugate system for controlling delivery of doxorubicin by 980 nm NIR pulse," *RSC Adv.*, vol. 8, no. 65, pp. 37492–37502, 2018.

[22] L. H. Gaabour, "Influence of silica nanoparticles incorporated with chitosan/polyacrylamide polymer nanocomposites," *J. Mater. Res. Technol.*, vol. 8, no. 2, pp. 2157–2163, 2019.

[23] S. A. Haddadi, A. R. Saadatabadi, A. Kheradmand, M. Amini, and M. Ramezanzadeh, "SiO2-covered graphene oxide nanohybrids for in situ preparation of UHMWPE/GO (SiO2) nanocomposites with superior mechanical and tribological properties," *J. Appl. Polym. Sci.*, vol. 136, no. 31, p. 47796, 2019.

[24] R. Dong, L. Wang, J. Zhu, L. Liu, and Y. Qian, “A novel SiO 2–GO/acrylic resin nanocomposite: Fabrication, characterization and properties,” *Appl. Phys. A*, vol. 125, pp. 1–11, 2019.

[25] O. H. Sabr, H. J. Kadhim, and M. M. Salman, “Studying the Effect of Silica Nanoparticles on Optical Properties of Polyvinyl Alcohol Thin Films for Semi-conductors Applications,” 2020.

[26] A. M. Alsaad, A. A. Ahmad, A. R. Al Dairy, A. S. Al-anbar, and Q. M. Al-Bataineh, “Spectroscopic characterization of optical and thermal properties of (PMMA-PVA) hybrid thin films doped with SiO2 nanoparticles,” *Results Phys.*, vol. 19, p. 103463, 2020.

[27] A. Hashim, “Fabrication and characteristics of flexible, lightweight, and low-cost pressure sensors based on PVA/SiO2/SiC nanostructures,” *J. Mater. Sci. Mater. Electron.*, vol. 32, no. 3, pp. 2796–2804, Feb. 2021, doi: 10.1007/s10854-020-05032-9.

[28] T. S. Soliman, S. A. Vshivkov, and S. I. Elkalashy, “Structural, thermal, and linear optical properties of SiO2 nanoparticles dispersed in polyvinyl alcohol nanocomposite films,” *Polym. Compos.*, vol. 41, no. 8, pp. 3340–3350, 2020.

[29] K. Abdali, “Structural, optical, electrical properties, and relative humidity sensor application of PVA/Dextrin polymeric blend loaded with silicon dioxide nanoparticles,” *J. Mater. Sci. Mater. Electron.*, vol. 33, no. 23, pp. 18199–18208, 2022.

[30] N. K. Al-Sharifi and M. A. Habeeb, “Synthesis and Exploring Structural and Optical Properties of Ternary PS/SiC/Sb2O3 Nanocomposites for Optoelectronic and Antimicrobial Applications,” *Silicon*, pp. 1–11, 2023.

[31] V. K. Sharma, D. G. Hayes, V. S. Urban, H. M. O’Neill, M. Tyagi, and E.

Mamontov, “Nanoscopic dynamics of bicontinous microemulsions: effect of membrane associated protein,” *Soft Matter*, vol. 13, no. 28, pp. 4871–4880, 2017.

[32] H. Zheng, “Polymers for structure design of dairy foods,” in *Polymers for food applications*, Springer, 2018, pp. 509–528.

[33] X. Zhang, Y. Su, L. Lei, S. Wu, and J. Shen, “Preparation of a three-dimensional modified graphene oxide via RAFT polymerization for reinforcing cement composites,” *Colloids Surfaces A Physicochem. Eng. Asp.*, vol. 610, p. 125925, 2021.

[34] G. Akovali, *Handbook of composite fabrication*. iSmithers Rapra Publishing, 2001.

[35] G. L. Wilkes, “Polymer Materials Science.: By Jerold Schultz, Department of Chemical Engineering, University of Delaware. Published by Prentice-Hall, Englewood Cliffs, NJ, 1974.” Elsevier, 1974.

[36] C. E. Carraher, *Carraher’s polymer chemistry*. CRC press, 2017.

[37] C. B. Crawford and B. Quinn, “Physiochemical properties and degradation,” *Microplastic Pollut.*, vol. 4, pp. 57–100, 2017.

[38] F. Auriemma, G. C. Alfonso, and C. De Rosa, “Polymer Crystallization I,” *Springer2017*, 2017.

[39] D. Liu *et al.*, “Surface functionalization of ZnO nanotetrapods with photoactive and electroactive organic monolayers,” *Langmuir*, vol. 24, no. 9, pp. 5052–5059, 2008.

[40] L. A. Kolahalam, I. V. K. Viswanath, B. S. Diwakar, B. Govindh, V. Reddy, and Y. L. N. Murthy, “Review on nanomaterials: Synthesis and applications,” *Mater. Today Proc.*, vol. 18, pp. 2182–2190, 2019.

[41] A. Thabet, Y. A. Mubarak, and M. Bakry, “A review of nano-fillers effects on industrial polymers and their characteristics,” *J. Eng. Sci*, vol. 39, pp. 377–403, 2011.

[42] M. Bhattacharya, “Polymer nanocomposites—a comparison between carbon nanotubes, graphene, and clay as nanofillers,” *Materials (Basel).*, vol. 9, no. 4, p. 262, 2016.

[43] K. Abdali, K. H. Abass, E. Al-bermany, E. M. Al-robayi, and A. M. Kadim, “Morphological, Optical, ElectricalCharacterizations and Anti-Escherichia coli Bacterial Efficiency (AECBE) of PVA/PAAm/PEO Polymer Blend Doped with Silver NPs,” *Nano Biomed. Eng.*, vol. 14, no. 2, pp. 114–122, 2022, doi: 10.5101/nbe.v14i2.p114-122.Abstract.

[44] F. W. Billmeyer, “Textbook of Polymer Science,” *Kobunshi*, vol. 12, no. 3, pp. 240–251, 1963, doi: 10.1295/kobunshi.12.240.

[45] Z. Guo *et al.*, “Effects of iron oxide nanoparticles on polyvinyl alcohol: interfacial layer and bulk nanocomposites thin film,” *J. Nanoparticle Res.*, vol. 12, no. 7, pp. 2415–2426, 2010.

[46] K. H. H. Al-Attiyah, A. Hashim, and S. F. Obaid, “Fabrication of novel (carboxy methyl cellulose–polyvinylpyrrolidone–polyvinyl alcohol)/lead oxide nanoparticles: structural and optical properties for gamma rays shielding applications,” *Int. J. Plast. Technol.*, vol. 23, no. 1, pp. 39–45, Jun. 2019, doi: 10.1007/s12588-019-09228-5.

[47] H.-D. Wu, I.-D. Wu, and F.-C. Chang, “The interaction behavior of polymer electrolytes composed of poly (vinyl pyrrolidone) and lithium perchlorate (LiClO4),” *Polymer (Guildf).*, vol. 42, no. 2, pp. 555–562, 2001.

[48] M. T. Razzak, S. P. Dewi, H. Lely, and E. Taty, “The characterization of

dressing component materials and radiation formation of PVA–PVP hydrogel," *Radiat. Phys. Chem.*, vol. 55, no. 2, pp. 153–165, 1999.

[49] C. M. Hassan and N. A. Peppas, "Structure and Applications of Poly(vinyl alcohol) Hydrogels Produced by Conventional Crosslinking or by Freezing/Thawing Methods," in *Biopolymers · PVA Hydrogels, Anionic Polymerisation Nanocomposites*, vol. 153, Berlin, Heidelberg: Springer Berlin Heidelberg, 2000, pp. 37–65. doi: 10.1007/3-540-46414-X_2.

[50] C. Ravindra, M. Sarswati, G. Sukanya, P. Shivalila, Y. Soumya, and K. Deepak, "Tensile and thermal properties of poly (vinyl pyrrolidone)/vanillin incorporated poly (vinyl alcohol) films," *Res. J. Phys. Sci*, vol. 3, no. 1, 2015.

[51] C. Srikanth, B. C. Sridhar, M. V. N. Prasad, and R. D. Mathad, "Characterization and DC conductivity of novel ZnO doped polyvinyl alcohol (PVA) nano-composite films," *J. Adv. Phys.*, vol. 5, no. 2, pp. 105–109, 2016.

[52] A. Gautam and S. Ram, "Preparation and thermomechanical properties of Ag-PVA nanocomposite films," *Mater. Chem. Phys.*, vol. 119, no. 1–2, pp. 266–271, 2010.

[53] A. Tawansi and H. M. Zidan, "Tunnelling and thermally stimulated phenomena in highly filled PMMA composites," *Int. J. Polym. Mater.*, vol. 15, no. 2, pp. 77–83, 1991.

[54] A.-K. J. Rashid, E. D. Jawad, B. Y. Kadem, A. K. J. Al-Bermany, E. Al-Bermany, and B. Y. Kadem, "A study of some mechanical properties of iraqi palm fiber-PVA composite by ultrasonic," *Eur. J. Sci. Res.*, vol. 61, no. 2, pp. 203–209, 2011.

[55] E. Jawad, S. H. Khudhair, and H. N. Ali, "A thermodynamic study of

adsorption of some days on Iraqi Bentoniet modified clay," *Eur. J. Sci. Res.*, vol. 60, no. 1, pp. 63–70, 2011.

[56] M. Liu, B. Guo, M. Du, and D. Jia, "Drying induced aggregation of halloysite nanotubes in polyvinyl alcohol/halloysite nanotubes solution and its effect on properties of composite film," *Appl. Phys. A*, vol. 88, no. 2, pp. 391–395, 2007.

[57] H. C. Schniepp *et al.*, "Functionalized single graphene sheets derived from splitting graphite oxide," *J. Phys. Chem. B*, vol. 110, no. 17, pp. 8535–8539, 2006.

[58] G. Wang, B. Wang, J. Park, J. Yang, X. Shen, and J. Yao, "Synthesis of enhanced hydrophilic and hydrophobic graphene oxide nanosheets by a solvothermal method," *Carbon N. Y.*, vol. 47, no. 1, pp. 68–72, 2009.

[59] E. H. Nicollian and J. R. Brews, *MOS (metal oxide semiconductor) physics and technology*. John Wiley & Sons, 2002.

[60] R. Salh, "Defect related luminescence in silicon dioxide network: a review," *Cryst. Silicon-Properties Uses*, pp. 135–172, 2011.

[61] A. Paleari, N. Chiodini, D. Di Martino, and F. Meinardi, "Radiative decay of vacuum-ultraviolet excitation of silica synthesized by molecular precursors of Si-Si sites: An indicator of intracenter relaxation of neutral oxygen vacancies," *Phys. Rev. B*, vol. 71, no. 7, p. 75101, 2005.

[62] P. Pellegrino *et al.*, "Time-resolved analysis of the white photoluminescence from SiO 2 films after Si and C coimplantation," *Appl. Phys. Lett.*, vol. 84, no. 1, pp. 25–27, 2004.

[63] G. Pacchioni, L. Skuja, and D. L. Griscom, *Defects in SiO2 and related dielectrics: science and technology*, vol. 2. Springer Science & Business

Media, 2012.

[64] P. D. Persans, A. Ruppert, and B. Abeles, “Crystallization kinetics of amorphous Si/SiO2 superlattice structures,” *J. Non. Cryst. Solids*, vol. 102, no. 1–3, pp. 130–135, 1988.

[65] S. Guo and E. Wang, “Synthesis and electrochemical applications of gold nanoparticles,” *Anal. Chim. Acta*, vol. 598, no. 2, pp. 181–192, 2007.

[66] R. Shukla *et al.*, “Optical and electrical properties of Si nanocrystals embedded in SiC matrix,” *Adv. Mater. Lett.*, vol. 3, no. 4, pp. 297–304, 2012.

[67] C. ATSDR and C. CDC-INFO, “Toxic Substances Portal.” 2010.

[68] W. S. Lau, *Infrared characterization for microelectronics*. World scientific, 1999.

[69] I. Ferreira, J. Ferreira-Strixino, M. L. Castilho, C. B. L. Campos, C. Tellez, and L. Raniero, “Characterization of Paracoccidioides brasiliensis by FT-IR spectroscopy and nanotechnology,” *Spectrochim. Acta Part A Mol. Biomol. Spectrosc.*, vol. 152, pp. 397–403, 2016.

[70] A. A. Bunaciu, E. G. UdriŞTioiu, and H. Y. Aboul-Enein, “X-ray diffraction: instrumentation and applications,” *Crit. Rev. Anal. Chem.*, vol. 45, no. 4, pp. 289–299, 2015.

[71] L. Reimer, *Transmission electron microscopy: physics of image formation and microanalysis*, vol. 36. Springer, 2013.

[72] G. Cao and C. J. Brinker, “Annual Review of Nano Research, Volume 1,” 2006.

[73] C. Kittel and P. McEuen, *Introduction to solid state physics*. John Wiley

& Sons, 2018.

[74] M. Qiu, Y. Zhang, and B. Wen, “Facile synthesis of polyaniline nanostructures with effective electromagnetic interference shielding performance,” *J. Mater. Sci. Mater. Electron.*, vol. 29, no. 12, pp. 10437–10444, 2018.

[75] S. L. Erlandsen, C. Frethem, and Y. Chen, “Field emission scanning electron microscopy (FESEM) entering the 21st century: nanometer resolution and molecular topography of cell structure,” *J. Histotechnol.*, vol. 23, no. 3, pp. 249–259, 2000.

[76] O. Stenzel, *The physics of thin film optical spectra*. Springer, 2015.

[77] M. A. Omar, *Elementary solid state physics: principles and applications*. Pearson Education India, 1975.

[78] T. K. Hamad, “Refractive index dispersion and analysis of the optical parameters of (PMMA/PVA) Thin film,” *Al-Nahrain J. Sci.*, vol. 16, no. 3, pp. 164–170, 2013.

[79] D. A. Neamen, “Semiconductor physics and devices: basic principles, Irwin,” *Inc, Universty New Mex.*, 1992.

[80] A. N. Alias, Z. M. Zabidi, A. M. M. Ali, M. K. Harun, and M. Z. A. Yahya, “Optical characterization and properties of polymeric materials for optoelectronic and photonic applications,” *Int. J. Appl. Sci. Technol.*, vol. 3, no. 5, 2013.

[81] J. I. Pankove, “Optical processes on semiconductors Dover publication,” *Inc. New york*, 1971.

[82] J. Tauc, A. Menth, and D. L. Wood, “Optical and magnetic investigations of the localized states in semiconducting glasses,” *Phys. Rev. Lett.*, vol.

25, no. 11, p. 749, 1970.

[83] D. A. Neamen, “Semiconductor Physics and Devices, University of New Mexico, Richard D. Irwin.” Inc, 1992.

[84] K. L. Chopra, P. D. Paulson, and V. Dutta, “Thin-film solar cells: an overview,” *Prog. Photovoltaics Res. Appl.*, vol. 12, no. 2-3, pp. 69–92, 2004.

[85] V. N. Suryawanshi, A. S. Varpe, M. D. Deshpande, A. S. Varpe, and M. D. Deshpande, “Band gap engineering in PbO nanostructured thin films by Mn doping,” 2017, doi: 10.1016/j.tsf.2017.10.016.

[86] A. Kirschning, W. Solodenko, and K. Mennecke, “Combining enabling techniques in organic synthesis: continuous flow processes with heterogenized catalysts,” *Chem. Eur. J.*, vol. 12, no. 23, pp. 5972–5990, 2006.

[87] N. A. Azahari, N. Othman, and H. Ismail, “Biodegradation studies of polyvinyl alcohol/corn starch blend films in solid and solution media,” *J. Phys. Sci.*, vol. 22, no. 2, pp. 15–31, 2011.

[88] M. Y. Nadeem and W. Ahmed, “Optical properties of ZnS thin films,” *Turkish J. Phys.*, vol. 24, no. 5, pp. 651–659, 2000.

[89] N. E. Hill, W. E. Vaughan, A. Price, and M. Davies, *Dielectric properties and molecular behaviour*. Van Nostrand Reinhold, 1969.

[90] A. J. Braihi, J. K. Ahmed, and D. abbass Kadham, “Preparing Medical (Polyvinyl Alcohol-Iodine) As A Pressure Sensor and Investigating Its Physical Properties,” *Int. J. Pharm. Phytopharm. Res.*, vol. 7, no. 1, pp. 34–41, 2017.

[91] H. Fröhlich, *Theory of dielectrics: dielectric constant and dielectric loss*,

vol. 190. Oxford University Press, USA, 1958.

[92] A. Muheisin, “Study of electrical conductivity for amorphous and semi crystalline polymers filled with Lithium Fluoride Additive.” M. Sc. Thesis, University of Mustansiriah, College of Science, 2009.

[93] J. D. Mackenzie and D. R. Ulrich, “Sol-gel optics, present status and future trends,” *Sol-gel Opt.*, vol. 1328, pp. 2–13, 1990.

[94] R. C. Dorf, *The engineering handbook*. CRC press, 2018.

[95] B. H. Rabee and R. Haider, “The effect of adding Ag nanoparticles on the electrical properties (AC) of the PMMA-SPO-PS blend,” in *Journal of Physics: Conference Series*, 2021, vol. 1973, no. 1, p. 12102.

[96] A. R. Blythe, T. Blythe, and D. Bloor, *Electrical properties of polymers*. Cambridge university press, 2005.

[97] J. D. Irwin, *The industrial electronics handbook*. CRC press, 1997.

[98] W. Levinson and E. Jawetz, *Medical microbiology and immunology: examination and board review*. Appleton & Lange, 1996.

[99] Z. L. Wang, “Zinc oxide nanostructures: growth, properties and applications,” *J. Phys. Condens. matter*, vol. 16, no. 25, p. R829, 2004.

[100] A. M. Cole *et al.*, “Determinants of Staphylococcus aureus nasal carriage,” *Clin. Diagnostic Lab. Immunol.*, vol. 8, no. 6, pp. 1064–1069, 2001.

[101] O. P. Sah, “Prescribing and sensitivity patterns of antimicrobials in uncomplicated urinary tract infections in females,” *J. Drug Deliv. Ther.*, vol. 4, no. 2, pp. 1–8, 2014.

[102] K. R. Park and Y. C. Nho, “Preparation and characterization by radiation

of hydrogels of PVA and PVP containing Aloe vera," *J. Appl. Polym. Sci.*, vol. 91, no. 3, pp. 1612–1618, 2004.

[103] A. L. Cogen, V. Nizet, and R. L. Gallo, "Skin microbiota: a source of disease or defence?," *Br. J. Dermatol.*, vol. 158, no. 3, pp. 442–455, 2008.

[104] P. R. Murray, E. J. Baron, J. H. Jorgensen, M. L. Landry, and M. A. Pfaller, "Manual of Clinical Microbiology. Ed. 9th." Washington DC: ASM Press American Society for Microbiology, 2007.

[105] H. Li, Q. Chen, J. Zhao, and K. Urmila, "Enhancing the antimicrobial activity of natural extraction using the synthetic ultrasmall metal nanoparticles," *Sci. Rep.*, vol. 5, no. 1, p. 11033, 2015.

[106] I. Armentano *et al.*, "The interaction of bacteria with engineered nanostructured polymeric materials: a review," *Sci. World J.*, vol. 2014, 2014.

[107] W. Gao, S. Thamphiwatana, P. Angsantikul, and L. Zhang, "Nanoparticle approaches against bacterial infections," *Wiley Interdiscip. Rev. nanomedicine nanobiotechnology*, vol. 6, no. 6, pp. 532–547, 2014.

[108] B. Luan, T. Huynh, and R. Zhou, "Complete wetting of graphene by biological lipids," *Nanoscale*, vol. 8, no. 10, pp. 5750–5754, 2016.

[109] A. Raghunath and E. Perumal, "Metal oxide nanoparticles as antimicrobial agents: a promise for the future," *Int. J. Antimicrob. Agents*, vol. 49, no. 2, pp. 137–152, 2017.

[110] N. R. Council, "BEIR VII: health risks from exposure to low levels of ionizing radiation: report in brief," in *Natl Acad*, 2006, vol. 93, p. 93.

[111] R. H. Mole, "Ionizing radiation as a carcinogen: practical questions and academic pursuits," *Br. J. Radiol.*, vol. 48, no. 567, pp. 157–169, 1975.

[112] M. Erdem, O. Baykara, M. Doğru, and F. Kuluöztürk, “A novel shielding material prepared from solid waste containing lead for gamma ray,” *Radiat. Phys. Chem.*, vol. 79, no. 9, pp. 917–922, 2010.

[113] E. Yılmaz, H. Baltas, E. Kırıs, İ. Ustabas, U. Cevik, and A. M. El-Khayatt, “Gamma ray and neutron shielding properties of some concrete materials,” *Ann. Nucl. Energy*, vol. 38, no. 10, pp. 2204–2212, 2011.

[114] C. Zeitlin, S. B. Guetersloh, L. H. Heilbronn, and J. Miller, “Measurements of materials shielding properties with 1 GeV/nuc 56Fe,” *Nucl. Instruments Methods Phys. Res. Sect. B Beam Interact. with Mater. Atoms*, vol. 252, no. 2, pp. 308–318, 2006.

[115] I. Akkurt, H. Akyildirim, B. Mavi, S. Kilincarslan, and C. Basyigit, “Gamma-ray shielding properties of concrete including barite at different energies,” *Prog. Nucl. Energy*, vol. 52, no. 7, pp. 620–623, 2010.

[116] İ. Türkmen, Y. Özdemir, M. Kurudirek, F. Demir, Ö. Simsek, and R. Demirboğa, “Calculation of radiation attenuation coefficients in Portland cements mixed with silica fume, blast furnace slag and natural zeolite,” *Ann. Nucl. Energy*, vol. 35, no. 10, pp. 1937–1943, 2008.

[117] C. Bootjomchai, J. Laopaiboon, C. Yenchai, and R. Laopaiboon, “Gamma-ray shielding and structural properties of barium–bismuth–borosilicate glasses,” *Radiat. Phys. Chem.*, vol. 81, no. 7, pp. 785–790, 2012.

[118] W. Tlaczala and M. Zaremba, “Virtual experiments in nuclear physics,” in *2007 IEEE Instrumentation & Measurement Technology Conference IMTC 2007*, 2007, pp. 1–6.

[119] A. Poškus, “Experiment No. 9. Absorption of alpha particles and electrons,” no. 9, 2015.

[120] D. Winkler, “Characterization of a HPGe Coaxial Well Detector for Low Energy Gamma Spectroscopy & Sensitivity Analysis of Germanium Spectrometers.” Ruprecht-Karls-Universität Heidelberg, 2018.

[121] R. Bhargava, S.-Q. Wang, and J. L. Koenig, “FTIR microspectroscopy of polymeric systems,” *Liq. Chromatogr. Microspectrosc. Assist. Synth.*, pp. 137–191, 2003.

[122] A. Di Gianfrancesco, “Technologies for chemical analyses, microstructural and inspection investigations,” in *Materials for ultra-supercritical and advanced ultra-supercritical power plants*, Elsevier, 2017, pp. 197–245.

[123] L.-S. Tang *et al.*, “Polyethylene glycol/graphene oxide aerogel shape-stabilized phase change materials for photo-to-thermal energy conversion and storage via tuning the oxidation degree of graphene oxide,” *Energy Convers. Manag.*, vol. 146, pp. 253–264, 2017.

[124] S. Pandey, A. Pandey, M. Deshmukh, and A. K. Shrivastava, “Role of Geiger Muller Counter in Modern Physics,” *J. Pure Appl. Ind. Phys.*, vol. 7, no. 5, pp. 192–196, 2017.

[125] H. Dweik, W. Sultan, M. Sowwan, and S. Makharza, “Analysis characterization and some properties of polyacrylamide copper complexes,” *Int. J. Polym. Mater.*, vol. 57, no. 3, pp. 228–244, 2008.

[126] H. S. Mansur, C. M. Sadahira, A. N. Souza, and A. A. P. Mansur, “FTIR spectroscopy characterization of poly (vinyl alcohol) hydrogel with different hydrolysis degree and chemically crosslinked with glutaraldehyde,” *Mater. Sci. Eng. C*, vol. 28, no. 4, pp. 539–548, 2008.

[127] H. Hendrawan, F. Khoerunnisa, Y. Sonjaya, and A. D. Putri, “Poly (vinyl alcohol)/glutaraldehyde/Premna oblongifolia merr extract hydrogel for

controlled-release and water absorption application," in *IOP Conference Series: Materials Science and Engineering*, 2019, vol. 509, no. 1, p. 12048.

[128] K. Abdali, E. Al, B. Khalid, and H. Abass, "Impact the silver nanoparticles on properties of new fabricated polyvinyl alcohol - polyacrylamide - polyacrylic acid nanocomposites films for optoelectronics and radiation pollution applications," *J. Polym. Res.*, vol. 30, no. 138, 2023, doi: 10.1007/s10965-023-03514-y.

[129] Z. Rashidi, G. Bagheri Marandi, and M. Taghvay Nakhjiri, "Carboxymethyl cellulose-based nanocomposite hydrogel grafted with vinylic comonomers: synthesis, swelling behavior and drug delivery investigation," *J. Macromol. Sci. Part A*, pp. 1–12, 2022.

[130] K. Abdali, "Structural, Morphological, and Gamma Ray Shielding (GRS) Characterization of HVCMC/PVP/PEG Polymer Blend Encapsulated with Silicon Dioxide Nanoparticles," *Silicon*, pp. 1–6, 2022.

[131] A. K. Al-shammari and E. Al-Bermany, "Polymer functional group impact on the thermo-mechanical properties of polyacrylic acid, polyacrylic amide-poly (vinyl alcohol) nanocomposites reinforced by graphene oxide nanosheetsAl-shammari AK, Al-Bermany E (2022) Polymer functional group impact on th," *J. Polym. Res.*, vol. 29, no. 8, pp. 1–12, 2022.

[132] N. R. Aldulaimi and E. Al-Bermany, "Tuning the bandgap and absorption behaviour of the newly-fabricated Ultrahigh Molecular weight Polyethylene Oxide-Polyvinyl Alcohol/Graphene Oxide hybrid nanocomposites," *Polym. Polym. Compos.*, vol. 30, p. 09673911221112196, 2022.

[133] N. R. Aldulaimi and E. Al-Bermany, "New Fabricated UHMWPEO-PVA Hybrid Nanocomposites Reinforced by GO Nanosheets: Structure and DC Electrical Behaviour," *J. Phys. Conf. Ser.*, vol. 1973, no. 1, p. 012164, Aug. 2021, doi: 10.1088/1742-6596/1973/1/012164.

[134] K. Abdali, "Synthesis, characterization and USW sensor of PEO/PMMA/PVP doped with zirconium dioxide nanoparticles," *Trans. Electr. Electron. Mater.*, vol. 23, no. 5, pp. 563–568, 2022, doi: 10.1007/s42341-022-00388-7.

[135] A. I. Ali, S. A. Salim, and E. A. Kamoun, "Novel glass materials-based (PVA/PVP/Al2O3/SiO2) hybrid composite hydrogel membranes for industrial applications: synthesis, characterization, and physical properties," *J. Mater. Sci. Mater. Electron.*, vol. 33, no. 13, pp. 10572–10584, 2022, doi: 10.1007/s10854-022-08043-w.

[136] A. K. Al-shammari and E. Al-Bermany, "New Fabricated (PAA-PVA/GO) and (PAAm-PVA/GO) Nanocomposites: Functional Groups and Graphene Nanosheets effect on the Morphology and Mechanical Properties," *J. Phys. Conf. Ser.*, vol. 1973, no. 1, p. 012165, Aug. 2021, doi: 10.1088/1742-6596/1973/1/012165.

[137] K. Rajesh, V. Crasta, N. B. Rithin Kumar, G. Shetty, and P. D. Rekha, "Structural, optical, mechanical and dielectric properties of titanium dioxide doped PVA/PVP nanocomposite," *J. Polym. Res.*, vol. 26, no. 4, 2019, doi: 10.1007/s10965-019-1762-0.

[138] M. A. Kadhim and E. Al-Bermany, "New fabricated PMMA-PVA/graphene oxide nanocomposites: Structure, optical properties and application," *J. Compos. Mater.*, vol. 55, no. 20, pp. 2793–2806, 2021.

[139] M. A. Q. Bhuiyan and S. Rahman, "MD; Rahaman, MS; Shajahan, M.;

Dafader, NC Improvement of Swelling Behaviour of Poly (Vinyl Pyrrolidone) and Acrylic Acid Blend Hydrogel Prepared By the Application of Gamma Radiation," *Org. Chem. Curr. Res*, vol. 4, no. 2, 2015.

[140] Y. Feng, X. Zhang, Y. Shen, K. Yoshino, and W. Feng, "A mechanically strong, flexible and conductive film based on bacterial cellulose/graphene nanocomposite," *Carbohydr. Polym.*, vol. 87, no. 1, pp. 644–649, 2012.

[141] A. N. Al-Jamal, K. A. O, K. H. Abbass, B. H. Rabee, and E. Al-Bermany, "Silver NPs reinforced the structural and mechanical properties of PVA-PAAm-PEG nanocomposites," in *AIP Conference Proceedings*, 2023, vol. 2414, no. 1, p. 30005.

[142] W. D. Callister and D. G. Rethwisch, *Introduction to Material Science and Engineering*. John wiley and Sons, Inc, 2018.

[143] S. H. Borova, O. M. Shevchuk, N. M. Bukartyk, E. Y. Nikitishyn, and V. S. Tokarev, "Nanocomposite films based on functional copolymers with embedded carbon nanotubes," 2014.

[144] Z. Yu, L. Guo, H. Du, T. Krauss, and J. Silcox, "Shell distribution on colloidal CdSe/ZnS quantum dots," *Nano Lett.*, vol. 5, no. 4, pp. 565–570, 2005.

[145] R. M. A. Domingues, G. D. A. Sousa, C. M. Silva, C. S. R. Freire, A. J. D. Silvestre, and C. P. Neto, "High value triterpenic compounds from the outer barks of several Eucalyptus species cultivated in Brazil and in Portugal," *Ind. Crops Prod.*, vol. 33, no. 1, pp. 158–164, 2011.

[146] P. Phukan and D. Saikia, "Optical and structural investigation of CdSe quantum dots dispersed in PVA matrix and photovoltaic applications," *Int. J. Photoenergy*, vol. 2013, 2013.

[147] P. Dhatarwal and R. J. Sengwa, “Nanofiller controllable optical parameters and improved thermal properties of (PVP/PEO)/Al2O3 and (PVP/PEO)/SiO2 nanocomposites,” *Optik (Stuttg).*, vol. 233, no. February, 2021, doi: 10.1016/j.ijleo.2021.166594.

[148] S. D. Meshram, R. V Rupnarayan, S. V Jagtap, V. G. Mete, and V. S. Sangawar, “Synthesis and characterization of lead oxide nanoparticles,” *Int. J. Chem. Phys. Sci.*, vol. 4, pp. 83–88, 2015.

[149] D. S. McLachlan *et al.*, “AC and DC percolative conductivity of single wall carbon nanotube polymer composites,” *J. Polym. Sci. Part B Polym. Phys.*, vol. 43, no. 22, pp. 3273–3287, 2005.

[150] S. A. Jabbar, S. M. Khalil, A. R. Abdulridha, E. Al-Bermany, and K. Abdali, “Dielectric, AC Conductivity and Optical Characterizations of (PVA-PEG) Doped SrO Hybrid Nanocomposites.pdf,” *Key Eng. Mater.*, vol. 936, pp. 83–92, 2022, doi: 10.4028/v-3lkwx9.

[151] M. Hussein and A. Hashim, “Study of Dielectric Properties For (Calcium Oxide-poly-vinyl alcohol) Composites,” *Basic Educ. Coll. Mag. Educ. Humanit. Sci.*, no. Special, 2012.

[152] Y.-L. Luo, L.-L. Chen, F. Xu, and Q.-S. Feng, “Fabrication and characterization of copper nanoparticles in PVA/PAAm IPNs and swelling of the resulting nanocomposites,” *Met. Mater. Int.*, vol. 18, no. 5, pp. 899–908, 2012.

[153] Y. Ts. of F. nanoparticles and its antibacterial application Prabhu, K. V. Rao, B. S. Kumari, V. S. S. Kumar, and T. Pavani, “Synthesis of Fe3O4 nanoparticles and its antibacterial application,” *Int. Nano Lett.*, vol. 5, no. 2, pp. 85–92, 2015.

[154] E. R. Atta, Z. K. M, and A. M. Madbouly, “Research Article Study on

Polymer Clay Layered Nanocomposites As Shielding Materials for Ionizing Radiation," *Int. J. Recent Sci. Res.*, vol. 6, pp. 4263–4269, 2015, [Online]. Available: http://www.recentscientific.com

الخلاصه

جذبت جسيمات أوكسيد السيليكون النانوي (SiO_2 NPs) المواد النانويه لتعديل و تحسين الهيكل و الخصائص وفجوة النطاق وخصائص العزل.ركزت هذه الدراسه على تاثير زيادة تركيز SiO_2 على مزيج ثلاثة بوليمرات بتراكيز مختلفة لتصنيع مركبات نانويه جديده. تم خلط بولي (أكريلاميد) (PAAm) ، بولي (فاينيل الكحول) (PVA) ، وبولي (فينيل بيروليدون) (PVP) مع نسب مختلفة وتحميلها بنسب مختلفة منSiO_2 ($x = 0.01, 0.03,$ and 0.05). باستخدام طريقة الاذابه والصب.

وقسمت الرساله إلى خمسة فصول، ركز الفصل الأول على الدراسة الاستقصائية للمقدمة والدراسات السابقة، وتضمن الفصل الثاني الجزء النظري، بينما تضمن الفصل الثالث الجزء العملي ثم الفصل الرابع النتائج والمناقشات واخيرا الفصل الخامس الاستنتاجات والدراسات المستقبلية. تم استخدام خصائص مختلفة للتحقيق في هذه المتراكبات النانوية الجديدة.

تم استخدام حيود الأشعة السينية (XRD) ، مطياف تحويل فورير بالأشعة تحت الحمراء (FTIR) ، الفحص المجهري البصري (OM) ، المجهر الإلكتروني الماسح للانبعاث الالكتروني (FE-SEM)، مقياس الطيف الضوئي المرئي للأشعة فوق البنفسجية (UV) ، ومقياس التيار الكهربائي المتردد والفعالية المضادة للبكتيريا لفحص العينات وعداد كايكر لكشف قابلية على امتصاص الاشعه المؤينه.

أظهرت أطياف FTIR تفاعلًا بينيًا كبيرًا بين خليط البوليمر والماده النانويه. أظهرت أنماط حيود الاشعة السينية (XRD) للعينات قمة واسعة بين $^{o}50$- 10~. أظهرت صور المجهر الضوئي و الالكتروني سطحًا متجانسًا وتوزيعًا ممتازًا للجسيمات النانوية في الخليط البلوليمري.

اظهرت الخصائص البصريه زيادة في الامتصاصية من 0.73 إلى 0.91 عند الطول الموجي 200 nm، وكذالك تحسنت فجوة الطاقة من 4.8 إلى 3.4 الكترون فولت للانتقال غير المباشر المسموح ومن 4.2 إلى 3.1 الكترون فولت للانتقال غير المباشر الممنوع. كذلك بينت النتائج تحسن معاملات الامتصاص و الانكسار الخمود، وثابت العزل الحقيقي والخيالي وكذلك التوصيلية البصرية مع زيادة تركيز الجسيمات النانوية SiO_2, بينما قلت النفاذية مع زيادة تركيزSiO_2 NPS. وككذلك تحسن ثابت العزل الكهربائي والفقدان من 0.20 إلى 0.53 بالاضافة الى تحسن بارز في التوصيله الكهربائي.

أظهرت اضافة و زيادة تركيز الجسيمات النانوية SiO_2 تحسنًا كبيرا في المنطقة المثبطة من النشاط المضاد للبكتيريا من 0.00 إلى 24 ملم من S. aureus و 23 ملم لبكتريا الشريطية القولونية مقارنة بالمزيج الثلاثي

للبوليمرات. كذلك اظهرت النتائج الامتصاص الاشعاعي لاشعه جاما انخفاض إشعاع مع زيادة تركيزات SiO_2 في لمركبات النانوية. حيث تزداد معاملات التوهين مع زيادة تركيز الجسيمات النانوية SiO_2. تعد هذه المركبات النانوية واعدة للخلايا الشمسية، والإلكترونيات الضوئية، وتطبيقات علم الاحياء وتطبيقات الحمايه من الضوء و الدروع الخفيفة الشفافة.

جمهورية العراق
وزارة التعليم العالي والبحث العلـمي
كلية التربية للعلوم الصرفة -جامعة بابل
قســم الفـيزياء

تاثير جسيمات ثنائي اوكسيد السيليكون النانويه على الخصائص الفيزيائيه للمتراكبات البوليمريه النانويه

رساله مقدمه

الى مجلس كلية التربيه للعلوم الصرفه في جامعة بابل وهي جزء من متطلبات

نيل درجة الماجستير في التربيه /الفيزياء

من قبل الطالبه

اثار اقبال عليوي عبد الشهيد

بكالوريوس في الفيزياء

جامعة بابل 2009 م

باشراف

أ.د احسان ضياء جواد البيرماني

1445هـ 2023م